# Semi-inclusive deep-inelastic scattering on a polarized spin-1 target. II. Deuteron and spectator nucleon tagging

W. Cosyn [1,*] and C. Weiss [2,†]

[1] *Department of Physics, Florida International University, Miami, Florida 33199, USA*

[2] *Theory Center, Jefferson Lab, Newport News, Virginia 23606, USA*

(Received 13 April 2026; accepted 2 June 2026; published 3 August 2026)

We develop the theoretical framework for semi-inclusive deep-inelastic scattering on a polarized spin-1 target and apply it to scattering on the polarized deuteron with spectator nucleon tagging. In Part I (previous article), we present the general form of the semi-inclusive cross section and polarization observables for the spin-1 target. In Part II (this article), we consider deep-inelastic scattering on the polarized deuteron with spectator nucleon tagging as a special case of target fragmentation. Methods of light-front quantization are employed to separate nuclear and hadronic structure in the high-energy process and achieve a composite description. The light-front wave function of the polarized deuteron is obtained from a rotationally covariant three-dimensional wave function in the center-of-mass frame of the proton-neutron system. The tagged structure functions are computed in the impulse approximation. The momentum and spin distribution of the active nucleon are controlled by the deuteron polarization and the detected spectator momentum ($D/S$ wave ratio). The cross section and spin asymmetries are evaluated for general deuteron polarization (vector and tensor, longitudinal and transverse) as functions of the spectator momentum. Tensor-polarized spin asymmetries of order unity are achieved for spectator momenta of approximately 300 MeV, which select configurations with a large $D$ wave. Sum rules for the tagged spin structure functions are derived. The results can be used for simulations of spectator tagging in future polarized fixed-target experiments (Jefferson Lab) or at the Electron-Ion Collider.

DOI: 10.1103/nf26-tkx7

## I. INTRODUCTION

This is Part II of a study of semi-inclusive deep-inelastic scattering on a polarized spin-1 target. Part I [1] presents the general form of the semi-inclusive cross section and polarization observables for the spin-1 target. Part II considers deep-inelastic scattering on the polarized deuteron with spectator nucleon tagging.

The deuteron nucleus plays an important role as a spin-1 target for inclusive and semi-inclusive deep-inelastic lepton scattering (DIS and SIDIS). A particular case of SIDIS is the detection of a "slow" nucleon (proton or neutron) with momentum $|\boldsymbol{p}_N|$ of a few 100 MeV in the target rest frame. It is an example of target fragmentation, or hadron production in the target rapidity region caused by soft interactions with rapidity range of order unity. In QCD, the target fragmentation cross section can be computed in a factorization scheme with so-called fracture functions, which combine aspects of parton distribution and fragmentation functions [2–4]. In the case of slow nucleon production in DIS on nuclei, the dominant production mechanism is the nuclear breakup, understood as the liberation of a bound nucleon in the initial nucleus by the DIS process, and the cross section can be computed in an approximation scheme on this basis [5,6]. In this context, the measurement is referred to as "spectator nucleon tagging." It presents a unique situation where the SIDIS cross section and polarization observables can be predicted on the basis of well-known nuclear structure and dynamics.

The deuteron in the initial state of the DIS process is described in terms of nucleon degrees of freedom [5,6] (regarding the role of non-nucleonic degrees of freedom in high-energy processes, see the references). It represents a quantum-mechanical system that exists as a superposition of $pn$ configurations in the space of relative momentum (or coordinate) and spin variables. The detection of the spectator nucleon and measurement of its momentum "selects" certain configurations from the superposition. This allows one to control the nuclear configurations during the DIS process and use that information for theoretical analysis.

The typical nucleon momenta in the deuteron are of the order of the so-called binding momentum $\sqrt{\epsilon_D m} = 45$ MeV, where $\epsilon_D$ is the deuteron binding energy and $m$ the nucleon mass. Tagging of nucleons with momenta $|\boldsymbol{p}_N|$ of a few 10 MeV (in the deuteron rest frame) selects average configurations in the deuteron, where interaction effects are moderate. Extrapolation to the nucleon pole at unphysical momenta

*Contact author: wcosyn@fiu.edu

†Contact author: weiss@jlab.org

*Published by the American Physical Society under the terms of the Creative Commons Attribution 4.0 International license. Further distribution of this work must maintain attribution to the author(s) and the published article's title, journal citation, and DOI. Funded by SCOAP³.*

$|\boldsymbol{p}_N|^2 = -\epsilon_D m$ selects configurations of infinite spatial size, where interactions are absent and the nucleons are free; this technique can be used to extract free neutron structure in a model-independent manner [7–10]. Tagging of nucleons with $|\boldsymbol{p}_N|$ of a few 100 MeV selects small-size configurations, where interactions are strong; this method can be used to study the interaction dependence of partonic structure modifications [11,12] and their connection with short-range $NN$ correlations [13–15]; see Ref. [16] for a review.

The orbital motion of the nucleons in the deuteron includes an $S$ and $D$ wave component, in which the spins are coupled parallel and antiparallel to the deuteron spin. The $S$ wave is dominant at average nucleon momenta; the $D$ wave becomes prominent at momenta $\gtrsim$200 MeV. By selecting configurations with a certain momentum using spectator tagging, one effectively controls the $D/S$ ratio and thus the spin state of the nucleons during the DIS process. In DIS on a vector-polarized deuteron, proton tagging controls the effective polarization of the active neutron [5,17,18]. This can be used to perform measurements of neutron spin structure functions in defined spin states and eliminate the $D$-wave depolarization. In DIS on the tensor-polarized deuteron, tagging controls the $D$ wave sustaining the tensor-polarized spin asymmetries. By selecting configurations with a large $D/S$ ratio, tensor-polarized asymmetries of order unity can be achieved, even saturating the mathematical bounds $A^T \in [-2, 1]$ (see Part I [1]) [5]. This is very different from inclusive DIS without spectator tagging, where scattering predominantly happens in average configurations with small $D$ wave and the tensor-polarized asymmetries are $\ll 1$ [5,19,20]. It offers a striking example of the entanglement of spin and orbital degrees of freedom in the deuteron and the idea of selection of configurations by spectator tagging.

Measurements of DIS on the deuteron with spectator tagging are performed in fixed-target scattering experiments at Jefferson Lab, using specialized detectors for detecting slow protons or neutrons emerging from the target, covering momenta $|\boldsymbol{p}_N| \lesssim 100$ MeV (BONuS, ALERT) [21–24] and a few 100 MeV (Deeps, BAND, LAD) [25–27]. Measurements of spectator tagging are also planned at the Electron-Ion Collider (EIC), using the far-forward detectors for charged and neutral beam fragments [10,28]. The collider setup offers several advantages for nuclear breakup detection: no target material preventing the detection of slow protons or neutrons; excellent coverage and momentum resolution for far-forward protons (magnetic spectrometer); possibility of detecting far-forward neutrons (zero-degree calorimeter). Measurements of DIS with spectator tagging could also be performed on the polarized deuteron if polarized deuteron beams become available at EIC; see Refs. [29–31] for the technical prospects. An important advantage of the collider in this regard is that the deuteron polarization does not interfere with the spectator detection (no holding magnets as in polarized fixed targets). This would make it possible to explore the spin effects of polarized spin-1 SIDIS using spectator tagging.

In Part I [1], we derived the general form of the cross section of semi-inclusive scattering on a polarized spin-1 target. In Part II here we consider the specific process of DIS on the polarized deuteron with spectator nucleon tagging. We focus on the description of nuclear structure in the DIS process and present quantitative predictions for the polarized tagged structure functions.

Methods of light-front (LF) quantization [32–36] are employed to separate nuclear and hadronic structure in the high-energy process and achieve a composite description [6]. The deuteron is described by an LF wave function in nucleon degrees of freedom. The LF wave function is matched with the rotationally covariant three-dimensional wave function in the center-of-mass frame of the $NN$ system [37,38]; this formulation ensures rotational invariance and is particularly useful for the LF description of spin degrees of freedom.

The polarized tagged DIS cross section is computed in the impulse approximation (IA). Two different formulations are employed: LF quantum mechanics [6] and the virtual nucleon scheme [39,40]; the comparison of the results illustrates the theoretical uncertainties of the method. The cross section is expressed in terms of the LF momentum distributions of the active nucleon in the deuteron, which depend on the tagged spectator momentum and the deuteron polarization. These distributions have the same structural properties as the transverse-momentum-dependent (TMD) parton distributions in QCD [41] (spin-orbit effects, $T$-even and -odd structures) and can be discussed in these terms. They exemplify the idea of the selection of configurations through spectator tagging.

The tagged deuteron structure functions are computed for general deuteron polarization (longitudinal vector, transverse vector, tensor) as functions of the spectator momentum. Predictions for the tagged polarization observables (differential cross section, azimuthal harmonics, spin asymmetries, see Part I [1]) are presented and studied as functions of the tagged spectator momentum. The role of the $D/S$ wave ratio in the vector and tensor-polarized spin asymmetries is explained. The dependence of the observables on the nuclear structure model is investigated.

The results of this study are interesting in two respects: (i) They can be used for the simulation and analysis of polarized spectator tagging experiments at EIC or future fixed-target facilities, focusing on measurements of neutron spin structure or nuclear structure effects in high-energy scattering. (ii) They illustrate the unique structures appearing in SIDIS on a polarized spin-1 target, in a realistic example where the dynamics is well understood and quantitative predictions can be made. The spin asymmetries in nuclear breakup in the target fragmentation region are generally much larger than those predicted or measured for quark fragmentation in the current fragmentation region SIDIS, presenting favorable conditions for experiments.

In the present study, we describe the nuclear DIS process in the IA, where it is assumed that the DIS final state and the spectator nucleon evolve independently after the DIS process. It is known that final-state interactions (FSIs) have a sizable effect on the observed spectator momentum distributions at momenta $|\boldsymbol{p}_N| \gtrsim 100$ MeV and need to be included in complete treatment [8,9,42–45]. The IA results presented here are useful as a baseline for the experimental analysis and for further theoretical treatment, including FSI. In the spin-dependent tagged structure functions only the $T$-even

structures are nonzero in the IA; the $T$-odd structures require explicit FSI (the situation is the same as with $T$-odd structures in the current fragmentation, such as the Sivers function [41,46]).

The production of a slow nucleon in DIS on the deuteron is a special case of target fragmentation. In QCD, the cross section of SIDIS in the target fragmentation region can be computed using a generalized factorization theorem, as the product of the cross section for electromagnetic scattering on a quark or gluon and the fracture function of the target [2,3]. The fracture function describes both the target structure in the initial state and the fragmentation process producing the identified hadron in the final state; as such it combines aspects of the parton densities and the parton fragmentation functions. In the present study we do not use QCD factorization but compute the cross section for "nucleon production" directly in terms of the nuclear wave function and the structure functions of the active nucleon (without factorizing them into quark or gluon coefficient functions and distributions in the nucleon). This approximation is justified in the present kinematics, where the nuclear breakup process is the dominant source of nucleon production. The results obtained in this approximation are compatible with the QCD factorization theorem and respect the underlying scale separation [9]. Our results may be regarded as a particular nonperturbative model of the fracture function for nucleon production in DIS on the deuteron (this interpretation appears literally when the active nucleon structure functions in our expressions are factorized into quark or gluon coefficient functions and distributions in the nucleon).

Polarization effects in electron-deuteron scattering have been studied extensively in quasi-elastic scattering (deuteron breakup into $NN$ final state), including general structural analysis [47–51] and dynamical calculations using nonrelativistic nuclear theory [52,53], relativistic bound state equations [54,55], and relativistic amplitude methods [56–58]; see also references in the quoted works. In the present study, we focus on the deep-inelastic regime and use methods of LF quantization to separate nuclear and hadronic structure. The necessity of using LF quantization in high-energy scattering processes and tests of the consistency of the approximations (momentum sum rule, spin sum rules) are discussed in the text.

The article is organized as follows: Section II summarizes the specific setup of the tagged DIS process, including the kinematic variables, collinear-frame coordinates, and deuteron polarization parameters, as a special case of the general framework developed in Part I [1]. Section III covers the treatment of nuclear structure in the DIS process, including LF quantization, spin structure, and the IA in both the three-dimensional quantum-mechanical and the four-dimensional virtual nucleon formulation. Section IV explores in detail the nucleon LF momentum distributions in the deuteron sampled in tagged DIS, including their definition and properties, dependence on the nucleon and deuteron spin, probabilistic formulation, and numerical estimates. Section V presents the tagged DIS structure functions in the IA, for unpolarized and polarized electron and vector- and tensor-polarized deuteron, and the sum rules for the tagged spin structure functions.

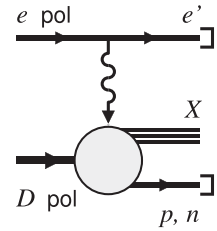



FIG. 1. DIS of polarized electrons on the polarized deuteron with detection of a proton (or neutron) in the nuclear fragmentation region (tagged DIS), Eq. (2.1).

Section VI presents examples of polarization observables in tagged DIS with the vector- and tensor-polarized deuteron, illustrating the idea of "selection of configurations" using the spectator momentum, and estimates of the nuclear structure model dependence. Section VII summarizes the conclusions and possible applications and extensions of the results. The Appendix gives the derivation of the spin sum rules for the polarized neutron distributions in spectator tagging, for both longitudinal and transverse spin.

## II. TAGGED DIS ON POLARIZED DEUTERON

### A. Kinematic variables

The semi-inclusive scattering process considered in this study is DIS of polarized electrons on a polarized deuteron with detection of a nucleon (proton or neutron) in the final state (see Fig. 1),

$$e(l|\lambda_e) + D(p_D|S_D, T_D) \to e'(l') + X + N(p_N), \qquad (2.1)$$

where $l$ ($l'$) are the initial (final) electron 4-momenta, $p_D$ is the initial deuteron 4-momentum, $p_N$ is the final nucleon 4-momentum. The electron polarization is specified by the helicity $\lambda_e$, the deuteron polarization by the vector and tensor parameters $S_D$ and $T_D$ (described in the following). We focus on the kinematic region where the detected nucleon momentum in the deuteron rest frame remains finite in the DIS limit (target fragmentation region) and has values $|\boldsymbol{p}_N| \lesssim$ few 100 MeV. In this region, the nucleon originates predominantly from the breakup of the deuteron nucleus, and the measurement is commonly referred to as "spectator nucleon tagging" or "tagged DIS"; this interpretation is not imposed a priori here but emerges from the theoretical analysis of Sec. III. For definiteness, we consider the case that the detected nucleon is a proton and refer to it as such in the following:

$$N \equiv p, \quad p_N \equiv p_p. \qquad (2.2)$$

equivalent formulas can be written for the case of a detected neutron.

The process Eq. (2.1) is characterized by the invariant kinematic variables described in Part I [1]. The original scaling variable for scattering on the deuteron is defined as

$$x_D \equiv \frac{Q^2}{2p_D \cdot q}, \quad 0 < x_D < 1. \qquad (2.3)$$

We use here the rescaled scaling variable

$$x \equiv 2x_D = \frac{Q^2}{p_D \cdot q}, \quad 0 < x < 2, \tag{2.4}$$

which can be regarded as the scaling variable for scattering on a nucleon in the absence of nuclear binding (this interpretation is optional; the variable is rigorously defined). We define the average nucleon mass as $m \equiv (m_n + m_p)/2$, so that the deuteron and nucleon masses are related as $M_D = 2m - \epsilon_D$, where $\epsilon_D = 2.2$ MeV is the binding energy. With these definitions,

$$x_D M_D = xm + O(\epsilon_D), \tag{2.5}$$

where the $O(\epsilon_D)$ terms are numerically irrelevant and can be neglected. Kinematic quantities depending on the combination $x_D M_D$ are therefore practically the same for scattering on the deuteron and on the unbound nucleon with the equivalent $x$. The $\gamma$ parameter defined in Part I [1], Eq. (2.9), is

$$\gamma \equiv \frac{2x_D M_D}{Q} = \frac{2xm}{Q} + O(\epsilon_D). \tag{2.6}$$

### B. Collinear frames

The theoretical analysis of tagged DIS is performed in the class of collinear frames introduced in Part I [1]. The deuteron momentum $\boldsymbol{p}_D$ and the momentum transfer $\boldsymbol{q}$ are along the $z$ axis, with $\boldsymbol{q}$ pointing in the negative $z$ direction. We describe four-vectors in the collinear frames by their LF components,

$$a^\pm \equiv a^0 \pm a^3, \quad \boldsymbol{a}_T \equiv (a^1, a^2), \tag{2.7a}$$

$$a \cdot b = \tfrac{1}{2}(a^+ b^- + a^- b^+) - \boldsymbol{a}_T \cdot \boldsymbol{b}_T. \tag{2.7b}$$

The components of $p_D$ and $q$ in the collinear frames are fixed by the invariant kinematic variables as

$$p_D^+ > 0 \text{ arbitrary}, \quad p_D^- = \frac{M_D^2}{p_D^+}, \tag{2.8a}$$

$$q^+ = -\frac{\xi p_D^+}{2}, \quad q^- = \frac{2Q^2}{\xi p_D^+}, \tag{2.8b}$$

$$\boldsymbol{p}_{DT} = \boldsymbol{q}_T = 0, \tag{2.8c}$$

where

$$\xi \equiv \frac{2x}{1 + \sqrt{1 + \gamma^2}}. \tag{2.9}$$

In the DIS limit, $Q \to \infty$ and $x$ fixed, one has $\xi \approx x$ up to power corrections.

The collinear frames are an equivalence class of frames connected by boosts along the $z$ axis (longitudinal boosts). A particular frame is selected by specifying the value of $p_D^+$. Longitudinal boosts between frames with different $p_D^+$ are performed by rescaling the LF components of the four-vector as

$$a^{+\prime} = \lambda a^+, \quad a^{-\prime} = \lambda^{-1} a^-, \quad \lambda \equiv p_D^{+\prime}/p_D^+. \tag{2.10}$$

If the $+$ and $-$ LF components of the four-vector are expressed as fractions of $p_D^+$ and $1/p_D^+$, as in Eq. (2.8), the boost is performed simply by changing the value of $p_D^+$ in the expressions. In particular, the class of collinear frames contains the deuteron rest frame, which is selected by setting

$$p_D^+ = M_D; \tag{2.11}$$

for other examples of collinear frames, see Ref. [9].

The final-state proton in the process Eq. (2.1) is characterized by its LF plus and transverse momentum (see Part I [1], Sec. II D),

$$p_p^+ = \frac{\alpha_p p_D^+}{2}, \quad \boldsymbol{p}_{pT}. \tag{2.12}$$

The LF momentum fraction $\alpha_p$ is invariant under longitudinal boosts and can be expressed in terms of the proton momentum in the deuteron rest frame as

$$\alpha_p = \frac{2\big[E_N(\boldsymbol{p}_p) + p_p^z\big]}{M_D}, \quad E_N(\boldsymbol{p}_p) \equiv \sqrt{|\boldsymbol{p}_p|^2 + m^2}. \tag{2.13}$$

For small rest-frame momenta $|\boldsymbol{p}_p| \ll m$,

$$\alpha_p \approx 1 + \frac{p_p^z}{m} + O\left(\frac{|\boldsymbol{p}_p|^2}{m^2}\right), \tag{2.14}$$

and the values of $\alpha_p$ are close to unity in the kinematic region under consideration. The invariant phase-space element in the final-state proton momentum is given by [see Part I [1], Eq. (2.38)]

$$d\Gamma_p = \frac{d^3 p_p}{(2\pi)^3 2E_N(\boldsymbol{p}_p)} = \frac{1}{[2(2\pi)^3]} \times \frac{d\alpha_p}{\alpha_p} d^2 p_{pT}, \tag{2.15a}$$

$$d^2 p_{pT} = |\boldsymbol{p}_{pT}|\, d|\boldsymbol{p}_{pT}|\, d\phi_p; \tag{2.15b}$$

for other equivalent forms, see Ref. [9]. The same factor $[2(2\pi)^3]$ will appear in the results for the tagged structure functions in Sec. V and will cancel in the final result for the cross section, see Eq. (2.19); we always write the factor in brackets to distinguish it.

The domain of the kinematic variables is restricted by the condition that the LF plus momentum of the unobserved hadronic final state $X$ must be positive,

$$p_X^+ = p_D^+ + q^+ - p_p^+ > 0, \tag{2.16}$$

which puts an upper limit on the proton plus momentum. In the DIS limit, neglecting power corrections $O(x^2 m^2/Q^2)$, the condition becomes

$$\alpha_p < 2 - x. \tag{2.17}$$

### C. Cross section

The general structure of the cross section for semi-inclusive scattering on a spin-1 target and its decomposition in structure functions is described in Part I [1], see master formula Eq. (4.36). In the application to tagged DIS on the deuteron ($A \equiv D$), we put $dx_D = dx/2$, Eq. (2.4), and consider the cross section differentially in $dx$. The expression takes the form

$$d\sigma = \frac{2\pi \alpha_{\rm em}^2 y^2}{Q^4(1-\epsilon)} \frac{dx}{2} dQ^2 \frac{d\psi_{l'}}{2\pi} \times (\mathcal{F}_U + \mathcal{F}_S + \mathcal{F}_T) d\Gamma_p, \tag{2.18}$$

where $d\Gamma_p$ is defined in Eq. (2.15), and $\mathcal{F}_U$, $\mathcal{F}_S$, $\mathcal{F}_T$ are the expressions containing the unpolarized, vector-polarized, and tensor-polarized structures as defined in Part I [1], Eqs. (4.37)–(4.39),

$$\mathcal{F}_U = F_{[UU,T]D} + \epsilon F_{[UU,L]D} + \cdots . \tag{2.19}$$

The azimuthal angle in the expressions is now the final-state proton angle, $\phi_h \equiv \phi_p$, defined as in Part I [1], Fig. 1. The structure functions depend on the DIS variables $x$ and $Q^2$ and the final-state proton variables $\alpha_p$ and $|\boldsymbol{p}_{pT}|$,

$$F_{[UU,T]D}(x, Q^2; \alpha_p, |\boldsymbol{p}_{pT}|), \text{ etc.} \tag{2.20}$$

The semi-inclusive DIS process of Eq. (2.1) can be measured and analyzed without making any assumption about the composite structure of deuteron. A composite description in terms of deuteron structure in nucleon degrees of freedom and a DIS process on the nucleon will be constructed in Sec. III, using methods of LF quantization.

For reference we note that the differential cross section in Eq. (2.19) can also be represented in the form [10]

$$d\sigma = \frac{2\pi\alpha_{\rm em}^2 y^2}{Q^4(1-\epsilon)x} dx\, dQ^2 \frac{d\psi_{l'}}{2\pi} \times \sigma_{{\rm red},D} d\Gamma_p, \tag{2.21a}$$

$$\sigma_{{\rm red},D} \equiv \frac{x}{2}(\mathcal{F}_U + \mathcal{F}_S + \mathcal{F}_T), \tag{2.21b}$$

where the flux factor is the same as in DIS on the nucleon, and $\sigma_{{\rm red},D}$ is the reduced cross section for tagged DIS on the deuteron. It is defined such that, up to nuclear binding effects,

$$\int d\Gamma_p\, \sigma_{{\rm red},D} \approx \sigma_{{\rm red},n} = F_{2n} - (1-\epsilon)F_{Ln}, \tag{2.22}$$

which is the reduced cross section of DIS on the neutron in the convention used in high-energy scattering experiments; see, e.g., Ref. [59]. This representation is useful for validating the normalization of the theoretical expressions, including nuclear structure, and for estimating experimental cross sections and rates.

### D. Deuteron polarization

The deuteron in the initial state of the tagged DIS process [Eq. (2.1)] is assumed to be in a mixed polarization state with vector and tensor polarization. The polarization is described by the spin-density matrix as introduced in Part I [1], Sec. III. The covariant spin density matrix is parametrized by the deuteron polarization four-vector and four-tensor

$$S_D^\alpha, \quad T_D^{\alpha\beta}, \tag{2.23}$$

whose components are specified by the invariant polarization parameters[1]

$$\{S_L, S_T, \phi_S\}, \quad \{T_{LL}, T_{LT}, T_{TT}, \phi_{T_L}, \phi_{T_T}\}. \tag{2.24}$$

In the class of collinear frames the polarization vector and tensor are described by their LF components and can be converted between frames in a simple manner using Eq. (2.10) [18].

In the nuclear structure calculations in Sec. III we start from the polarization vector and tensor in the deuteron rest frame and transport that information to the other collinear frames through boosts. The rest-frame polarization three-vector and three-tensor are expanded in the three-dimensional basis vectors $\{\boldsymbol{e}_{x'}, \boldsymbol{e}_{y'}, \boldsymbol{e}_z\}$ in the deuteron rest frame defined in Part I [1], Sec. II C and Fig. 1. The unit vector $\boldsymbol{e}_z$ is along the collinear axis in the direction opposite to $\boldsymbol{q}$. The $x'$ direction is along the final-state proton transverse momentum; the $y'$ direction is the right-handed normal to it; the transverse unit vectors are thus given by

$$\boldsymbol{e}_{x'} = \boldsymbol{p}_{pT}/|\boldsymbol{p}_{pT}|, \quad \boldsymbol{e}_{y'} = \boldsymbol{e}_z \times \boldsymbol{e}_{x'}. \tag{2.25}$$

The rest-frame polarization vector is expanded in terms of the basis vectors as in Part I [1], Eqs. (3.22),

$$\boldsymbol{S}_D = S_L \boldsymbol{e}_z + S_T[\cos(\phi_p - \phi_S)\boldsymbol{e}_{x'} + \sin(\phi_p - \phi_S)\boldsymbol{e}_{y'}], \tag{2.26}$$

where $\phi_p$ is the azimuthal angle of $\boldsymbol{p}_{pT}$ and $\phi_S$ is the spin-polarization angle, measured relative to the lepton scattering plane as specified in Part I [1], Fig. 1 ($\phi_p \equiv \phi_h$ in the figure). The rest-frame polarization tensor is expanded in the three-dimensional spherical tensors formed from the basis vectors as in Part I [1], Eq. (3.23),

$$\begin{aligned} T_D^{ij} = &\sqrt{\frac{3}{2}}\, T_{LL} e_{LL}^{ij} + \sqrt{2}\, T_{LT} \cos\big(\phi_p - \phi_{T_L}\big) e_{LT}^{ij} \\ &+ \sqrt{2}\, T_{LT} \sin\big(\phi_p - \phi_{T_L}\big) e_{LT'}^{ij} \\ &+ \frac{1}{\sqrt{2}}\, T_{TT} \cos\big(2\phi_p - 2\phi_{T_T}\big) e_{TT}^{ij} \\ &+ \frac{1}{\sqrt{2}}\, T_{TT} \sin\big(2\phi_p - 2\phi_{T_T}\big) e_{TT'}^{ij}; \end{aligned} \tag{2.27}$$

the expressions of the three-dimensional spherical tensors are given in Part I [1], Eq. (3.24).

The values of the invariant polarization parameters Eq. (2.24) are determined by the experimental setup. The values for standard setups (deuteron polarization relative to the electron beam axis in the deuteron rest frame) can be computed using the formulas of Part I [1], Sec. V A. The nuclear structure calculations here are aimed at the structure functions and do not require the experimental values of the invariant polarization parameters.

In the nuclear structure calculations it will be useful to have the polarization parameters corresponding to pure deuteron spin states in the rest frame. In a pure spin state, with spin projection $\Lambda = (+1, 0, -1)$ along an axis defined by the unit vector $\boldsymbol{N}$ in the deuteron rest frame, the rest-frame polarization vector and tensor are given by

$$\boldsymbol{S}_D = \Lambda \boldsymbol{N}, \tag{2.28a}$$

$$T_D = W(\Lambda)\big(-\tfrac{1}{6} + \tfrac{1}{2}\boldsymbol{N}\otimes\boldsymbol{N}\big), \tag{2.28b}$$

$$W(\Lambda) \equiv (1, -2, 1) \quad \text{for } \Lambda = (+1, 0, -1), \tag{2.28c}$$

see Part I [1], Eq. (5.2). Note that $\boldsymbol{S}_D \neq 0$ only in the states with spin projections $\Lambda = \pm 1$, while $T_D \neq 0$ in all spin

[1]For brevity we do not put a label $D$ on the invariant polarization parameters; it is clear that they refer to the deuteron.

projections. The polarization vector and tensor of Eq. (2.28) can be expanded in the basis vectors and tensors as in Eqs. (2.26) and (2.27). In particular, if the axis is along the longitudinal direction, $\boldsymbol{N} = \boldsymbol{e}_z$, Eq. (2.28) gives[2]

$$\boldsymbol{S}_D = \Lambda \boldsymbol{e}_z, \tag{2.29a}$$

$$T_D = W(\Lambda)\left[\frac{1}{\sqrt{6}} e_{LL}\right], \tag{2.29b}$$

and the invariant polarization parameters are

$$S_L = \Lambda, \quad S_T = 0, \tag{2.30a}$$

$$\{T_{LL}, T_{LT}, T_{TT}\} = W(\Lambda) \times \left\{\tfrac{1}{3}, 0, 0\right\}. \tag{2.30b}$$

If the axis is along a transverse direction, $\boldsymbol{N} = \boldsymbol{N}_T$ with $|\boldsymbol{N}_T| = 1$ and azimuthal angle $\phi_N$ relative to the lepton plane (see Part I [1], Fig. 1),

$$\boldsymbol{N}_T = \cos(\phi_p - \phi_N)\boldsymbol{e}_{x'} + \sin(\phi_p - \phi_N)\boldsymbol{e}_{y'}, \tag{2.31}$$

the rest-frame polarization parameters are

$$\boldsymbol{S}_D = \Lambda[\cos(\phi_p - \phi_N)\boldsymbol{e}_{x'} + \sin(\phi_p - \phi_N)\boldsymbol{e}_{y'}], \tag{2.32a}$$

$$T_D = W(\Lambda)\left[-\frac{1}{2\sqrt{6}} e_{LL} + \frac{1}{2\sqrt{2}} \cos(2\phi_p - 2\phi_N) e_{TT} + \frac{1}{2\sqrt{2}} \sin(2\phi_p - 2\phi_N) e_{TT'}\right], \tag{2.32b}$$

and the invariant polarization parameters are

$$S_L = 0, \quad S_T = |\Lambda|, \tag{2.33a}$$

$$\{T_{LL}, T_{LT}, T_{TT}\} = W(\Lambda) \times \left\{-\tfrac{1}{6}, 0, \tfrac{1}{2}\right\}, \tag{2.33b}$$

$$\phi_S = \phi_N, \quad \phi_{T_T} = \phi_N. \tag{2.33c}$$

## III. NUCLEAR STRUCTURE AND DIS PROCESS

### A. Light-front quantization

The tagged DIS process involves strong interaction dynamics at very different scales: the DIS process at energy and momentum transfers $\gg$1 GeV, and the nuclear binding and breakup process at momenta of a few 10 to 100 MeV. The theoretical analysis aims to separate the dynamics at the two scales and construct a composite description of the nuclear scattering process in terms of nucleon degrees of freedom.

The description of high-energy scattering processes on nuclei (projectile energy $\gg$1 GeV in the nuclear rest frame) in terms of nucleon degrees of freedom presents some specific challenges, resulting from the combination of quantum mechanics and relativity. (i) Because of nuclear binding, the projectile-nucleon scattering amplitudes are generally "off-shell," meaning off the energy shell in the time-ordered description of the process, or off the mass shell in the covariant description. One must ensure that the off-shellness does not lead to artifacts that grow proportionally to the projectile energy and become large in the high-energy limit. (ii) Because of relativity, non-nucleonic degrees of freedom of the nucleus (mesons, excited baryons) can contribute as initial states of the high-energy scattering process. One must justify why a truncation to nucleonic degrees of freedom is possible, and corrections to this approximation are expected.

LF quantization is an appropriate method for describing high-energy scattering on relativistic composite systems [6]. In this approach, the structure of the target is described at fixed LF time $x^+ = x^0 + x^3 = 0$, as "seen" by the high-energy projectile propagating through the system [33,36]. It has several unique features: (i) The off-shellness of the projectile-nucleon scattering amplitudes remains finite in the high-energy limit [6]. This permits the matching of the off-shell amplitudes in scattering on the nucleus with on-shell amplitudes measured in scattering of the free nucleon. (ii) The contributions of non-nucleonic degrees of freedom as initial states of the scattering process remain finite in the high-energy limit and can be controlled [6]. Using a dispersion-theoretical representation of the LF nuclear scattering amplitudes, one can quantify the contributions of non-nucleonic degrees of freedom in the initial state and study the convergence of the nuclear scattering amplitudes as functions of the invariant mass of the nuclear initial state. In high-energy scattering on the deuteron, the truncation to the $NN$ initial state (neglecting $NN\pi$ and $\Delta\Delta$ configurations) is a good approximation if the final state is restricted to breakup momenta $|\boldsymbol{p}_N| \lesssim$ a few 100 MeV [6]. Altogether, LF quantization permits the factorization of nuclear and hadronic structure in high-energy scattering, with finite effects due to nuclear binding.

In the LF description of nuclear high-energy scattering, the nucleus in the initial state is described by an LF wave function in nucleon degrees of freedom. The LF wave function encodes the low-energy nuclear structure as relevant for the high-energy process and is boost-invariant (independent of the reference frame) [36]. The frame independence allows one to consider the LF wave function in the nuclear rest frame, where it can be matched with the nonrelativistic wave function. In this way, the extensive theoretical and empirical knowledge of nonrelativistic nuclear few-body systems can be recruited for describing high-energy processes.

The LF description of nuclear high-energy scattering processes can be implemented using two formulations:

(1) a three-dimensional formulation based on LF quantum mechanics (LFQM);
(2) a four-dimensional formulation based on Feynman diagrams, referred to as the virtual nucleon approximation (VNA) [39,40].

When used as approximations with on-shell nucleon structure as input, the two formulations give equivalent results up to instantaneous terms in $x^+$ (LFQM) or off-shell contributions (VNA), which represent the systematic uncertainty arising from the lack of complete knowledge of the dynamics. In the following, we calculate the tagged DIS cross section in the IA using first the LFQM formulation (Secs. III B–III D). We then repeat the calculation in the VNA formulation and show that the results are identical up to instantaneous or off-shell terms (Sec. III E).

[2]The following expressions are special cases of the general formula Part I [1], Eq. (5.4).

### B. Quantum-mechanical formulation

In LFQM the nucleon states are characterized by their LF momenta, consisting of the plus component $p_N^+$ and the transverse momentum $\boldsymbol{p}_{NT}$, defined as in Eq. (2.7) (here $N = p$ or $n$). The LF energy or minus component is fixed by the mass-shell condition $p_N^2 = m^2$ as

$$p_N^- = \frac{|\boldsymbol{p}_{NT}|^2 + m^2}{p_N^+}. \tag{3.1}$$

The spin degrees of freedom are described by the LF helicity $\lambda_N$ (details are discussed in Sec. III C). The nucleon states are denoted as

$$|N(p_N, \lambda_N)\rangle \equiv |N(p_N^+, \boldsymbol{p}_{NT}, \lambda_N)\rangle. \tag{3.2}$$

for brevity we label them by the 4-momentum $p_N$; it is understood that the independent variables are $p_N^+$ and $\boldsymbol{p}_{NT}$, and that $p_N^-$ is always fixed by Eq. (3.1). The states are normalized as

$$\begin{aligned}&\langle N(p'_N, \lambda'_N)|N(p_N, \lambda_N)\rangle \\ &\quad = (2\pi)^3\, 2p_N^+\, \delta(p_N^{+\prime} - p_N^+)\delta^{(2)}(\boldsymbol{p}'_{NT} - \boldsymbol{p}_{NT})\delta(\lambda'_N, \lambda_N).\end{aligned} \tag{3.3}$$

The deuteron state is expanded in $pn$ states. We assume that the deuteron state has arbitrary LF plus momentum $p_D^+ > 0$ and transverse momentum $\boldsymbol{p}_{DT} = 0$; this is sufficient for describing DIS processes in the class of collinear frames (see Sec. II B). Because LF momentum is conserved in LFQM, the LF momenta of the $p$ and $n$ in the $pn$ configurations in the deuteron satisfy

$$p_p^+ + p_n^+ = p_D^+, \tag{3.4a}$$

$$\boldsymbol{p}_{pT} + \boldsymbol{p}_{nT} = \boldsymbol{p}_{DT} = 0. \tag{3.4b}$$

The plus components are parametrized as fractions of the deuteron plus momentum [see Eq. (2.12)],

$$p_p^+ = \alpha_p \frac{p_D^+}{2}, \quad p_n^+ = \alpha_n \frac{p_D^+}{2}, \quad \alpha_p + \alpha_n = 2. \tag{3.5}$$

The expansion of the deuteron state in $pn$ states is written in the form

$$\begin{aligned}&\langle p(p_p, \lambda_p), n(p_n, \lambda_n)|D(p_D, \lambda_D)\rangle \\ &\quad = (2\pi)^3\, 2p_D^+\, \delta(p_p^+ + p_n^+ - p_D^+)\, \delta^{(2)}(\boldsymbol{p}_{pT} + \boldsymbol{p}_{nT}) \\ &\qquad \times\ (2\pi)^{3/2}\Psi_D(\alpha_p, \boldsymbol{p}_{pT}; \lambda_p, \lambda_n|\lambda_D),\end{aligned} \tag{3.6}$$

where the LF wave function $\Psi_D$ depends on the proton LF momentum variables $\alpha_p$ and $\boldsymbol{p}_{pT}$; the corresponding values for the neutron in the configuration are

$$\alpha_n = 2 - \alpha_p, \quad \boldsymbol{p}_{nT} = -\boldsymbol{p}_{pT}. \tag{3.7}$$

The wave function is normalized such that

$$\begin{aligned}&\sum_{\lambda_p, \lambda_n} \int \frac{d\alpha_p d^2 p_{pT}}{\alpha_p(2-\alpha_p)}\, \Psi_D^*(\alpha_p, \boldsymbol{p}_{pT}; \lambda_p, \lambda_n|\lambda'_D) \\ &\qquad \times \Psi_D(\alpha_p, \boldsymbol{p}_{pT}; \lambda_p, \lambda_n|\lambda_D) = \delta(\lambda'_D, \lambda_D).\end{aligned} \tag{3.8}$$

The LF wave function is invariant under longitudinal boosts; it does not depend on $p_D^+$ but only on the boost-invariant fraction $\alpha_p$. Under transverse boosts it transforms kinematically [36]; only states with $\boldsymbol{p}_{DT} = 0$ are needed in the present calculation.

In the expansion Eq. (3.6) the LF energy of the $pn$ states is different from that of the deuteron state,

$$p_p^- + p_n^- \neq p_D^-. \tag{3.9}$$

It implies that the 4-momentum of the $pn$ states is different from that of the deuteron state

$$p_p + p_n \neq p_D. \tag{3.10}$$

The transition is therefore accompanied by a difference in the invariant masses of the states, defined as the square of their 4-momenta,

$$M_{pn}^2 \equiv (p_p + p_n)^2, \quad M_D^2 = p_D^2. \tag{3.11}$$

The invariant mass of the $pn$ state is a function of the LF momentum variables

$$M_{pn}^2 \equiv M_{pn}^2(\alpha_p, \boldsymbol{p}_{pT}) = \frac{4(|\boldsymbol{p}_{pT}|^2 + m^2)}{\alpha_p(2-\alpha_p)} \tag{3.12}$$

(this form applies to the states with zero overall transverse momentum). The LF energy difference Eq. (3.9) is proportional to the invariant-mass difference between the $pn$ state and the deuteron state,

$$p_p^- + p_n^- - p_D^- = \frac{M_{pn}^2 - M_D^2}{p_D^+}. \tag{3.13}$$

The invariant-mass difference thus acts as the invariant representation of the LF "energy denominator" and plays a central role in LFQM. In the deuteron rest frame ($p_D^+ = M_D$), expressing the LF variables $\alpha_p$ and $\boldsymbol{p}_{pT}$ in terms of the proton 3-momentum $\boldsymbol{p}_p$, and expanding in $|\boldsymbol{p}_p|/m$, one obtains

$$M_{pn}^2 - M_D^2 = 4m\left(\frac{|\boldsymbol{p}_p|^2}{m} + \epsilon_D\right)\left[1 + O\left(\frac{p_p^z}{m}\right)\right], \tag{3.14}$$

and the invariant-mass difference becomes proportional to the energy difference between the $pn$ and deuteron states in the nonrelativistic theory.

The deuteron LF wave function satisfies a two-body bound-state equation with an $NN$ potential or effective interaction at fixed LF time [6,60]. The equation determines, in particular, the analytic structure of the wave function. On general grounds the wave function can be written in

the form

$$\Psi_D(\alpha_p, \boldsymbol{p}_{pT}; \lambda_p, \lambda_n|\lambda_D) = (2\pi)^{-3/2} \frac{\Gamma_{Dpn}(\alpha_p, \boldsymbol{p}_{pT}; \lambda_p, \lambda_n|\lambda_D)}{M_{pn}^2(\alpha_p, \boldsymbol{p}_{pT}) - M_D^2}. \tag{3.15}$$

The invariant-mass difference in the denominator of Eq. (3.15) is independent of the $NN$ interaction. It describes the propagation of the nucleons in intermediate states between interactions. The form Eq. (3.15) contains the free nucleon pole (Bethe-Peierls pole), which occurs at $|\boldsymbol{p}_p|^2 + m\epsilon_D = 0$ in the nonrelativistic approximation of Eq. (3.14) and is a universal feature of a two-body system bound by a short-range interaction. The vertex function in the numerator of Eq. (3.15) depends on the $NN$ interaction. It describes the binding effects and the spin structure of the system. It can be determined by solving the LF bound-state equation with specific models of the $NN$ interaction. Alternatively, it can be obtained by matching the LF and nonrelativistic deuteron wave functions in the rest frame.

### C. Spin structure

In LFQM the spin states of particles are chosen as LF helicity states [36,61]. The LF helicity states are obtained from the rest-frame spin states through a sequence of LF boosts along the longitudinal and transverse momentum directions. They differ from the canonical spin states by the so-called Melosh rotation [62] if the transverse momentum of the state is nonzero, $\boldsymbol{p}_T \neq 0$. In the deuteron bound state, the nucleons have transverse momenta $\boldsymbol{p}_{pT} = -\boldsymbol{p}_{nT} \neq 0$, and their LF helicity states are affected by the rotation. The deuteron state as a whole has $\boldsymbol{p}_{DT} = 0$ in the collinear frames, and its LF helicity states are the same as canonical spin states.

In formulating the LF helicity structure of the deuteron, one faces the challenge that three-dimensional rotational invariance is not manifest in LF quantization. In equal-time quantization (i.e., in nonrelativistic theory), where rotational invariance is manifest, the deuteron has two internal spin states, corresponding to the $S$ and $D$ waves of the orbital motion. The LF version of this structure can be obtained by expressing the LF wave function in a form that exhibits rotational invariance and can be matched with the spin structure in equal-time quantization. A practical way to do this is to express the deuteron LF wave function as a function of the 3-momentum of the nucleons in the center-of-mass (c.m.) frame of the $pn$ system [5,6,18,37].

The c.m. frame is the special collinear frame in which the LF components of the total 4-momentum of the $pn$ system satisfy

$$(p_p + p_n)^+ = (p_p + p_n)^- \tag{3.16}$$

such that

$$(p_p + p_n)^z = \tfrac{1}{2}[(p_p + p_n)^+ - (p_p + p_n)^-] = 0. \tag{3.17}$$

From Eqs. (3.1) and (3.12), one can see that this is realized in the collinear frame with $p_D^+ = M_{pn}$. Note that this frame is not the deuteron rest frame, but a frame that differs from it by a boost with parameter $\lambda = M_{pn}/M_D$, see Eq. (2.10). The condition Eq. (3.17), together with $\boldsymbol{p}_{pT} + \boldsymbol{p}_{nT} = 0$ valid in any collinear frame, implies that the ordinary 3-momentum of the $pn$ system is zero, and the 4-momentum is [here $(p^0, \boldsymbol{p})$ denote the ordinary four-vector components]

$$p_p + p_n = (M_{pn}, \boldsymbol{0}). \tag{3.18}$$

In this frame, the $p$ and $n$ have equal and opposite ordinary 3-momenta, and their 4-momenta can be written as

$$p_p = (E, \boldsymbol{k}), \quad p_n = (E, -\boldsymbol{k}), \tag{3.19a}$$

$$E \equiv E(\boldsymbol{k}) \equiv \sqrt{|\boldsymbol{k}|^2 + m^2}. \tag{3.19b}$$

The relation of the c.m. momentum $\boldsymbol{k}$ to the LF variables $\alpha_p$ and $\boldsymbol{p}_{pT}$ is

$$k^z = \frac{M_{pn}}{2}(\alpha_p - 1), \quad \boldsymbol{k}_T = \boldsymbol{p}_{pT}, \tag{3.20a}$$

$$\alpha_p = 1 + \frac{k^z}{E}, \quad M_{pn} = 2E. \tag{3.20b}$$

The relation between the integration measures is

$$\int \frac{d\alpha_p d^2 p_{pT}}{\alpha_p(2-\alpha_p)} = \int \frac{d^3k}{E(k)}. \tag{3.21}$$

The c.m. momentum thus serves as an alternative variable to the LF momenta and can be used as an argument of the LF wave function. This representation allows one to formulate the LF helicity structure of the wave functions such that it respects three-dimensional rotational covariance.

The explicit form of the deuteron LF wave function in terms of the c.m. momentum variable has been derived in Refs. [5,18,37]; we follow the notation of Ref. [18]:

$$\Psi_D(\alpha_p, \boldsymbol{p}_{pT}; \lambda_p, \lambda_n|\lambda_D) = \sum_{\lambda_p', \lambda_n'} \widetilde{\Psi}_D(\boldsymbol{k}, \lambda_n', \lambda_p'|\lambda_D)\, U^*(\boldsymbol{k}, \lambda_p', \lambda_p)\, U^*(-\boldsymbol{k}, \lambda_n', \lambda_n), \tag{3.22a}$$

$$\widetilde{\Psi}_D(\boldsymbol{k}, \lambda_n', \lambda_p'|\lambda_D) = \frac{1}{\sqrt{2}} \epsilon_D^i(\lambda_D) \left[\delta^{ij} f_0(k) + \frac{1}{\sqrt{2}}\left(\frac{3k^i k^j}{k^2} - \delta^{ij}\right) f_2(k)\right] \chi^\dagger(\lambda_n')[\sigma^j (i\sigma^2)]\, \chi^*(\lambda_p'), \tag{3.22b}$$

$$U(\boldsymbol{k}, \lambda_p', \lambda_p) = \chi^\dagger(\lambda_p') \left[\frac{E + k^z + m + \boldsymbol{k}_T \cdot \boldsymbol{\sigma}_T \sigma^3}{\sqrt{2(E + k^z)(E + m)}}\right] \chi(\lambda_p), \tag{3.22c}$$

$$U(-\boldsymbol{k}, \lambda_n', \lambda_n) = \chi^\dagger(\lambda_n') \left[\frac{E - k^z + m - \boldsymbol{k}_T \cdot \boldsymbol{\sigma}_T \sigma^3}{\sqrt{2(E - k^z)(E + m)}}\right] \chi(\lambda_n), \tag{3.22d}$$

where $\boldsymbol{k}$ is related to $\alpha_p$ and $\boldsymbol{p}_{pT}$ by Eq. (3.20). $\widetilde{\Psi}_D$ in Eq. (3.22b) is the three-dimensional relativistic wave function in the c.m. momentum $\boldsymbol{k}$ and the canonical spin variables $\lambda'_p$ and $\lambda'_n$. The three-vector $\epsilon^i_D(\lambda_D)$ is the polarization three-vector of the $pn$ configuration in the c.m. frame and is identical to the deuteron polarization three-vector in the deuteron rest frame. The 2-spinors $\chi(\lambda'_p)$ and $\chi(\lambda'_n)$ describe the spin degrees of freedom of the proton and neutron at rest, quantized along the $z$ axis. The form of $\widetilde{\Psi}_D$ is constrained by three-dimensional rotational invariance in $\boldsymbol{k}$ and includes the $S$ and $D$ waves of the orbital motion, similar to the nonrelativistic deuteron wave function. The radial wave functions are normalized as ($k \equiv |\boldsymbol{k}|$)

$$4\pi \int \frac{dk\, k^2}{E(k)} \left[f_0^2(k) + f_2^2(k)\right] = 1. \tag{3.23}$$

The functions $U(\boldsymbol{k}, \lambda'_p, \lambda_p)$ and $U(-\boldsymbol{k}, \lambda'_n, \lambda_n)$ in Eqs. (3.22c) and (3.22d) are the Melosh rotations of the proton and neutron spins. They connect the canonical spin variables $\lambda'_p$ and $\lambda'_n$ with the LF helicities $\lambda_p$ and $\lambda_n$ and depend on the proton or neutron momentum in the c.m. frame, with $U(\boldsymbol{k}_T = 0) = 1$. The asterisk (*) in Eq. (3.22) denotes complex conjugation, which appears because the wave function describes the matrix element $\langle pn|D\rangle$, Eq. (3.6), where the proton or neutron appears in the complex-conjugate state.

Equation (3.22) serves as a general parametrization of the deuteron LF wave function and is used in all applications in the present study. The dynamical content is in the radial wave functions in the c.m. momentum variable $f_L(k)$ ($L = 0, 2$). They can be obtained by solving the dynamical equation for the two-body bound state in LFQM with specific models of the $NN$ interaction [6,60,63]. Alternatively, the radial wave functions can be approximated by the nonrelativistic radial wave functions as

$$f_L(k) = \sqrt{E(k)}\, f_{L,\mathrm{nr}}(k) \quad (L = 0, 2), \tag{3.24}$$

where the factor $\sqrt{E}$ accounts for the difference between the normalization Eq. (3.23) and the standard nonrelativistic normalization

$$4\pi \int dk\, k^2 \left[f_{0,\mathrm{nr}}^2(k) + f_{2,\mathrm{nr}}^2(k)\right] = 1. \tag{3.25}$$

The approximation Eq. (3.24) has been shown to be accurate for $|\boldsymbol{k}| \lesssim 300$ MeV [6,63] and is used in the present study.

LFQM in principle permits "nonspherical" components of the deuteron wave function, beyond the $S$ and $D$ waves in the c.m. frame included in the parametrization Eq. (3.22) [64,65]. The incomplete $P$ wave described in Ref. [65] is connected with the presence of non-nucleonic degrees of freedom in the deuteron at very large c.m. momenta $|\boldsymbol{k}| \gtrsim 800$ MeV, which causes a departure from the logic based on the requirement of rotational invariance in the $NN$ sector. These structures can be neglected at the nucleon momenta of a few 100 MeV considered in the present study.

The deuteron LF wave function can also be represented in four-dimensional form, as a sum of bilinear forms in the nucleon 4-spinors describing the LF helicity states, contracted with the four-dimensional polarization vector of the $pn$ system

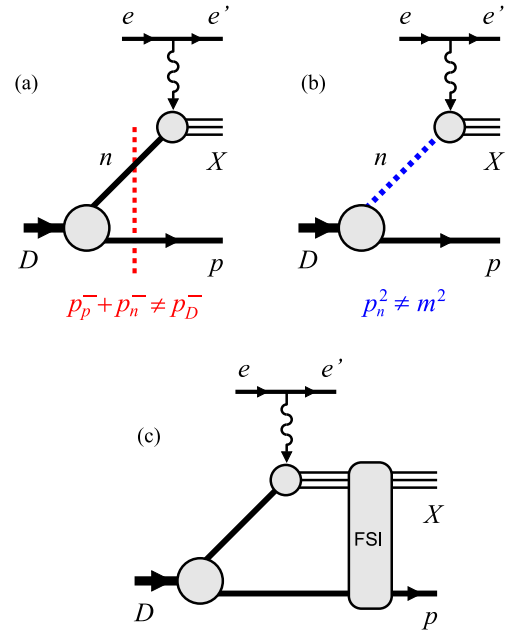



FIG. 2. Composite description of the tagged DIS process in LF quantization. (a) IA in the quantum-mechanical formulation (LFQM). (b) IA in the virtual nucleon formulation (VNA). (c) FSI.

[5,18,37]. The invariant functions accompanying the bilinear forms can be connected with the radial functions in the c.m. frame parametrization [Eq. (3.22)]. The four-dimensional form of the deuteron LF wave function permits the evaluation of spin sums using gamma matrix algebra. It will not be used explicitly in the present study, but the results obtained with it will be quoted in Sec. IV.

### D. Impulse approximation

LF quantization permits a composite description of tagged DIS on the deuteron as a DIS process on the nucleons and a distribution of the nucleons in the deuteron. One distinguishes two contributions (see Fig. 2):

(1) The impulse approximation (IA), where the electromagnetic current interacts with a single nucleon, and the final state produced in the DIS process evolves independently from the other nucleon ("spectator") [see Fig. 2(a)]. The tagged nucleon in the final state is assumed to be the spectator nucleon (production of slow nucleons in the DIS process is kinematically restricted and can be neglected at $x \gtrsim 0.1$ [9]). Measurement of the tagged nucleon LF momentum fixes the relative momentum of the nucleons in $pn$ configuration, and therefore the LF momentum of the active nucleon.

(2) Final-state interactions (FSIs), where certain components of the DIS final state interact with the spectator [see Fig. 2(c)]. The interactions transfer momentum to the spectator nucleon and require integration over all relevant $pn$ configurations in the initial state [9]. The $pn$ configurations in the initial state are therefore only indirectly related to the LF momentum of the tagged nucleon. The phase space for the integration strongly

grows with the tagged nucleon momentum, leading to a strong kinematic dependence of the FSI effects. The FSI process can also transfer quantum numbers (charge, spin) to the spectator nucleon.

The IA dominates the tagged DIS cross section at low momenta of the tagged nucleon, $|\boldsymbol{p}_p| \lesssim 300$ MeV in the deuteron rest frame, where the phase space for FSI is suppressed [9]. The IA becomes exact when extrapolating to the free nucleon pole, which occurs at a slightly nonphysical value of the tagged proton nucleon momentum; this feature is related to the analytic properties of the deuteron wave function and can be used to extract free neutron structure from tagged DIS [7,9,10,17]. In the present study, we use the IA to compute the cross section of tagged DIS on the deuteron with general vector and tensor polarization. The IA provides the baseline for the theoretical and experimental analysis and permits a simple study of the various polarization effects. Dynamical models of the FSI in unpolarized tagged DIS were developed in Refs. [8,9,42–45]. The inclusion of FSI in polarized tagged DIS requires further theoretical development and will be the object of a further study.

We now compute the polarized tagged DIS cross section in the IA using LFQM [9]. In this formulation, the scattering process is viewed as a transition between quantum-mechanical states induced by the electromagnetic current operator. The nuclear initial state is expanded in free nucleon states using the LF wave function, and the electromagnetic current couples to a single free nucleon with definite LF momentum. The single-nucleon states are on the mass shell, but the LF energy of the two-nucleon intermediate states is different from that of the initial or final state. This formulation is in close correspondence to the IA in nonrelativistic quantum mechanics [66].

The calculation is performed in the frame where the deuteron and virtual photon momenta are collinear and along the $z$ axis, see Eq. (2.8) and Part I [1]. We consider the current matrix element for the $D \to X + p$ transition (see Fig. 2),

$$\langle X, p(p_p, \lambda_p)|J^\mu|D(p_D, \lambda_D)\rangle, \tag{3.26}$$

and insert a complete set of intermediate proton and neutron states using

$$1_{pn} = \sum_{\lambda'_p,\lambda_n} \int \frac{dp_n^+ d\boldsymbol{p}_{nT}}{(2\pi)^3 2p_n^+} \int \frac{dp_p^{+\prime} d\boldsymbol{p}'_{pT}}{(2\pi)^3 2p_p^{+\prime}} |p(p'_p, \lambda'_p), n(p_n, \lambda_n)\rangle\langle p(p'_p, \lambda'_p), p(p_n, \lambda_n)| \tag{3.27}$$

(we put a prime on the intermediate-state proton variables to distinguish them from those of the final-state proton). Assuming that the current couples to the neutron, and expressing the $D \to pn$ matrix element in terms of the deuteron LF wave function, Eq. (3.6), we obtain

$$\begin{aligned}
&\langle X, p(p_p, \lambda_p)|J^\mu|D(p_D, \lambda_D)\rangle \\
&= \sum_{\lambda'_p,\lambda_n} \int \frac{dp_n^+ d\boldsymbol{p}_{nT}}{(2\pi)^3 2p_n^+} \int \frac{dp_p^{+\prime} d\boldsymbol{p}'_{pT}}{(2\pi)^3 2p_p^{+\prime}} \langle X|J^\mu|n(p_n, \lambda_n)\rangle\langle p(p_p, \lambda_p)|p(p'_p, \lambda'_p)\rangle\langle p(p'_p, \lambda'_p), n(p_n, \lambda_n)|D(p_D, \lambda_D)\rangle \\
&= \sum_{\lambda_n} \langle X|J^\mu|n(p_n, \lambda_n)\rangle \frac{2(2\pi)^{3/2}}{2-\alpha_p} \Psi_D(\alpha_p, \boldsymbol{p}_{pT}; \lambda_p, \lambda_n|\lambda_D).
\end{aligned} \tag{3.28}$$

The neutron LF momentum variables are fixed in terms of the final-state proton variables by Eq. (3.7),

$$\alpha_n = 2 - \alpha_p, \quad \boldsymbol{p}_{nT} = -\boldsymbol{p}_{pT}. \tag{3.29}$$

The factor

$$p_D^+/p_n^+ = 2/\alpha_n = 2/(2-\alpha_p) \tag{3.30}$$

in Eq. (3.28) arises from the normalization of the nucleon and deuteron states, Eq. (3.6), and represents a relativistic flux factor specific to LF quantization. The hadronic tensor for tagged DIS [see Part I, Eq. (4.7)] is then obtained as

$$\begin{aligned}
W_D^{\mu\nu}(p_D, q, p_p|\lambda'_D, \lambda_D) &= (4\pi)^{-1} \sum_{\lambda_p} \sum_X (2\pi)^4 \delta^4(p_D + q - p_p - p_X) \langle D(p_D, \lambda'_D)|J^\mu|X, p(p_p, \lambda_p)\rangle\langle X, p(p_p, \lambda_p)|J^\nu|D(p_D, \lambda_D)\rangle \\
&= \frac{2[2(2\pi)^3]}{(2-\alpha_p)^2} \sum_{\lambda_p} \sum_{\lambda_n,\lambda'_n} \Psi_D^*(\alpha_p, \boldsymbol{p}_{pT}; \lambda_p, \lambda'_n|\lambda'_D) \Psi_D(\alpha_p, \boldsymbol{p}_{pT}; \lambda_p, \lambda_n|\lambda_D) \\
&\quad \times (4\pi)^{-1} \sum_X (2\pi)^4 \delta^4(q + p_D - p_p - p_X) \langle n(p_n, \lambda'_n)|J^{\dagger\mu}(0)|X\rangle\langle X|J^\nu(0)|n(p_n, \lambda_n)\rangle.
\end{aligned} \tag{3.31}$$

The particular arrangement of the prefactors is explained in the following.

The hadronic tensor Eq. (3.31) is a matrix in the LF helicities of the initial-state deuteron appearing in the current matrix element and its complex conjugate, $\lambda_D$ and $\lambda'_D$. As such, it is to be averaged with the deuteron spin-density matrix in the LF helicity representation [see Part I, Eq. (4.9)],

$$\langle W_D^{\mu\nu}\rangle(p_D, q, p_p) = \sum_{\lambda_D,\lambda'_D} \rho_D(\lambda_D, \lambda'_D)\, W_D^{\mu\nu}(p_D, q, p_p|\lambda'_D, \lambda_D). \tag{3.32}$$

The final-state proton helicity $\lambda_p$ is summed over in Eq. (3.31), since the proton polarization is not observed in the measurements considered here.

The deuteron hadronic tensor Eq. (3.31) can be expressed in terms of the hadronic tensor of the active neutron. This allows one to connect the cross section of tagged scattering on the deuteron with that of scattering on the free neutron. In this step one must take into account the energy off-shellness in LFQM, which causes nonconservation of 4-momentum in the intermediate states of the scattering process, see Eq. (3.10). In the IA hadronic tensor, this implies

$$p_n \neq p_D - p_p \quad \text{(four-vectors)}, \tag{3.33}$$

so that the "internal" 4-momentum of the neutron is not equal to the difference of the "external" 4-momenta $p_D$ and $p_p$. The neutron hadronic tensor in Eq. (3.31) therefore cannot be identified with the free neutron hadronic tensor with 4-momenta $q$ and $p_n$, as this would lead to

$$q + p_n \neq q + p_D - p_p = p_X, \tag{3.34}$$

so that 4-momentum is not nonconserved between the initial and final state of the virtual photon-neutron–scattering process. However, the neutron hadronic tensor in Eq. (3.31) can be identified with the free neutron tensor at the effective 4-momentum transfer

$$\widetilde{q} \equiv q + p_D - p_n - p_p \neq q, \tag{3.35}$$

which takes into account that the virtual photon-neutron interaction occurs in an intermediate state where the 4-momentum of the nucleons is shifted. With Eq. (3.35)

$$\widetilde{q} + p_n = q + p_D - p_p = p_X, \tag{3.36}$$

and 4-momentum is conserved in the virtual photon-neutron scattering process. The neutron hadronic tensor at the effective momentum transfer is defined as

$$\begin{aligned} &W_n^{\mu\nu}(p_n, \widetilde{q}|\lambda'_n, \lambda_n) \\ &\quad\equiv (4\pi)^{-1} \sum_X (2\pi)^4\, \delta^{(4)}(\widetilde{q} + p_n - p_X) \\ &\qquad\times \langle n(p_n, \lambda'_n)|J^{\dagger\mu}(0)|X\rangle\, \langle X|J^{\nu}(0)|n(p_n, \lambda_n)\rangle. \end{aligned} \tag{3.37}$$

Substituting this expression in Eq. (3.31), the spin-averaged deuteron hadronic tensor (3.32) is finally obtained as

$$\begin{aligned} &\langle W_D^{\mu\nu}\rangle(p_D, q, p_p) \\ &\quad= \frac{2[2(2\pi)^3]}{(2-\alpha_p)^2} \sum_{\lambda_D,\lambda'_D} \rho_D(\lambda_D, \lambda'_D) \sum_{\lambda_p} \sum_{\lambda_n,\lambda'_n} \\ &\qquad\times \Psi_D^*(\alpha_p, \boldsymbol{p}_{pT}; \lambda_p, \lambda'_n|\lambda'_D)\Psi_D(\alpha_p, \boldsymbol{p}_{pT}; \lambda_p, \lambda_n|\lambda_D) \\ &\qquad\times W_n^{\mu\nu}(p_n, \widetilde{q}|\lambda'_n, \lambda_n), \end{aligned} \tag{3.38}$$

where the neutron LF momentum variables are again given by Eq. (3.29). Equation (3.38) is the IA result for the tagged DIS cross section in LFQM and exhibits the factorization of deuteron and nucleon structure, in the form of a product of a density in the deuteron LF wave function and the effective neutron hadronic tensor. In Sec. V, we use Eq. (3.38) to derive the expressions of the various structure functions appearing in the tagged DIS cross section.

The arrangement of the prefactors in Eq. (3.38) is explained as follows: The factor $[2(2\pi)^3]$ ensures that the tagged cross section is differential in the physical phase space element Eq. (2.15) with the normalization of the LF wave function given by Eq. (3.8). The factor $1/(2-\alpha_p)^2$ is a relativistic flux factor arising from LF quantization. The factor of 2 provides the connection between the deuteron and nucleon hadronic tensors and ensures the proper relation between the structure functions (see Sec. V).

Some comments on the accuracy of the LFQM calculation are in order. First, the 4-momentum nonconservation arising from the off-shellness of the LF energy does not produce large invariants in the DIS limit,

$$p_D \cdot q \sim Q^2 \to \infty, \quad Q^2/(p_D \cdot q) = x \text{ fixed}. \tag{3.39}$$

Using the LF components of $p_n + p_p - p_D$ given by Eqs. (3.4) and (3.13), and the LF components of $q$ in the collinear frame given by Eq. (2.8b), one obtains [6,9]

$$\begin{aligned} (p_p + p_n - p_D)\cdot q &= \frac{1}{2}(p_p^- + p_n^- - p_D^-)q^+ \\ &= -\frac{\xi}{4}\big(M_{pn}^2 - M_D^2\big) \approx -\frac{x}{4}\big(M_{pn}^2 - M_D^2\big), \end{aligned} \tag{3.40}$$

which remains finite in the DIS limit. Note that the individual invariants $p_p \cdot q$, $p_n \cdot q$, and $p_D \cdot q$ all become large $\sim Q^2$, because the momenta $p_p$, $p_n$, and $p_D$ have nonzero plus components, but the difference in Eq. (3.40) remains finite because the difference of the 4-momenta has zero plus component. The effects caused by the off-shellness of the LF energy are therefore power-suppressed in the DIS limit as

$$\frac{(p_p + p_n - p_D)\cdot q}{p_D \cdot q} \approx \frac{x^2\big(M_{pn}^2 - M_D^2\big)}{4Q^2}. \tag{3.41}$$

This feature is unique to LF quantization and arises because the quantization axis is aligned with the direction of the high-energy process. In other quantization schemes (i.e., equal-time quantization, where the 0-component of the 4-momentum is off-shell) the invariants produced by the energy off-shellness generally grow as $Q^2$. This is the principal reason for the use of LF quantization in high-energy scattering. In particular, Eq. (3.40) implies that

$$\widetilde{q}^2 = q^2\left[1 - \frac{x\big(M_{pn}^2 - M_D^2\big)}{2Q^2}\right], \tag{3.42}$$

so that the invariant momentum transfer in the electron-nucleon scattering process is equal to that in the electron-deuteron process (which is fixed by the kinematics), up to power corrections governed by the nuclear motion.

Second, in LF quantization the components of the current operator differ in how they involve the interactions of the system and are affected by instantaneous terms in $x^+$; see Ref. [9] for a summary. The "good" current $J^+$ is free of interactions and instantaneous terms; the "bad" current $J_T$ involves the interactions and is affected by instantaneous terms; the "worst" current $J^-$ is entirely dependent on the interactions. The matrix elements of $J^+$ can be computed reliably in the LFQM approach, leading to Eq. (3.38). The matrix elements of $J^-$ can be reconstructed from the transversality condition in the collinear frame (current conservation),

$$q^\mu \langle \dots | J_\mu | \dots \rangle = \frac{q^+}{2} \langle \dots | J^- | \dots \rangle + \frac{q^-}{2} \langle \dots | J^+ | \dots \rangle = 0, \tag{3.43}$$

and one does not need to know the form of the operator $J^-$. The matrix elements of $J_T$ involve unknown instantaneous terms, which are not included in Eq. (3.38). Studies comparing LFQM calculations using different current components in different frames (good and bad currents in a collinear frame vs good currents in a noncollinear frame) indicate that the effect of the instantaneous terms is power-suppressed in the DIS limit as $(\text{mass})^2/Q^2 \to 0$ [67]. The use of Eq. (3.38) without instantaneous terms is therefore a reasonable approximation for the leading-twist structure functions in tagged DIS. Its accuracy for higher-twist structure functions cannot be established at present, absent a dynamical theory that would allow one to consistently generate instantaneous terms. Our results for higher-twist structure functions quoted below should therefore be regarded as a rough estimate.

### E. Virtual nucleon formulation

We now compute the tagged DIS cross section in the equivalent four-dimensional formulation of LF nuclear structure based on Feynman diagrams (virtual nucleon approximation, VNA) [40,68]. In this formulation, the 4-momenta are conserved in the intermediate states of the scattering process, but the active nucleon momentum is off the mass-shell $p^2 \neq m^2$. The VNA formulation provides an alternative definition of the deuteron LF wave function in terms of the four-dimensional deuteron-proton-neutron vertex function. It also offers a different perspective on the instantaneous terms in the bad-current matrix element in the LFQM, by relating them to off-mass-shell terms in the VNA.

In the VNA, the $D \to p + X$ electromagnetic transition amplitude is regarded as an effective Feynman diagram [see Fig. 2(b)]. As with Feynman diagrams for point-particle interactions, 4-momenta are conserved at all the vertices. Applying 4-momentum conservation to the $D \to p + n$ effective vertex, the 4-momentum of the active neutron is now given by

$$\widetilde{p}_n \equiv p_D - p_p \quad \text{(4-momenta)}, \tag{3.44}$$

and is off the nucleon mass-shell,

$$\widetilde{p}_n^2 - m^2 \neq 0. \tag{3.45}$$

Applying the effective Feynman rules of Ref. [40], the IA current matrix element is obtained as

$$\langle X(p_X), p(p_p, \lambda_p) | J^\mu | D(p_D, \lambda_D) \rangle = -\Gamma^\mu_{\gamma^* nX} \frac{\widetilde{\not{p}}_n + m}{\widetilde{p}_n^2 - m^2} \Gamma^\nu_{Dpn} \epsilon_{D\nu}(\lambda_D) v(p_p, \lambda_p). \tag{3.46}$$

Here, $\Gamma^\mu_{\gamma^* nX}$ denotes the abstract vertex of the electromagnetic transition between the active neutron and the DIS final state $X$; its relation to the neutron structure function will be explained below. The following factor is the Feynman propagator of a point-like nucleon with 4-momentum $\widetilde{p}_n$. $\Gamma^\nu_{Dpn}$ is the deuteron-proton-neutron vertex, which is a four-vector and a matrix in bispinor space. It is contracted with the deuteron polarization four-vector $\epsilon_D(\lambda_D)$ and the bispinor of the final proton, $v(p_p, \lambda_p)$. [In the four-dimensional formulation of the deuteron-proton-neutron vertex, the proton is described by a charge-conjugated bispinor $v \equiv C\bar{u}^T$, the neutron by a regular bispinor $u$, so that the vertex can be represented as the bilinear form $\bar{u}\Gamma^\nu_{Dpn} v$; see Ref. [17] for details. This is the same assignment as in the three-dimensional formulation of the wave function in Eq. (3.22), where the proton is described by the complex-conjugate 2-spinor, and the neutron by the regular 2-spinor.]

The neutron virtuality $\widetilde{p}_n^2 - m^2$ in Eq. (3.46) is a function of the LF momentum variables of the final-state proton, $\alpha_p$ and $\boldsymbol{p}_{pT}$, which determine the neutron 4-momentum through Eq. (3.44). The correspondence between the VNA and LFQM formulations is established by noting that the virtuality in the VNA amplitude is proportional to the invariant-mass difference Eq. (3.15) in LFQM,

$$\widetilde{p}_n^2 - m^2 = -\frac{2 - \alpha_p}{2} \left( M_{pn}^2 - M_D^2 \right). \tag{3.47}$$

This allows one to express the VNA amplitude in terms of an effective LF wave function. To do so one needs to connect also the numerators in the two approaches. Here one encounters the problem that a representation in terms of nucleon spin states is defined *a priori* only for 4-momenta on the mass-shell, $p_n^2 = m^2$. To extend it to off-mass-shell momenta one has to adopt a prescription relating the off-shell nucleon momentum to an on-shell momentum,

$$\widetilde{p}_n \to p_n \quad \text{with} \quad p_n^2 = m^2. \tag{3.48}$$

This prescription is not unique; geometrically, it means projecting the vector $\widetilde{p}_n$ on the manifold defined by the mass-shell condition. The freedom is related to the choice of quantization axis in the noncovariant formulation and determines what kind of wave function (LF, equal-time, etc.) we want to recover from the VNA expression. In our case we identify the effective on-shell momentum through a projection along a light-like direction. Introducing a light-like four-vector $V$, $V^2 = 0$, we define an effective on-shell momentum as

$$p_n = \widetilde{p}_n - \frac{(\widetilde{p}_n^2 - m^2) V}{2 V \cdot \widetilde{p}_n}. \tag{3.49}$$

Notice that the modification of $\widetilde{p}_n$ along the light-like direction $V$ is proportional to the virtuality $\widetilde{p}_n^2 - m^2$. Specifically, if $V$ is chosen along the $z$ axis in the LF minus direction, $V^\mu \propto$

$(1,0,0,-1)$, $V^+=0$, $V^-\neq 0$, the LF 4-momentum components of the effective on-shell momentum Eq. (3.49) are

$$p_n^+ = \tilde{p}_n^+ = p_D^+ - p_p^+, \tag{3.50a}$$

$$\boldsymbol{p}_{nT} = \tilde{\boldsymbol{p}}_{nT} = -\boldsymbol{p}_{pT}, \tag{3.50b}$$

$$p_n^- = \frac{|\boldsymbol{p}_{nT}|^2 + m^2}{p_n^+}, \tag{3.50c}$$

which conincide with the 4-momentum components of the active neutron in the LFQM formulation, Eqs. (3.4) and (3.1).

At the effective on-shell momentum, we then introduce neutron spin states as LF helicity states, described by the LF helicity bispinors $u_{\rm LF}(p_n,\lambda_n)$. The final-state proton spin states we describe by $v_{\rm LF}(p_p,\lambda_p)$; the explicit expressions of the LF helicity spinors are given in Ref. [17]. With these spinors, the numerator of the Feynman propagator in Eq. (3.46) can be expressed as

$$\tilde{\not{p}}_n + m = \sum_{\lambda_n} u_{\rm LF}(p_n,\lambda_n)\bar{u}_{\rm LF}(p_n,\lambda_n) + \frac{(\tilde{p}_n^2 - m^2)}{2V\cdot\tilde{p}_n} V\cdot\gamma \tag{3.51a}$$

$$= \sum_{\lambda_n} u_{\rm LF}(p_n,\lambda_n)\bar{u}_{\rm LF}(p_n,\lambda_n) + \frac{1}{2}(\tilde{p}_n^- - p_n^-)\gamma^+. \tag{3.51b}$$

The first term in the expressions on the right-hand side is the on-shell spin projector for nucleon states with momentum $p_n$; the second term is proportional to the nucleon virtuality and accounts for the difference between the off-shell and on-shell projectors.

The deuteron spin state in Eq. (3.46) is described by the polarization four-vector $\epsilon_D(\lambda_D)$, which is defined relative to the deuteron 4-momentum $p_D$ and satisfies

$$p_D\cdot\epsilon_D = (p_p+\tilde{p}_n)\cdot\epsilon_D = 0, \quad \epsilon_D^2 = -1. \tag{3.52}$$

When the neutron 4-momentum is changed by the on-shell projection Eq. (3.48), the polarization vector is no longer aligned with the sum of the proton and neutron 4-momenta because $p_p+p_n\neq p_D$. We define a polarization vector $\epsilon_{pn}(\lambda_D)$ aligned with $p_p+p_n$ as

$$\epsilon_{pn} \equiv \epsilon_D + \frac{(\tilde{p}_n^2 - m^2)(V\cdot\epsilon_D)p_D}{M_D^2\, V\cdot\tilde{p}_n} + O\big[(\tilde{p}_n^2-m^2)^2\big] \tag{3.53}$$

(same argument $\lambda_D$ in $\epsilon_{pn}$ and $\epsilon_D$), which satisfies

$$(p_p+p_n)\cdot\epsilon_{pn} = 0 + O\big[(\tilde{p}_n^2-m^2)^2\big], \tag{3.54a}$$

$$\epsilon_{pn}^2 = -1 + O\big[(\tilde{p}_n^2-m^2)^2\big], \tag{3.54b}$$

where we have used Eq. (3.48) and neglected terms of higher order in the virtuality. The new vector $\epsilon_{pn}(\lambda_D)$ describes the spin wave function of the $pn$ system after the on-shell projection, and the vertex formed with it satisfies LF helicity selection rules with the nucleon spinors.

We now define the deuteron LF wave function in the context of the VNA as

$$\Psi_D(p_p;\lambda_p,\lambda_n|\lambda_D)[\text{VNA}] \equiv -\frac{\bar{u}_{\rm LF}(p_n,\lambda_n)\Gamma^\mu_{Dpn}\epsilon_{pn,\mu}(\lambda_D)v_{\rm LF}(p_p,\lambda_p)}{2(2\pi)^{3/2}\,(\tilde{p}_n^2-m^2)}. \tag{3.55}$$

The covariant expression on the right-hand side is a function of the proton 4-momentum $p_p$ and depends on the invariants $V\cdot\tilde{p}_n$ and $p_D\cdot p_p$, which can be related to the LF variables $\alpha_p$ and $|\boldsymbol{p}_{pT}|$. By virtue of Eq. (3.47), the virtuality denominator is proportional to the invariant-mass denominator of Eq. (3.15). The contraction of the deuteron vertex with the proton and on-shell neutron spinors is equal to the deuteron-proton-neutron vertex function in Eq. (3.15). The wave function defined by Eq. (3.55) therefore coincides with that of the LFQM formulation,

$$\Psi_D(p_p;\lambda_p,\lambda_n|\lambda_D)[\text{VNA}] = \frac{\Psi_D(\alpha_p,\boldsymbol{p}_{pT};\lambda_p,\lambda_n|\lambda_D)[\text{LF}]}{2-\alpha_p}. \tag{3.56}$$

The exact connection between the spin structure of the two wave functions is described in Ref. [17]. The covariant decomposition of the bilinear form in the numerator of the VNA wave function can be matched with the spin decomposition of the LFQM wave function in the rotationally symmetric representation in the c.m. frame (see Sec. III C).

The electromagnetic $\gamma^* nX$ vertex in Eq. (3.46) is evaluated at the off-shell neutron momentum $\tilde{p}_n$. It can be expanded around the on-shell momentum, resulting in corrections proportional to the virtuality,

$$\Gamma^\mu_{\gamma^* nX}(\tilde{p}_n) = \Gamma^\mu_{\gamma^* nX}(p_n) + \text{terms} \propto (\tilde{p}_n^2 - m^2). \tag{3.57}$$

The contraction of the on-shell vertex $\Gamma^\mu_{\gamma^* nX}(p_n)$ with the on-shell neutron spinor $u(p_n,\lambda_n)$ in the projector Eq. (3.51) of the propagator reproduces the current matrix element between a physical neutron state with momentum $p_n$ and the state $X$,

$$\Gamma^\mu_{\gamma^* nX}(p_n)u(p_n,\lambda_n) = \langle X|J^\mu|n(p_n,\lambda_n)\rangle. \tag{3.58}$$

The momentum transfer in the matrix element is

$$p_X - p_n = q + p_D - p_p - p_n = \tilde{q} \neq q, \tag{3.59}$$

which agrees with the effective momentum transfer in the LFQM calculation, Eq. (3.35). Altogether, neglecting the off-shell terms in the projector Eq. (3.51) and in the vertex Eq. (3.57), the IA current matrix element for deuteron breakup in the VNA, Eq. (3.46), becomes

$$\begin{aligned}
&\langle X, p(p_p,\lambda_p)|J^\mu|D(p_D,\lambda_D)\rangle \\
&\quad = 2(2\pi)^{3/2}\sum_{\lambda_n}\langle X|J^\mu|n(p_n,\lambda_n)\rangle \\
&\qquad \times \Psi_D(p_p;\lambda_p,\lambda_n|\lambda)[\text{VNA}] \\
&\quad = 2(2\pi)^{3/2}\sum_{\lambda_n}\langle X|J^\mu|n(p_n,\lambda_n)\rangle \\
&\qquad \times \frac{\Psi_D(\alpha_p,\boldsymbol{p}_{pT};\lambda_p,\lambda_n|\lambda)[\text{LF}]}{2-\alpha_p} \\
&\qquad \big[\text{up to terms} \propto (\tilde{p}_n^2 - m^2)\big].
\end{aligned} \tag{3.60}$$

This agrees with the result obtained in LFQM, Eq. (3.28). After squaring the matrix element, one again obtains the hadronic tensor, which can be expressed through the effective neutron hadronic tensor, see Eq. (3.38).

Some comments are in order regarding the correspondence between the VNA and LFQM formulations and the role of the off-shell terms.

(a) The off-shell terms in the VNA correspond to "instantaneous" terms in the LFQM formulation—contributions to the transition amplitude that do not involve physical intermediate states propagating over LF finite times. The neutron virtuality in the VNA is proportional to the LF energy off-shellness of the intermediate state in LFQM,

$$\widetilde{p}_n^2 - m^2 = -\frac{2-\alpha_p}{2} p_D^+ (p_p^- + p_n^- - p_D^-). \tag{3.61}$$

In the terms where the LF energy denominator is canceled by off-shell terms in the numerator, no propagation takes place.

(b) The off-shell terms arising from the numerator of the Feynman propagator Eq. (3.51) are proportional to $\gamma^+$. Because $(\gamma^+)^2 = 0$ these terms do not affect structures in the neutron electromagnetic vertex that are $\propto \gamma^+$. These are precisely the good components $J^+$ of the neutron current matrix element. In contrast, structures $\propto \gamma_T$ or $\gamma^-$ in the neutron vertex correspond to the bad or worst current components and have nonzero contraction with the off-shell terms in the propagator.

(c) The off-shellness is caused by nuclear binding. In the nonrelativistic limit,

$$\begin{aligned} \widetilde{p}_n^2 - m^2 &= -2(|\boldsymbol{p}_p|^2 + m\epsilon_D) \\ &= -4m(E_{\mathrm{kin},p} + \epsilon_D/2), \end{aligned} \tag{3.62}$$

where $E_{\mathrm{kin},p} \equiv |\boldsymbol{p}_p|^2/2m$ is the proton (or neutron) kinetic energy, and $\epsilon_D/2$ is the binding energy per nucleon. The typical values of the virtuality are therefore determined by the nucleon energy in the nucleus.

(d) In tagged DIS the neutron virtuality in the Feynman diagram is equal to the invariant momentum transfer between the deuteron and the tagged proton,

$$\widetilde{p}_n^2 - m^2 = (p_D - p_p)^2 - m^2 \equiv t' < 0, \tag{3.63}$$

which is a kinematic variable computed from the proton momentum. In tagged DIS experiments one can therefore control the virtuality of the active nucleon in the IA and measure the dependence of the structure functions on the virtuality in the physical region $|t'| < 2m\epsilon_D$. The extrapolation to $t' \to 0$ (on-shell point, or free nucleon point) eliminates off-shell terms in the cross section and allows one to access the structure function of the free neutron with tagged DIS [7]. The method also eliminates FSI effects through the analytic structure of the cross section [7–9]. On-shell extrapolation in polarized tagged DIS is discussed in Ref. [17].

## IV. NEUTRON DISTRIBUTION IN DEUTERON

### A. Neutron spin density matrix

The IA expresses the hadronic tensor of tagged DIS in terms of the deuteron LF wave function and the hadronic tensor of the active neutron. The LF momentum of the active neutron is fixed by the tagged proton momentum. Because of the entanglement of momentum and spin degrees of freedom in the deuteron wave function, also the LF helicity of the active neutron is influenced by the spectator momentum. It is useful to present this dependence in the form of a momentum and spin density of the active neutron that depends on the tagged proton momentum. This form allows one to present the expressions for the tagged DIS structure function in a compact and transparent form. It also allows one to study the LF structure of the deuteron in nucleon degrees of freedom and exhibit the analogies with the parton picture of hadrons. For the spin-1/2 nucleus of $^3$He, similar nucleon LF momentum distributions have been introduced in Ref. [69].

We write the IA result for the deuteron hadronic tensor with proton tagging, Eq. (3.38), in the form

$$\begin{aligned} \left\langle W_D^{\mu\nu} \right\rangle (p_D, q, p_p) &= \frac{2[2(2\pi)^3]}{(2-\alpha_p)^2} \sum_{\lambda_n, \lambda_n'} \rho_n(p_p|\lambda_n, \lambda_n') \\ &\quad \times W_n^{\mu\nu}(p_n, \widetilde{q}|\lambda_n', \lambda_n), \end{aligned} \tag{4.1a}$$

$$\begin{aligned} \rho_n(p_p|\lambda_n, \lambda_n') \equiv \sum_{\lambda_D, \lambda_D'} \rho_D(\lambda_D, \lambda_D') \sum_{\lambda_p} \\ \times \Psi_D^*(\alpha_p, \boldsymbol{p}_{pT}; \lambda_p, \lambda_n'|\lambda_D') \\ \times \Psi_D(\alpha_p, \boldsymbol{p}_{pT}; \lambda_p, \lambda_n|\lambda_D). \end{aligned} \tag{4.1b}$$

The effective neutron density $\rho_n$ is a density matrix in the neutron LF helicities. It depends on the tagged proton LF momentum and the deuteron polarization parameters contained in the deuteron spin density matrix.

It is convenient to introduce a covariant representation of the neutron density matrix [18], in analogy to the covariant representation of the deuteron density matrix, see Part I [1], Sec. III A. The matrix element of a neutron operator between neutron LF helicity states can be represented as a bilinear form in LF bispinors

$$\langle n(p_n, \lambda_n')|\mathcal{O}|n(p_n, \lambda_n)\rangle = \bar{u}_{\mathrm{LF}}(p_n, \lambda_n')\, \Gamma u_{\mathrm{LF}}(p_n, \lambda_n), \tag{4.2}$$

where $\Gamma$ is a matrix in bispinor indices whose form depends on the operator. The covariant neutron spin density matrix in the deuteron is defined as

$$\Pi_n \equiv \sum_{\lambda_n, \lambda_n'} \rho_n(\lambda_n, \lambda_n') u_{\mathrm{LF}}(p_n, \lambda_n) \bar{u}_{\mathrm{LF}}(p_n, \lambda_n'). \tag{4.3}$$

The average over the neutron LF helicities can then be computed as

$$\sum_{\lambda_n, \lambda_n'} \rho_n(p_p|\lambda_n, \lambda_n')\, \langle n(p_n, \lambda_n')|\mathcal{O}|n(p_n, \lambda_n)\rangle = \mathrm{tr}[\Pi_n \Gamma]. \tag{4.4}$$

The neutron density matrix $\rho_n$, Eq. (4.1b), arises as an average over the deuteron spin ensemble and depends linearly on the vector and tensor polarization parameters. Its covariant representation $\Pi_n$, Eq. (4.3), can be expressed as the sum of an unpolarized, vector-polarized, and tensor-polarized term,

$$\Pi_n = \tfrac{1}{2}(\not{p}_n + m)(u_n + \not{s}_n \gamma^5 + t_n), \tag{4.5}$$

where $\gamma^5 \equiv -i\gamma^0\gamma^1\gamma^2\gamma^3$ in our convention. The construction is described in Ref. [18]; here we only state the results. The expressions take a simple form when written in terms of the deuteron wave function in the $pn$ c.m. frame (see Sec. III C). The scalar functions $u_n$ and $t_n$ are obtained as [here $f_{0,2} \equiv f_{0,2}(k)$]

$$u_n = f_0^2 + f_2^2, \tag{4.6a}$$

$$t_n = -\frac{3\,\boldsymbol{k}\cdot T_D\cdot\boldsymbol{k}}{|\boldsymbol{k}|^2}\left(2f_0+\frac{f_2}{\sqrt{2}}\right)\frac{f_2}{\sqrt{2}}, \tag{4.6b}$$

where $T_D$ is the three-tensor describing the tensor polarization in the deuteron rest frame, Eq. (2.27). These functions have the same value in any collinear frame; the relation between the c.m. momentum $\boldsymbol{k}$ and the LF momentum variables $\alpha_p$ and $\boldsymbol{p}_{pT}$ is given in Eq. (3.20). Of the four-vector function $s_n$ in Eq. (4.5), the ordinary vector components in the c.m. frame are obtained as

$$s_n[\text{c.m.}] = \left(s_n^0, \boldsymbol{s}_n\right), \tag{4.7a}$$

$$s_n^0 = -\frac{\boldsymbol{S}_D\cdot\boldsymbol{k}}{m}\left(f_0-\frac{f_2}{\sqrt{2}}\right)^2, \tag{4.7b}$$

$$\boldsymbol{s}_n = \left(f_0-\frac{f_2}{\sqrt{2}}\right)\left[\frac{(\boldsymbol{S}_D\cdot\boldsymbol{k})\boldsymbol{k}}{|\boldsymbol{k}|^2}\,\frac{E}{m}\left(f_0-\frac{f_2}{\sqrt{2}}\right) + \left(\boldsymbol{S}_D-\frac{(\boldsymbol{S}_D\cdot\boldsymbol{k})\boldsymbol{k}}{|\boldsymbol{k}|^2}\right)(f_0+\sqrt{2}f_2)\right], \tag{4.7c}$$

where $\boldsymbol{S}_D$ is the three-vector describing the vector polarization in the deuteron rest frame, Eq. (2.26). The LF components of $s_n$ in an arbitrary collinear frame are then obtained by forming the LF plus and minus components in the c.m. frame, $(s^0 \pm s^3)$ [c.m.], and performing a boost to the desired value of $p_D^+$, see Eq. (2.10), with the boost parameter given by $p_D^+/p_D^+$ [c.m.] $= p_D^+/M_{pn} = p_D^+/(2E)$, resulting in

$$s_n^+ = \frac{p_D^+}{2E}\left(s_n^0+s_n^3\right)\text{ [c.m.]}, \tag{4.8a}$$

$$s_n^- = \frac{2E}{p_D^+}\left(s_n^0-s_n^3\right)\text{ [c.m.]}, \tag{4.8b}$$

$$\boldsymbol{s}_{nT} = \boldsymbol{s}_{nT}\text{ [c.m.]}. \tag{4.8c}$$

It is worth emphasizing that the deuteron polarization parameters appearing in Eqs. (4.6b) and (4.7) are the polarization three-tensor and three-vector in the deuteron rest frame (see Sec. II D). The c.m. frame expressions of the neutron density have been derived by importing the deuteron polarization from the rest frame, using the fact that both frames are in the class of collinear frames, where boosts can be performed in a simple manner (see Sec. II B) [18]. The representation in terms of c.m. frame variables thus describes the LF spin structure very efficiently, expressing the neutron LF helicity distribution in any collinear frame in terms of the deuteron rest frame polarization parameters.

### B. Neutron momentum distributions

From the neutron spin density matrix one can derive the distributions of neutrons with a given spin projection in the deuteron with proton tagging. These distributions depend on the deuteron polarization, the tagged proton momentum, and the neutron spin projections, and exhibit rich structure. They can be used to present the IA result for the tagged cross section and its decomposition in structure functions in a compact form, exhibiting the connection with the nucleon spin structure functions.

TABLE I. Spin matrices used in the definition of the spin-projected neutron distributions, Eqs. (4.9) and (4.11). Upper rows: Distributions of unpolarized, longitudinally polarized, and transversely polarized neutrons. Lower rows: Distributions in pure spin states with projection $\pm 1/2$ along the longitudinal axis or a transverse axis set by the vector $\boldsymbol{n}$.

| $a$ | $\Gamma$ | Symbol | Name |
|---|---|---|---|
| 1 | $\gamma^+ \,/\, p_n^+$ | $U$ | Unpolarized |
| $\sigma^3$ | $-\gamma^+\gamma_5 \,/\, p_n^+$ | $S_L$ | Longitud. polarized |
| $\sigma^i$ (i = 1,2) | $i\sigma^{i+}\gamma_5 \,/\, p_n^+$ | $S_T$ | Transv. polarized |
| $\frac{1}{2}(1\pm\sigma^3)$ | | $L\pm$ | $\pm 1/2$ longitud. |
| $\frac{1}{2}(1\pm\boldsymbol{n}_T\cdot\boldsymbol{\sigma})$ | | $T\pm$ | $\pm 1/2$ transv. $\boldsymbol{n}_{\rm T}$ |

We define the spin-projected distribution of neutrons in proton tagging as

$$\begin{aligned} &P(\alpha_p, \boldsymbol{p}_{pT}|\boldsymbol{S}_D, T_D) \\ &\equiv \frac{1}{2-\alpha_p}\sum_{\lambda_n,\lambda_n'} a(\lambda_n',\lambda_n)\rho_n(\alpha_p,\boldsymbol{p}_{pT};\lambda_n,\lambda_n'|\boldsymbol{S}_D,T_D) \\ &= \frac{1}{2-\alpha_p}\sum_{\lambda_n,\lambda_n'} a(\lambda_n',\lambda_n)\sum_{\lambda_D,\lambda_D'}\rho_D(\lambda_D,\lambda_D'|\boldsymbol{S}_D,T_D) \\ &\quad\times\sum_{\lambda_p}\Psi_D^*(\alpha_p,\boldsymbol{p}_{pT};\lambda_p,\lambda_n'|\lambda_D')\Psi_D(\alpha_p,\boldsymbol{p}_{pT};\lambda_p,\lambda_n|\lambda_D), \end{aligned} \tag{4.9}$$

where $\rho_n$ is the neutron spin density matrix Eq. (4.1b) and $a(\lambda_n',\lambda_n)$ is a matrix in the neutron LF helicities. We have explicitly indicated the dependence on the deuteron rest-frame polarization three-vector and tensor, $\boldsymbol{S}_D$ and $T_D$. It is convenient to evaluate the neutron spin projection using the covariant representation of the density matrix Eq. (4.3). Writing the matrix $a$ as a bilinear form in LF bispinors as in Eq. (4.2),

$$a(\lambda_n',\lambda_n) = \bar{u}(p_n,\lambda_n')\,\Gamma\,u(p_n,\lambda_n), \tag{4.10}$$

the average Eq. (4.9) is computed using Eq. (4.4),

$$P(\alpha_p,\boldsymbol{p}_{pT}|\boldsymbol{S}_D,T_D) = \frac{\text{tr}[\Pi_n\Gamma]}{2-\alpha_p}. \tag{4.11}$$

The spin matrices used in the present study are summarized in Table I.[3] They describe the unpolarized, longitudinally polarized, and transversely polarized distributions of neutrons, as

[3]The form of the bispinor matrices $\Gamma$ is not unique. They are contracted with on-shell bispinors satisfying the Dirac equation and can be modified by terms that vanish due to the Dirac equation. The form in Table I are the standard projectors used in partonic structure in QCD.

well as the probabilistic distributions of neutrons in states with a defined longitudinal or transverse spin projection $\pm 1/2$. These distributions are analogous to the leading-twist quark parton distributions in a hadron and provide a complete characterization of the one-body LF momentum distributions in a system with spin-1/2 constituents. We use the notation

$$P_{[\text{neutron}]}(\alpha_p, \boldsymbol{p}_{pT} | \boldsymbol{S}_D, T_D)$$
$$\text{neutron} = U, S_L, S_T \tag{4.12}$$

to denote the neutron spin projection in the distribution. The neutron distributions here depend on the deuteron polarization parameters $\boldsymbol{S}_D$ and $T_D$ and refer to a general mixed polarization state; normalized distributions in particular deuteron spin states will be defined in Secs. IV C and IV D.

The neutron distributions defined here are functions of the tagged proton LF momentum variables $\alpha_p$ and $\boldsymbol{p}_{pT}$ and are to be integrated as

$$\int \frac{d\alpha_p}{\alpha_p} d^2 p_{pT} P(\alpha_p, \boldsymbol{p}_{pT}). \tag{4.13}$$

When the deuteron LF wave function is expressed in terms of the c.m. wave function, the neutron densities are obtained as functions of the c.m. momentum variable $\boldsymbol{k}$, related to $\alpha_p$ and $\boldsymbol{p}_{pT}$ by Eq. (3.20). In the c.m. frame one can also consider a neutron distribution $N(\boldsymbol{k})$ defined as

$$P(\alpha_p, \boldsymbol{p}_{pT}) = \frac{N(\boldsymbol{k})}{2 - \alpha_p}, \tag{4.14}$$

which differs from the distribution $P$ by the flux factor $1/(2-\alpha_p)$. The distribution $N(\boldsymbol{k})$ corresponds to the three-dimensional particle density of the c.m. frame wave function and is to be integrated as [see Eq. (3.21)]

$$\int \frac{d^3k}{E(k)} N(\boldsymbol{k}). \tag{4.15}$$

The unpolarized neutron projection of $N(\boldsymbol{k})$ exhibits three-dimensional rotational symmetry (see below); in the longitudinally and transversely polarized projections the rotational symmetry is broken only by the Melosh rotations [see Eq. (3.22)]. The neutron distribution in tagged DIS can be described either by the LF distribution $P$ or the c.m. momentum distribution $N$. The distribution $P$ is identical to the spectral function as defined in Refs. [9,17] and appears in the tagged cross section differential in the phase space element Eq. (2.15). In the following we quote the expressions for $P$; the expressions for $N$ are obtained simply by stripping away the factor $1/(2-\alpha_p)$, see Eq. (4.14).

The functions introduced in Eqs. (4.9) and (4.11) describe the neutron distribution in a general mixed polarization state of the deuteron, characterized by the rest-frame polarization three-vector and three-tensor, $\boldsymbol{S}_D$ and $T_D$. It is useful to define normalized distributions corresponding to unit polarization along given directions, i.e., distributions corresponding to unit values of the scalar parameters $S_L, S_T$ and $T_{LL}, T_{LT}, T_{TT}$. These normalized distributions can then be multiplied by the scalar parameters and combined to obtain the distributions in the general polarization state. This enables easy calculation of the tagged DIS cross section and produces simple expressions of the tagged structure functions (see Sec. V). We use the notation

$$P_{[\text{deuteron,neutron}]}(\alpha_p, \boldsymbol{p}_{pT}),$$
$$\text{deuteron} = U, S_L, S_T, T_{LL}, T_{LT}, T_{TT}, \tag{4.16}$$
$$\text{neutron} = U, S_L, S_T,$$

where "deuteron" characterizes the deuteron polarization, and "neutron" characterizes the neutron polarization as in Eq. (4.12) and Table I. The normalized neutron distributions are analogous to the unpolarized and polarized parton densities defined for hadron states with unit polarization. In the following, we compute the normalized neutron distributions needed for tagged DIS and discuss their properties.

### C. Unpolarized neutron distributions

The distribution of unpolarized neutrons obtained from Eq. (4.11) with the density matrix Eq. (4.5) and the projector in Table I is

$$\begin{aligned} P_{[U]}(\alpha_p, \boldsymbol{p}_{pT} | T_D) &\equiv \frac{\text{tr}[\Pi_n \gamma^+]}{(2-\alpha_p)^2\, p_D^+} \\ &= \frac{f_0^2 + f_2^2}{2-\alpha_p} - \frac{3}{2-\alpha_p} \frac{\boldsymbol{k} \cdot T_D \cdot \boldsymbol{k}}{|\boldsymbol{k}|^2} \\ &\quad \times \left(2 f_0 + \frac{f_2}{\sqrt{2}}\right) \frac{f_2}{\sqrt{2}}. \end{aligned} \tag{4.17}$$

With respect to deuteron polarization, it contains a term independent of the deuteron polarization and a term proportional to the polarization tensor $T_D$, but no term involving the polarization vector $\boldsymbol{S}_D$. For the unpolarized deuteron, we define the normalized distribution in the notation of Eq. (4.16) as

$$P_{[U,U]}(\alpha_p, \boldsymbol{p}_{pT}) \equiv \frac{f_0^2 + f_2^2}{2-\alpha_p}. \tag{4.18}$$

For the tensor-polarized deuteron, we define normalized distributions corresponding to the three-dimensional spherical tensors in the expansion of the rest-frame polarization tensor, Eq. (2.27).

$$\begin{aligned} &\left.\begin{matrix} P_{[T_{LL},U]} \\ P_{[T_{LT},U]} \\ P_{[T_{TT},U]} \end{matrix}\right\} (\alpha_p, \boldsymbol{p}_{pT}) \\ &\quad \equiv \begin{Bmatrix} P_{[U]}(T_D = e_{LL}) \\ P_{[U]}(T_D = e_{LT}) \\ P_{[U]}(T_D = e_{TT}) \end{Bmatrix} \\ &\quad = -\frac{3}{2-\alpha_p} \left(2 f_0 + \frac{f_2}{\sqrt{2}}\right) \frac{f_2}{\sqrt{2}} \begin{Bmatrix} \frac{\boldsymbol{k} \cdot e_{LL} \cdot \boldsymbol{k}}{|\boldsymbol{k}|^2} \\ \frac{\boldsymbol{k} \cdot e_{LT} \cdot \boldsymbol{k}}{|\boldsymbol{k}|^2} \\ \frac{\boldsymbol{k} \cdot e_{TT} \cdot \boldsymbol{k}}{|\boldsymbol{k}|^2} \end{Bmatrix}. \end{aligned} \tag{4.19}$$

The three distributions have the same dependence on the radial wave functions, as they arise from projections of the same rotationally covariant structure in Eq. (4.17). They are proportional to the $D$ wave radial function $f_2$, showing that the deuteron tensor polarization can influence the neutron distribution only through the $L = 2$ state in the orbital motion. The angular dependence is governed by the contraction of the

spherical basis tensors with the vector $\boldsymbol{k}$. Using the explicit expressions in Part I [1], Eq. (3.24), we obtain

$$\frac{\boldsymbol{k}\cdot e_{LL}\cdot\boldsymbol{k}}{|\boldsymbol{k}|^2} = \frac{1}{\sqrt{6}}\left(\frac{3(k^z)^2}{|\boldsymbol{k}|^2}-1\right) = \frac{1}{\sqrt{6}}(3\cos^2\theta_k - 1)$$
$$= \sqrt{\frac{2\cdot 4\pi}{3\cdot 5}}Y_{20}(\theta_k,\phi_k=0), \tag{4.20a}$$

$$\frac{\boldsymbol{k}\cdot e_{LT}\cdot\boldsymbol{k}}{|\boldsymbol{k}|^2} = \sqrt{2}\frac{k^z|\boldsymbol{k}_T|}{|\boldsymbol{k}|^2} = \sqrt{2}\cos\theta_k\sin\theta_k$$
$$= \sqrt{\frac{2\cdot 4\pi}{3\cdot 5}}\frac{1}{\sqrt{2}}[-Y_{21}+Y_{2-1}](\theta_k,\phi_k=0), \tag{4.20b}$$

$$\frac{\boldsymbol{k}\cdot e_{TT}\cdot\boldsymbol{k}}{|\boldsymbol{k}|^2} = \frac{1}{\sqrt{2}}\frac{|\boldsymbol{k}_T|^2}{|\boldsymbol{k}|^2} = \frac{1}{\sqrt{2}}\sin^2\theta_k$$
$$= \sqrt{\frac{2\cdot 4\pi}{3\cdot 5}}\frac{1}{\sqrt{2}}[Y_{22}+Y_{2-2}](\theta_k,\phi_k=0). \tag{4.20c}$$

The polar angle of the vector $\boldsymbol{k}$ in the $x'y'z$ coordinate system is defined as

$$\cos\theta_k \equiv \boldsymbol{e}_z\cdot\boldsymbol{k}, \quad \sin\theta_k \equiv \boldsymbol{e}_{x'}\cdot\boldsymbol{k}; \tag{4.21}$$

the azimuthal angle is zero, $\phi_k = 0$, because the $x'$ axis is chosen along the direction of $\boldsymbol{k}_T \equiv \boldsymbol{p}_{pT}$; see Eq. (2.25) and Part I [1], Fig. 1. The contractions of the spherical tensors $e_{LT'}$ and $e_{TT'}$ with $\boldsymbol{k}$ are zero; these components of the deuteron tensor polarization therefore do not influence the neutron momentum distribution.

In terms of the normalized distributions, the unpolarized neutron distribution in a deuteron with general tensor polarization, Eq. (4.17), can be expressed as

$$P_{[U]}(\alpha_p,\boldsymbol{p}_{pT}|T_D)$$
$$= P_{[U,U]}(\alpha_p,\boldsymbol{p}_{pT}) + \sqrt{\frac{3}{2}}\,T_{LL}\,P_{[T_{LL},U]}(\alpha_p,\boldsymbol{p}_{pT})$$
$$+ \sqrt{2}\,T_{LT}\,\cos(\phi_p-\phi_{T_L})\,P_{[T_{LT},U]}(\alpha_p,\boldsymbol{p}_{pT})$$
$$+ \frac{1}{\sqrt{2}}\,T_{TT}\,\cos(2\phi_p-2\phi_{T_T})\,P_{[T_{TT},U]}(\alpha_p,\boldsymbol{p}_{pT}), \tag{4.22}$$

where we have used the expansion of $T_D$ in the basis tensors, Eq. (2.27). Equation (4.22) shows the explicit dependence of the neutron distributions on the deuteron tensor polarization parameters and can be used in the calculation of tagged scattering observables.

The integral of the unpolarized neutron distribution Eq. (4.18) is

$$\int_0^2 \frac{d\alpha_p}{\alpha_p}\,d^2p_{pT}\,P_{[U,U]}(\alpha_p,\boldsymbol{p}_{pT}) = \int\frac{d^3k}{E}\,\left(f_0^2+f_2^2\right) = 1, \tag{4.23}$$

because of the normalization condition of the deuteron wave function [Eq. (3.23)]. Furthermore,

$$\int_0^2 \frac{d\alpha_p}{\alpha_p}\,d^2p_{pT}\,(2-\alpha_p)P_{[U,U]}(\alpha_p,\boldsymbol{p}_{pT})$$
$$= \int\frac{d^3k}{E}\left(1-\frac{k^z}{E}\right)\left(f_0^2+f_2^2\right) = 1, \tag{4.24}$$

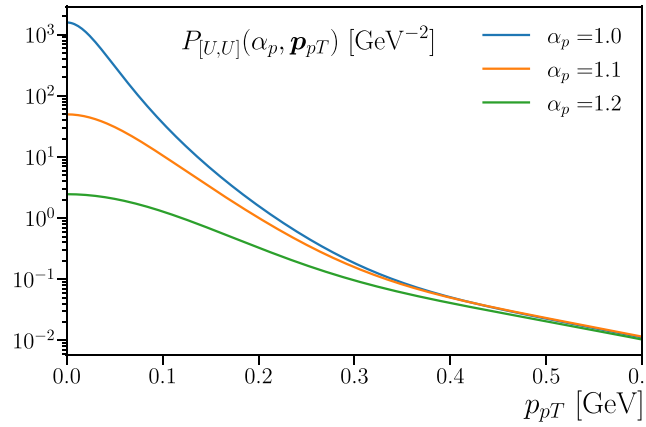



FIG. 3. The distribution of unpolarized neutrons in the unpolarized deuteron, $P_{[U,U]}$, Eq. (4.18), as a function of the tagged proton transverse momentum $p_{pT}$, for several values of the longitudinal momentum fraction $\alpha_p$.

because the term $\propto k^z$ integrates due to rotational symmetry (the relation can also be derived using the symmetry of the deuteron LF wave function under $\alpha_p \to 2-\alpha_p$). The integrals of the tensor-polarized distributions Eq. (4.19) are zero,

$$\int_0^2 \frac{d\alpha_p}{\alpha_p}\,d^2p_{pT}\,P_{[T_{LL},U]}(\alpha_p,\boldsymbol{p}_{pT}) = 0, \tag{4.25a}$$

$$\int_0^2 \frac{d\alpha_p}{\alpha_p}\,d^2p_{pT}\,(2-\alpha_p)P_{[T_{LL},U]}(\alpha_p,\boldsymbol{p}_{pT}) = 0$$
$$\text{(same for } T_{LT},\ T_{TT}\text{)}, \tag{4.25b}$$

because the polarization tensor is traceless ($L=2$) and cannot produce any scalars. Equations (4.23) and (4.24) express the baryon number and LF momentum sum rule at the nucleon level and play an essential role in the applications to DIS. The fact that both sum rules are realized is an achievement of LF quantization and the implementation of rotational symmetry through the c.m. frame formulation. Equation (4.25) guarantees that the sum rules hold in a deuteron state with arbitrary tensor polarization.

Numerical distributions are obtained by evaluating the expressions with models of the radial wave functions $f_{0,2}(k)$. We use the nonrelativistic approximation Eq. (3.24) and the nonrelativistic radial wave functions obtained from empirical $NN$ interactions. All distributions shown in the following are computed with the AV18 radial wave functions [70]; the nuclear model dependence is investigated in Sec. VI D.

Figure 3 shows the distribution of unpolarized neutrons in the unpolarized deuteron, $P_{[U,U]}$, as a function of $p_{pT} \equiv |\boldsymbol{p}_{pT}|$ for several values of $\alpha_p$. The dependence on the variables is determined by the way in which $p_{pT}$ and $\alpha_p$ combine to form the c.m. momentum $k$, Eq. (3.20), and by the behavior of the radial wave functions. One observes: (i) $P_{[U,U]}$ is maximal at $\alpha_p = 1$ and $p_{pT} = 0$, where $k = 0$. The distribution decreases with growing $|\alpha_p - 1|$ or $p_{pT}$. (ii) The bulk of the strength is at values $|\alpha_p - 1| \leqslant 0.2$; $p_{pT} \leqslant 0.3$ GeV. (iii) The effective dependence on $\alpha_p$ at fixed $p_{pT}$ changes with the value of $p_{pT}$, and vice versa. At small $p_{pT} \leqslant 0.1$ GeV, $P_{[U,U]}$ decreases

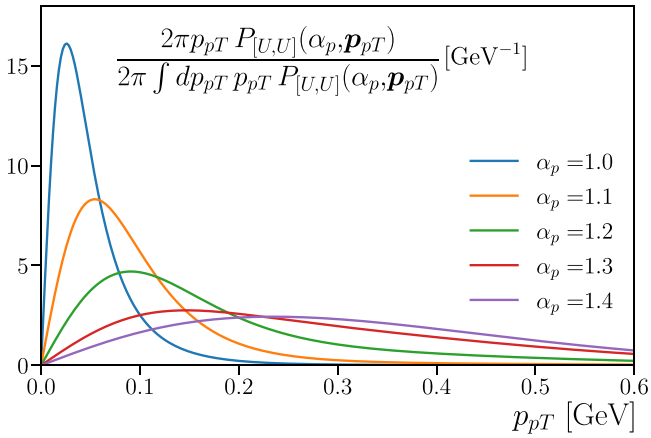



FIG. 4. Same as Fig. 3, but showing the distributions multiplied by the phase-space factor $2\pi p_{pT}$, and divided by the integral over $p_{pT}$ (normalized radial distributions in $p_{pT}$).

roughly by an order of magnitude if $|\alpha_p - 1|$ is increased by 0.1. At large $p_{pT} \gtrsim 0.5$ GeV, $P_{[U,U]}$ decreases much more slowly in $|\alpha_p - 1|$.

Figure 4 shows the radial distributions in transverse momentum, $2\pi p_{pT} P_{[U,U]}$, as functions of $p_{pT}$ for fixed values of $\alpha_p$. The functions are divided by the integral $2\pi \int dp_{pT}\, p_{pT} P_{[U,U]} = \int d^2 p_{pT} P_{[U,U]}$ and represent the normalized $p_{pT}$ distributions at the given value of $\alpha_p$. One observes that the shape of the normalized $p_{pT}$ distributions strongly changes with $\alpha_p$. For $\alpha_p$ close to 1, the distribution has a strong peak at a $p_{pT}$ value below 0.1 GeV and a long tail at larger $p_{pT}$. For larger values of $\alpha_p$ the strength of the distribution diffuses to larger values of $p_{pT}$, with a peak at larger values of $p_{pT}$ and a greatly increased width.

Figure 5 shows the distributions of unpolarized neutrons in the unpolarized and tensor-polarized deuteron, $P_{[U,U]}$ and $P_{[T_{LL},U]}$, $P_{[T_{LT},U]}$, $P_{[T_{TT},U]}$, as functions of $\alpha_p$ and $p_{pT}$. The scales on the axes are such that the longitudinal and transverse 3-momentum of the proton in the deuteron rest frame are represented in (approximately) the same graphical units, such that the plot conveys an image of the shape of the distribution in physical 3-momentum in the deuteron rest frame. One observes the following: (i) $P_{[U,U]}$ is positive and strongly centered around $\alpha_p = 1$ and $p_{pT} = 0$ (see also Fig. 3). The distribution is approximately spherical in the proton 3-momentum; the small deviations from spherical shape are relativistic effects caused by the use of LF momentum variables. (ii) $P_{[T_{LL},U]}$, $P_{[T_{LT},U]}$ and $P_{[T_{TT},U]}$ take positive and negative values. They are numerically smaller than $P_{[U,U]}$ at $\alpha_p \approx 1$ and $p_{pT} \approx 0$ but become comparable at values $|\alpha_p - 1| \gtrsim 0.2$ and/or $p_{pT} \gtrsim 0.2$ GeV, where the $D$ wave becomes large. All three tensor-polarized distributions have a node from the $(2f_0 + f_2/\sqrt{2})$ factor, see Eq. (4.19). (iii) The angular dependence is governed by the polar angle dependence of the spherical harmonics in Eq. (4.20) and exhibits a quadrupole pattern. These features are expressed in the tagged DIS observables (see Sec. VI) and can be tested experimentally.

### D. Polarized neutron distributions

The longitudinally polarized neutron distribution obtained from Eq. (4.11) with the density matrix Eq. (4.5) and the

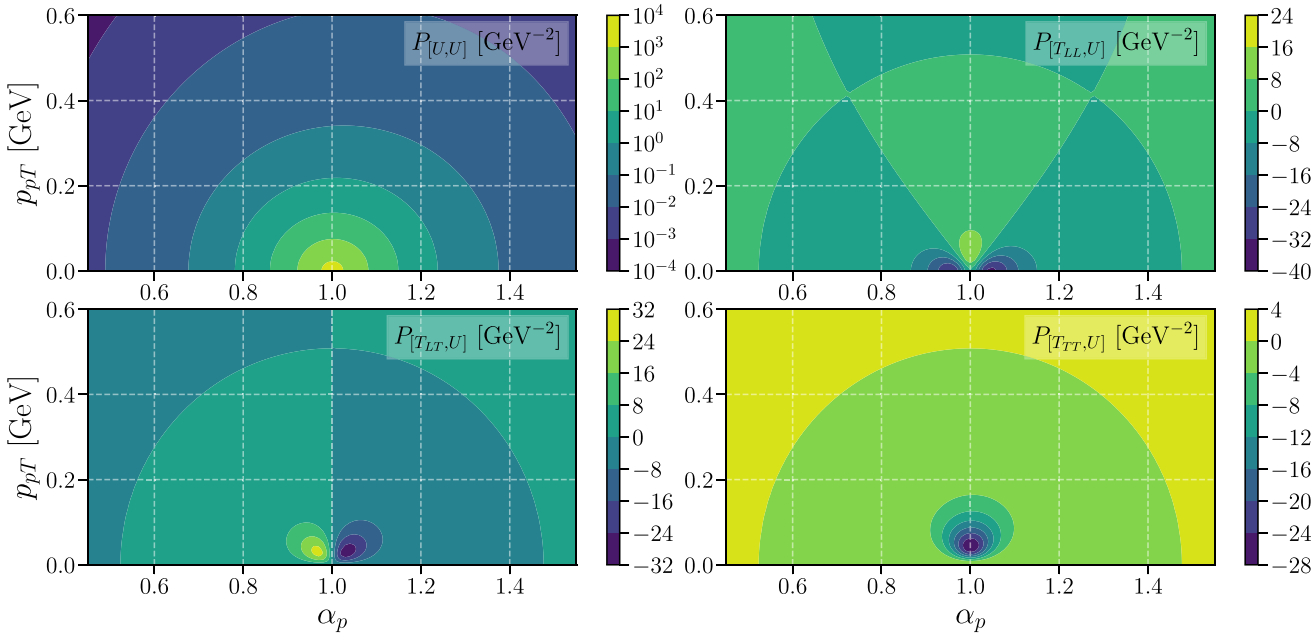



FIG. 5. The distributions of unpolarized neutrons in the unpolarized and tensor-polarized deuteron, Eqs. (4.18) and (4.19), as functions of $\alpha_p$ and $p_{pT}$. The upper-left panel shows the distribution in the unpolarized deuteron, $P_{[U,U]}$, and the upper-right panel shows the $T_{LL}$ tensor-polarized deuteron, $P_{[T_{LL},U]}$. The lower-left panel shows the $T_{LT}$ tensor-polarized deuteron, $P_{[T_{LT},U]}$. The lower-right panel shows the $T_{TT}$ tensor-polarized deuteron, $P_{[T_{TT},U]}$.

projector in Table I is

$$P_{[S_L]}(\alpha_p, \boldsymbol{p}_{pT}|\boldsymbol{S}_D) \equiv \frac{\mathrm{tr}[\Pi_n(-\gamma^+\gamma^5)]}{(2-\alpha_p)^2\ p_D^+} = \frac{2ms_n^+}{(2-\alpha_p)^2 p_D^+}. \tag{4.26}$$

Due to the presence of $\gamma^5$, only the term proportional to the polarization four-vector $s_n$ in the density matrix Eq. (4.5) contributes. Using the explicit expressions of $s_n$ in the c.m. frame, Eq. (4.7), we obtain

$$P_{[S_L]}(\alpha_p, \boldsymbol{p}_{pT}|\boldsymbol{S}_D) = \frac{1}{2-\alpha_p}\left(f_0 - \frac{f_2}{\sqrt{2}}\right)\left[A\left(f_0 - \frac{f_2}{\sqrt{2}}\right) + B(f_0 + \sqrt{2}f_2)\right], \tag{4.27a}$$

$$A = S_D^z - \frac{E(E+k^z)|\boldsymbol{k}_T|^2}{(m^2+|\boldsymbol{k}_T|^2)|\boldsymbol{k}|^2} S_D^z + \frac{(E+k^z)[-|\boldsymbol{k}|^2 + Ek^z]}{(m^2+|\boldsymbol{k}_T|^2)|\boldsymbol{k}|^2}\boldsymbol{S}_{DT}\cdot\boldsymbol{k}_T, \tag{4.27b}$$

$$B = \frac{m(E+k^z)|\boldsymbol{k}_T|^2}{(m^2+|\boldsymbol{k}_T|^2)|\boldsymbol{k}|^2} S_D^z - \frac{mk^z(E+k^z)}{(m^2+|\boldsymbol{k}_T|^2)|\boldsymbol{k}|^2}\boldsymbol{S}_{DT}\cdot\boldsymbol{k}_T. \tag{4.27c}$$

At zero transverse nucleon momentum,

$$A(\boldsymbol{k}_T = 0) = S_D^z, \quad B(\boldsymbol{k}_T = 0) = 0. \tag{4.28}$$

The deviations from these values for $\boldsymbol{k}_T \neq 0$ are due to the relativistic spin effects in LF quantization (Melosh rotations).

With respect to the deuteron polarization, the distribution Eq. (4.27) depends only on the polarization vector $\boldsymbol{S}_D$. As such, it contains terms proportional to the longitudinal and transverse vector polarization in the collinear frame. We define normalized distributions in the longitudinally and transversely polarized deuteron by choosing $\boldsymbol{S}_D$ as the unit vectors Eq. (2.25) (with $\boldsymbol{p}_{pT} \equiv \boldsymbol{k}_T$),

$$\boldsymbol{e}_z, \quad \boldsymbol{e}_{x'} = \boldsymbol{k}_T/|\boldsymbol{k}_T|, \quad \boldsymbol{e}_{y'} = \boldsymbol{e}_z \times \boldsymbol{e}_{x'}. \tag{4.29}$$

We define

$$P_{[S_L,S_L]}(\alpha_p, \boldsymbol{p}_{pT}) \equiv P_{[S_L]}(\boldsymbol{S}_D = \boldsymbol{e}_z) = \frac{1}{2-\alpha_p}\left(f_0 - \frac{f_2}{\sqrt{2}}\right)\left[A_{[=]}\left(f_0 - \frac{f_2}{\sqrt{2}}\right) + B_{[=]}(f_0 + \sqrt{2}f_2)\right], \tag{4.30a}$$

$$A_{[=]} \equiv 1 - \frac{E(E+k^z)|\boldsymbol{k}_T|^2}{(m^2+|\boldsymbol{k}_T|^2)|\boldsymbol{k}|^2}, \tag{4.30b}$$

$$B_{[=]} \equiv \frac{m(E+k^z)|\boldsymbol{k}_T|^2}{(m^2+|\boldsymbol{k}_T|^2)|\boldsymbol{k}|^2}, \tag{4.30c}$$

and

$$P_{[S_T,S_L]}(\alpha_p, \boldsymbol{p}_{pT}) \equiv P_{[S_L]}(\boldsymbol{S}_D = \boldsymbol{e}_{x'}) = \frac{1}{2-\alpha_p}\left(f_0 - \frac{f_2}{\sqrt{2}}\right)\left[A_{[\neq]}\left(f_0 - \frac{f_2}{\sqrt{2}}\right) - B_{[\neq]}(f_0 + \sqrt{2}f_2)\right], \tag{4.31a}$$

$$A_{[\neq]} \equiv \frac{(E+k^z)[-|\boldsymbol{k}|^2 + Ek^z]|\boldsymbol{k}_T|}{(m^2+|\boldsymbol{k}_T|^2)|\boldsymbol{k}|^2}, \tag{4.31b}$$

$$B_{[\neq]} \equiv \frac{mk^z(E+k^z)|\boldsymbol{k}_T|}{(m^2+|\boldsymbol{k}_T|^2)|\boldsymbol{k}|^2}. \tag{4.31c}$$

At $\boldsymbol{k}_T = 0$, the coefficients become

$$A_{[=]}(\boldsymbol{k}_T = 0) = 1, \quad B_{[=]}(\boldsymbol{k}_T = 0) = 0, \tag{4.32a}$$

$$A_{[\neq]}(\boldsymbol{k}_T = 0) = 0, \quad B_{[\neq]}(\boldsymbol{k}_T = 0) = 0. \tag{4.32b}$$

Equation (4.30) describes the distribution of longitudinally polarized neutrons in a longitudinally polarized deuteron. This distribution would also be present in a nonrelativistic system and is nonzero at $\boldsymbol{k}_T = 0$. Equation (4.31) describes the distribution of longitudinally polarized neutrons in a transversely polarized deuteron. This distribution arises from relativistic spin effects in the LF formulation and vanishes at $\boldsymbol{k}_T = 0$. We refer to the two functions as the "favored" and "unfavored" distributions. The terms will be explained further when comparing the longitudinally and transversely polarized distributions.

The distribution of transversely polarized neutrons obtained from Eq. (4.11) with the density matrix Eq. (4.5) and the projector in Table I is

$$P^i_{[S_T]}(\alpha_p, \boldsymbol{p}_{pT}|\boldsymbol{S}_D) \equiv \frac{\mathrm{tr}[\Pi_n(i\sigma^{+i}\gamma^5)]}{(2-\alpha_p)^2\ p_D^+} = \frac{2\left(p_n^+ s_n^i - s_n^+ p_n^i\right)}{(2-\alpha_p)^2 p_D^+}. \tag{4.33}$$

As in the distribution of longitudinally polarized neutrons, only the term proportional to the polarization four-vector $s_n$ in the neutron density matrix contributes. With the explicit expression of $s_n$ in the c.m. frame, Eq. (4.7), we obtain

$$\boldsymbol{P}_{[S_T]}(\alpha_p, \boldsymbol{p}_{pT}|\boldsymbol{S}_D) = \frac{1}{2-\alpha_p}\left(f_0 - \frac{f_2}{\sqrt{2}}\right)\left[\boldsymbol{A}_T(f_0+\sqrt{2}f_2) + \boldsymbol{B}_T\left(f_0 - \frac{f_2}{\sqrt{2}}\right)\right], \tag{4.34a}$$

$$\boldsymbol{A}_T \equiv \boldsymbol{S}_{DT} - \frac{E(E+k^z)\boldsymbol{k}_T}{(m^2+|\boldsymbol{k}_T|^2)|\boldsymbol{k}|^2}\,\boldsymbol{S}_{DT}\cdot\boldsymbol{k}_T - \frac{(E+k^z)[-|\boldsymbol{k}|^2 + Ek^z]\boldsymbol{k}_T}{(m^2+|\boldsymbol{k}_T|^2)|\boldsymbol{k}|^2}\,S_D^z, \tag{4.34b}$$

$$\boldsymbol{B}_T \equiv \frac{m(E+k^z)\boldsymbol{k}_T}{(m^2+|\boldsymbol{k}_T|^2)|\boldsymbol{k}|^2}\,\boldsymbol{S}_{DT}\cdot\boldsymbol{k}_T + \frac{mk^z(E+k^z)\boldsymbol{k}_T}{(m^2+|\boldsymbol{k}_T|^2)|\boldsymbol{k}|^2}\,S_D^z. \tag{4.34c}$$

At zero transverse nucleon momentum,

$$\boldsymbol{A}_T(\boldsymbol{k}_T=0) = \boldsymbol{S}_{DT}, \quad \boldsymbol{B}_T(\boldsymbol{k}_T=0) = 0. \tag{4.35}$$

With respect to deuteron polarization, Eq. (4.34) contains terms proportional to the longitudinal and transverse vector polarization in the collinear frame. The transverse neutron polarization described by the direction of $\boldsymbol{P}_{[S_T]}$ has terms proportional to $\boldsymbol{k}_T$ and to $\boldsymbol{S}_{DT}$. We define normalized distributions corresponding to deuteron and neutron polarizations along the transverse unit vectors $\boldsymbol{e}_{x'}$ and $\boldsymbol{e}_{y'}$, Eq. (4.29). For transverse deuteron polarization,

$$P^{\parallel}_{[S_T,S_T]} \equiv \boldsymbol{e}_{x'}\cdot\boldsymbol{P}_{[S_T]}(\boldsymbol{S}_D=\boldsymbol{e}_{x'}) = \frac{1}{2-\alpha_p}\left(f_0 - \frac{f_2}{\sqrt{2}}\right)\left[A_{[=]}(f_0+\sqrt{2}f_2) + B_{[=]}\left(f_0 - \frac{f_2}{\sqrt{2}}\right)\right], \tag{4.36a}$$

$$P^{\perp}_{[S_T,S_T]} \equiv \boldsymbol{e}_{y'}\cdot\boldsymbol{P}_{[S_T]}(\boldsymbol{S}_D=\boldsymbol{e}_{y'}) = \frac{1}{2-\alpha_p}\left(f_0 - \frac{f_2}{\sqrt{2}}\right)(f_0+\sqrt{2}f_2). \tag{4.36b}$$

The other projections are zero,

$$\boldsymbol{e}_{y'}\cdot\boldsymbol{P}_{[S_T]}(\boldsymbol{S}_D=\boldsymbol{e}_{x'}) = 0, \tag{4.37a}$$

$$\boldsymbol{e}_{x'}\cdot\boldsymbol{P}_{[S_T]}(\boldsymbol{S}_D=\boldsymbol{e}_{y'}) = 0. \tag{4.37b}$$

For longitudinal deuteron polarization,

$$P_{[S_L,S_T]} \equiv \boldsymbol{e}_{x'}\cdot\boldsymbol{P}_{[S_T]}(\boldsymbol{S}_D=\boldsymbol{e}_z) = \frac{1}{2-\alpha_p}\left(f_0 - \frac{f_2}{\sqrt{2}}\right)\left[-A_{[\neq]}(f_0+\sqrt{2}f_2) + B_{[\neq]}\left(f_0 - \frac{f_2}{\sqrt{2}}\right)\right], \tag{4.38a}$$

$$\boldsymbol{e}_{y'}\cdot\boldsymbol{P}_{[S_T]}(\boldsymbol{S}_D=\boldsymbol{e}_z) = 0. \tag{4.38b}$$

The functions $A_{[=]}$, $B_{[=]}$ and $A_{[\neq]}$, $B_{[\neq]}$ in Eqs. (4.36) and (4.38) are those defined in Eqs. (4.30) and (4.31) and thus the same as in the helicity-dependent distributions.

In terms of the normalized distributions, the distributions of longitudinally and transversely polarized neutrons in a deuteron with general vector polarization, Eqs. (4.27) and (4.34), can be expressed as

$$P_{[S_L]}(\alpha_p, \boldsymbol{p}_{pT}|\boldsymbol{S}_D) = S_D^z P_{[S_L,S_L]}(\alpha_p, \boldsymbol{p}_{pT}) + |\boldsymbol{S}_{DT}|\cos(\phi_p-\phi_S)P_{[S_T,S_L]}(\alpha_p, \boldsymbol{p}_{pT}), \tag{4.39a}$$

$$\begin{aligned}\boldsymbol{P}_{[S_T]}(\alpha_p, \boldsymbol{p}_{pT}|\boldsymbol{S}_D) = {}& |\boldsymbol{S}_{DT}|\big[\cos(\phi_p-\phi_S)P^{\parallel}_{[S_T,S_T]}(\alpha_p, \boldsymbol{p}_{pT})\boldsymbol{e}_{x'} + \sin(\phi_p-\phi_S)P^{\perp}_{[S_T,S_T]}(\alpha_p, \boldsymbol{p}_{pT})\boldsymbol{e}_{y'}\big] \\ & + S_D^z P_{[S_L,S_T]}(\alpha_p, \boldsymbol{p}_{pT})\boldsymbol{e}_{x'},\end{aligned} \tag{4.39b}$$

where we have used the expansion of $\boldsymbol{S}_D$ in the basis vectors, Eq. (2.26). Equations (4.39) show the explicit dependence of the neutron distributions on the deuteron vector polarization parameters and can be used in the calculation of tagged scattering observables.

The integrals of the polarized neutron distributions over the tagged proton momentum describe the fraction of the deuteron spin carried by the neutron spin degrees of freedom in LF quantization ("spin sum rules"). The integrals can be computed as integrals over the c.m. momentum variable as in Eqs. (4.23) and (4.24), in which rotational invariance is manifest and an expansion in $k/m$ can be performed (see Appendix). For the longitudinally polarized neutron distributions we obtain

$$\int_0^2 \frac{d\alpha_p}{\alpha_p}\,d^2p_{pT}\,P_{[S_L,S_L]}(\alpha_p, \boldsymbol{p}_{pT}) = 1 - \frac{3}{2}\omega_2, \tag{4.40a}$$

$$\int_0^2 \frac{d\alpha_p}{\alpha_p}\,d^2p_{pT}\,P_{[S_T,S_L]}(\alpha_p, \boldsymbol{p}_{pT}) = \varepsilon_{[S_L]}. \tag{4.40b}$$

Here $\omega_2$ is the $D$-state probability of the deuteron wave function in the c.m. frame, given by the integral of $f_2^2$, Eq. (A7). $\varepsilon_{[S_L]}$ is an integral of a quadratic form in $f_0$ and $f_2$, weighted by $k/m$, Eq. (A12) (so-called relativistic correction). For the

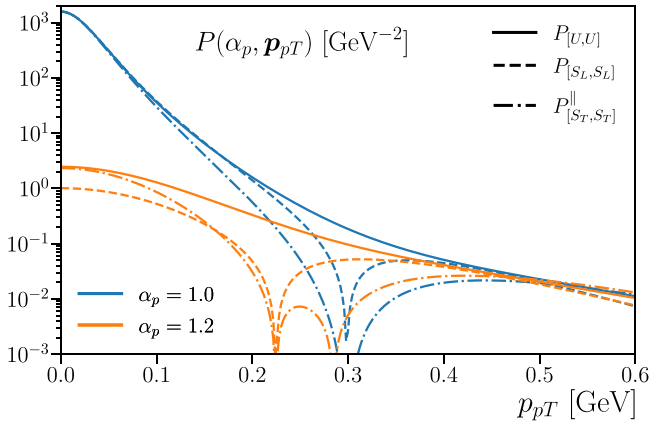



FIG. 6. Comparison of the distribution of unpolarized neutrons, $P_{[U,U]}$, Eq. (4.18), and the favored distributions of longitudinally and transversely polarized neutrons, $P_{[S_L,S_L]}$ and $P^{\parallel}_{[S_T,S_T]}$, Eqs. (4.30) and (4.36). The distributions are shown as functions of $p_{pT}$ for two values of $\alpha_p$.

transversely polarized neutron distributions we obtain

$$\int_0^2 \frac{d\alpha_p}{\alpha_p}\, d^2p_{pT} P^{\parallel}_{[S_T,S_T]}(\alpha_p, \boldsymbol{p}_{pT}) = 1 - \delta^{\parallel}, \quad \text{(4.41a)}$$

$$\int_0^2 \frac{d\alpha_p}{\alpha_p}\, d^2p_{pT} P^{\perp}_{[S_T,S_T]}(\alpha_p, \boldsymbol{p}_{pT}) = 1 - \delta^{\perp}, \quad \text{(4.41b)}$$

$$\int_0^2 \frac{d\alpha_p}{\alpha_p}\, d^2p_{pT} P_{[S_L,S_T]}(\alpha_p, \boldsymbol{p}_{pT}) = \varepsilon_{[S_T]}. \quad \text{(4.41c)}$$

Here, $\delta^{\parallel}$ and $\delta^{\perp}$ are integrals of terms $f_0 f_2$ and $f_2^2$ (linear and quadratic in the $D$ wave), Eqs. (A21) and (A23). $\varepsilon_{[S_T]}$ is the relativistic correction integral Eq. (A29), of similar form as $\varepsilon_{[S_L]}$. The numerical values of the integrals are summarized in Table III.

One observes the following: (i) The favored polarized neutron distributions (neutron polarization and deuteron spin along same axis) integrate to unity up to depolarization corrections resulting from the $D$ wave of the deuteron wave function, see Eqs. (4.40a), (4.41a), and (4.41b). It shows the preservation of spin when the deuteron state is expanded in $pn$ states. (ii) The unfavored distributions (neutron polarization and deuteron spin along different axes) integrate to zero, up to relativistic corrections, see Eqs. (4.40b) and (4.41c). It shows that some conversion of net transverse to longitudinal polarization (and vice versa) happens because of the preferred direction in LF quantization.

The results for the integrals of the polarized neutron distributions are obtained thanks to the manifest realization of three-dimensional rotational invariance in the c.m. frame representation of the LF wave function. They are essential for ensuring the sum rules for the tagged spin structure functions in the IA (see Sec. V D).

Numerical distributions of the polarized neutrons are obtained using the same setup as in the unpolarized case. We want to compare the unpolarized and polarized, and the favored and unfavored distributions.

Figure 6 compares the unpolarized neutron distribution $P_{[U,U]}$ with the favored distributions of longitudinally and transversely polarized neutrons, $P_{[S_L,S_L]}$ and $P^{\parallel}_{[S_T,S_T]}$. For $\alpha_p = 1$ and $p_{pT} \leqslant 0.1$ GeV, the deuteron $S$ wave dominates and there are very small depolarization effects. Basically any deuteron polarization is transferred to the nucleon, independent of the deuteron state, and all three distributions consequently coincide. For larger internal deuteron momenta ($\alpha_p$ away from 1 or $p_{pT} \gtrsim 0.2$ GeV), the $D$ wave dominates and there is significant depolarization. In this region the favored helicity-dependent distributions are suppressed relative to $P_{[U,U]}$ and have a node for momenta where $f_0(k) = f_2(k)/\sqrt{2}$, which is around $k \approx 0.3$ GeV.

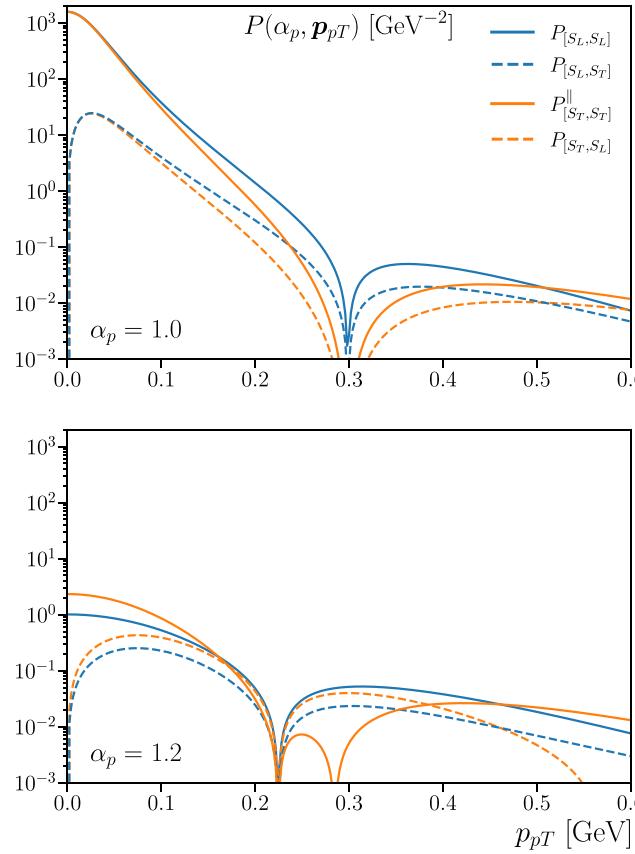



FIG. 7. Comparison of the favored and unfavored polarized neutron distributions in the longitudinally polarized deuteron, $P_{[S_L,S_L]}$ and $P_{[S_L,S_T]}$, and in the transversely polarized deuteron, $P^{\parallel}_{[S_T,S_T]}$ and $P_{[S_T,S_L]}$. The distributions are plotted as functions of $p_{pT}$ for fixed values of $\alpha_p$. Upper panel: $\alpha_p = 1.0$. Lower panel: $\alpha_p = 1.2$. Both panels use the same vertical axis scale to facilitate comparison of the magnitude of the functions.

Figure 7 compares the favored and unfavored polarized distributions for all four combinations of deuteron and neutron polarization: $P_{[S_L,S_L]}$, $P_{[S_L,S_T]}$ (deuteron longitudinal, neutron longitudinal or transverse), and $P^{\parallel}_{[S_T,S_T]}$, $P_{[S_T,S_L]}$ (deuteron transverse, neutron transverse or longitudinal). As observed in Fig. 6, all the polarized distributions have a node for momenta where $f_0(k) = f_2(k)/\sqrt{2}$. A second node can appear (see examples in the bottom panel of Fig. 7) for momenta where the factor containing $A_{[=]}, B_{[=]}$ (or $A_{[\neq]}, B_{[\neq]}$) goes to zero. For all momenta away from those nodes, the unfavored

distributions are significantly suppressed relative to the favored distributions with the same deuteron polarization.

Overall, the results of this section show a remarkable similarity of the longitudinally and transversely polarized distributions of neutrons in the deuteron, when comparing favored with favored and unfavored with unfavored distributions. It appears even though the distributions refer to LF momentum and spin variables and include relativistic effects and spin rotations. The similarity is realized because: (i) the construction of the LF wave function in the c.m. frame implements three-dimensional rotational invariance; (ii) relativistic effects in the deuteron are moderate up to momenta of a few 100 MeV.

### E. Probabilistic distributions

The neutron distributions discussed so far correspond to definite types of neutron polarization (unpolarized, longitudinally polarized, transversely polarized) and deuteron polarization (unpolarized, vector, tensor). It is interesting to study the distributions describing the probability to find a neutron with spin projection along a given axis in a deuteron state with given polarization state. These probabilistic distributions are positive and bounded and have a simple interpretation. They illustrate how the internal structure of the deuteron "polarizes" or "depolarizes" the nucleons depending on the nuclear configuration selected by the spectator momentum.

The spin matrices defining the neutron distributions in states with spin projection $\pm 1/2$ along the longitudinal or a transverse axis are given in Table I (bottom rows). In the transverse case the spin matrix depends on the transverse unit vector $\boldsymbol{n}_T$ specifying the quantization axis. In the convention of Eq. (4.16), we denote the probabilistic distributions as

$$\begin{aligned} &P_{[\text{neutron}]}(\alpha_p, \boldsymbol{p}_{pT} | \boldsymbol{S}_D, T_D), \\ &\text{neutron} = L\pm,\ T\pm\,. \end{aligned} \tag{4.42}$$

The probabilistic distributions are linear combinations of the unpolarized and longitudinally or transversely polarized neutron distributions defined in Eqs. (4.17), (4.27), and (4.34),

$$\begin{aligned} &P_{[L\pm]}(\alpha_p, \boldsymbol{p}_{pT} | \boldsymbol{S}_D, T_D) \\ &\quad = \tfrac{1}{2}\big[P_{[U]} \pm P_{[S_L]}\big](\alpha_p, \boldsymbol{p}_{pT} | \boldsymbol{S}_D, T_D), \qquad (4.43a) \\ &P_{[T\pm]}(\alpha_p, \boldsymbol{p}_{pT} | \boldsymbol{S}_D, T_D) \\ &\quad = \tfrac{1}{2}\big[P_{[U]} \pm \boldsymbol{n}_T \cdot \boldsymbol{P}_{[S_T]}\big](\alpha_p, \boldsymbol{p}_{pT} | \boldsymbol{S}_D, T_D). \qquad (4.43b) \end{aligned}$$

Equations (4.43) describe the probabilistic neutron distributions in a deuteron with a general (mixed) polarization state characterized by the polarization parameters $\boldsymbol{S}_D$ and $T_D$.

For a pure deuteron spin state, with spin projection $\Lambda = (+1, 0, -1)$ along an axis described by the unit vector $\boldsymbol{N}$ in the deuteron rest frame, the polarization parameters $\boldsymbol{S}_D$ and $T_D$ are given by Eqs. (2.28) *et seq*. Evaluating Eq. (4.43) with these expressions, we can compute the probabilistic neutron distributions in a pure deuteron spin state. They depend on the deuteron spin direction, the neutron spin direction, and the tagged proton momentum, and exhibit a rich structure. We consider the following situations:

(1) Neutron spin longitudinal, or transverse along the proton transverse momentum direction ($\boldsymbol{n}_T = \boldsymbol{e}_{x'}$), with spin projections $\pm 1/2$;
(2) Deuteron polarization longitudinal ($\boldsymbol{N} = \boldsymbol{e}_z$), or transverse along the proton transverse momentum direction ($\boldsymbol{N} = \boldsymbol{e}_{x'}$), with spin projections $\pm 1$.

We denote these distributions by

$$\begin{aligned} &P_{[\text{deuteron,neutron}]}(\alpha_p, \boldsymbol{p}_{pT}), \\ &\text{deuteron} = L\pm,\ T\pm, \\ &\text{neutron} = L\pm,\ T\pm\,. \end{aligned} \tag{4.44}$$

We evaluate the distributions using the definitions Eq. (4.43), the values of the deuteron polarization parameters in Eqs. (2.29)–(2.33), and the expressions of the distributions $P_{[U]}$, $P_{[S_L]}$, $\boldsymbol{P}_{[S_T]}$ in Eqs. (4.22) and (4.39). The result is expressed in terms of the normalized distributions introduced in Secs. IV C and IV D.

The probabilistic distributions of neutrons with longitudinal spin $\pm 1/2$ in a deuteron state with longitudinal spin $+1$, or with transverse spin $+1$ (along the proton transverse momentum $\boldsymbol{p}_{pT}$), are obtained as

$$\begin{aligned} &P_{[L+,L\pm]}(\alpha_p, \boldsymbol{p}_{pT}) \\ &\quad = \frac{1}{2}\bigg[P_{[U,U]} + \frac{1}{\sqrt{6}} P_{[T_{LL},U]} \pm P_{[S_L,S_L]}\bigg](\alpha_p, \boldsymbol{p}_{pT}), \qquad (4.45a) \\ &P_{[T+,L\pm]}(\alpha_p, \boldsymbol{p}_{pT}) \\ &\quad = \frac{1}{2}\bigg[P_{[U,U]} - \frac{1}{2\sqrt{6}} P_{[T_{LL},U]} + \frac{1}{2\sqrt{2}} P_{[T_{TT},U]} \\ &\qquad \pm P_{[S_T,S_L]}\bigg](\alpha_p, \boldsymbol{p}_{pT}). \qquad (4.45b) \end{aligned}$$

The corresponding distributions in the deuteron states with longitudinal or transverse spin projections $-1$ are given by

$$P_{[L-,L\pm]} = P_{[L+,L\mp]}, \quad P_{[T-,L\pm]} = P_{[T+,L\mp]}, \tag{4.46a}$$

as follows from the fact that the neutron spin-dependent distributions Eq. (4.27) are proportional to the deuteron polarization vector and change sign when the deuteron polarization is reversed.

The probabilistic distributions of neutrons with transverse spin $\pm 1/2$ in a deuteron state with transverse spin $+1$ (both along the proton transverse momentum $\boldsymbol{p}_{pT}$), or with longitudinal spin $+1$, are obtained as

$$\begin{aligned} &P_{[T+,T\pm]}(\alpha_p, \boldsymbol{p}_{pT}) \\ &\quad = \frac{1}{2}\bigg[P_{[U,U]} - \frac{1}{2\sqrt{6}} P_{[T_{LL},U]} + \frac{1}{2\sqrt{2}} P_{[T_{TT},U]} \\ &\qquad \pm P^{\parallel}_{[S_T,S_T]}\bigg](\alpha_p, \boldsymbol{p}_{pT}), \qquad (4.47a) \\ &P_{[L+,T\pm]}(\alpha_p, \boldsymbol{p}_{pT}) \\ &\quad = \frac{1}{2}\bigg[P_{[U,U]} + \frac{1}{\sqrt{6}} P_{[U,T_{LL}]} \pm P_{[S_L,S_T]}\bigg](\alpha_p, \boldsymbol{p}_{pT}). \qquad (4.47b) \end{aligned}$$

The corresponding distributions in the deuteron spin states with spin projections $-1$ are obtained from relations analogous to Eq. (4.46).

The distributions obtained in Eqs. (4.45) and (4.47) are positive (as can be verified by explicit computation) and can be interpreted as the number densities of neutrons with a given spin projection in a deuteron with given spin projection. The distributions in which the directions of the neutron and deuteron spins are the same (both longitudinal or both transverse), Eqs. (4.45a) and (4.47a), involve the favored polarized distributions $P_{[S_L,S_L]}$ and $P_{[S_T,S_T]}$, Eqs. (4.30) and (4.36). The distributions in which the directions of the neutron and deuteron polarization are the different (one longitudinal, one transverse), Eqs. (4.45b) and (4.47b), involve the unfavored polarized distributions $P_{[S_T,S_L]}$ and $P_{[S_L,S_T]}$, Eqs. (4.31) and (4.38).

From the distributions Eqs. (4.45) and (4.47) we can form the ratios

$$R_{[L+,L+]} \equiv \frac{P_{[L+,L+]}}{P_{[L+,L+]} + P_{[L+,L-]}}, \tag{4.48a}$$

$$R_{[T+,L+]} \equiv \frac{P_{[T+,L+]}}{P_{[T+,L+]} + P_{[T+,L-]}}, \tag{4.48b}$$

and

$$R_{[T+,T+]} \equiv \frac{P_{[T+,T+]}}{P_{[T+,T+]} + P_{[T+,T-]}}, \tag{4.49a}$$

$$R_{[L+,T+]} \equiv \frac{P_{[L+,T+]}}{P_{[L+,T+]} + P_{[L+,T-]}}. \tag{4.49b}$$

The ratios in Eq. (4.48) describe the probability for the neutron to be in the $+1/2$ longitudinal spin state in a deuteron polarized in the longitudinal or transverse direction, as a function of the tagged proton LF momentum. Those in Eq. (4.49) describe the same probability for the neutron to be in the $+1/2$ transverse spin state in a deuteron polarized in the transverse or longitudinal direction. The ratios are bounded by $[0, 1]$ (because of the positivity of the pure-state distributions) and can be interpreted as probabilities. Eqs. (4.48a) and (4.49a), where the direction of polarization of the deuteron and neutron are the same, describe the polarization transfer from the deuteron to the nucleon, as determined by the orbital motion and its angular momentum. Equations (4.48b) and (4.49b), where the direction of polarization of the deuteron and neutron are different, describe the effective polarization perpendicular to the deuteron spin as induced by the orbital motion. The corresponding ratios with the $-1/2$ neutron spin state in the numerator are obtained as

$$R_{[L+,L-]} \equiv \frac{P_{[L+,L-]}}{P_{[L+,L+]} + P_{[L+,L-]}} = 1 - R_{[L+,L+]}, \tag{4.50}$$

etc. and describe the complementary probability for the neutron to be polarized in the "opposite" direction.

Note that, in the ratios of Eqs. (4.48) and (4.49), the denominators are defined as the sums of the neutron spin distributions in a deuteron with pure polarization state $+1$ (longitudinal or transverse). They are not the same as the distributions in the unpolarized deuteron because they contain some degree of tensor polarization, see Eqs. (4.45) and (4.47).

Figure 8 shows the neutron polarization probabilities as functions of the tagged proton LF momentum variables $\alpha_p$ and $p_{pT} \equiv |\boldsymbol{p}_{pT}|$. The left column shows the neutron $L+$ polarization probabilities in the $L+$ and $T+$ polarized deuteron, Eq. (4.48); the right column shows the neutron $T+$ probabilities in the $L+$ and $T+$ polarized deuteron. The probabilities exhibit a complex dependence on the tagged proton momentum, which controls the $D/S$ wave ratio in the deuteron wave function and thus the effective neutron polarization. One observes the following:

(1) At proton momenta with $0.8 < \alpha_p < 1.2$ and $p_{pT} < 0.2$ GeV the neutron is almost completely polarized along the deuteron spin direction, in both the longitudinally and transversely polarized deuteron. Such LF momenta correspond to c.m. momenta $|\boldsymbol{k}| \lesssim 0.2$ GeV, where the $S$ wave dominates. The $[L+, L+]$ (upper left) and $[T+, T+]$ (lower right) probabilities show an effective neutron polarization $\approx 1$. The $[L+, T+]$ (lower left) and $[T+, L+]$ (upper right) probabilities have values $\approx 1/2$, showing the 50-50 probability for the neutron to be polarized in either direction along the axis perpendicular to the deuteron spin direction.

(2) At proton momenta with $\alpha_p < 0.7$ or $> 1.3$, or at $p_{pT} > 0.3$ GeV, the $D$ wave becomes prominent and causes significant depolarization of the neutron. The $[L+, L+]$ probability (upper left) becomes zero at $p_{pT} \approx 0.5$ GeV and $\alpha_p \approx 1$, showing that the neutron is polarized opposite to the direction of the deuteron spin. These LF momenta correspond to c.m. momenta $|\boldsymbol{k}| \approx 0.5$ GeV, where the $S$ wave has a node and the $D$ wave dominates. Likewise, the $[T+, T+]$ probability (lower right) becomes zero for $\alpha_p \approx 0.5$ or 1.5 and $p_{pT} \approx 0$. The $[L+, T+]$ (lower left) and $[T+, L+]$ (upper right) probabilities again have values $\approx 1/2$ in these regions.

(3) Some interesting effects of the LF spin structure can be seen in the probabilities at zero transverse momentum, $p_{pT} = 0$. The $[L+, L+]$ probability (upper left) at $p_{pT} = 0$ remains exactly 1 for all values of $\alpha_p$. This happens because the LF spin structure causes the $D$ wave to vanish at $p_{pT} = 0$. Using the explicit expressions of the distributions in Eqs. (4.45) and in Eqs. (4.18), (4.19), and (4.30), we obtain

$$R_{[L+,L+]}(\alpha_p, \boldsymbol{p}_{pT} = 0) = 1 \quad (\alpha_{\rm p} \text{ arbitrary}). \tag{4.51}$$

In contrast, the $[T+, T+]$ probability (lower right) at $p_{pT} = 0$ changes as $\alpha_p$ moves away from unity. Using the expressions in Eqs. (4.47), and Eqs. (4.18), (4.19), and (4.36), we find

$$R_{[T+,T+]}(\alpha_p, \boldsymbol{p}_{pT} = 0) = 1 - \frac{\frac{9}{8} f_2^2}{\left(f_0 + \frac{1}{2\sqrt{2}} f_2\right)^2 + \frac{9}{8} f_2^2}, \tag{4.52}$$

which shows that the probability decreases proportionally to the square of the $D$ wave as $\alpha_p$ moves away from unity. Nonzero $(1 - \alpha_p)$ implies $p_p^z \neq 0$, where for a transversely polarized deuteron the $D$ wave

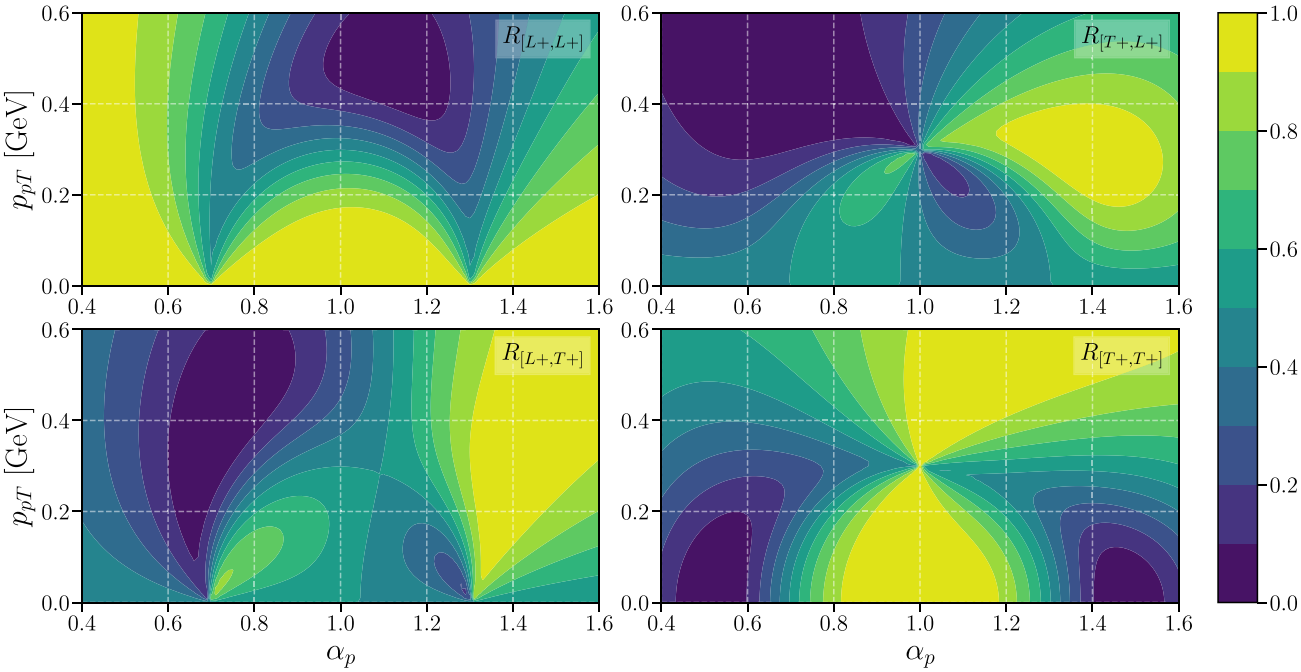



FIG. 8. The neutron polarization probabilities in spectator tagging with a polarized deuteron (pure spin states with projections $\pm 1$, longitudinal or transverse), Eqs. (4.48) and (4.49), as functions of the tagged proton LF momentum variables $\alpha_p$ and $p_{pT} \equiv |\boldsymbol{p}_{pT}|$. The left/right column shows the longitudinal (transverse) deuteron polarization. The upper/lower row shows the longitudinal (transverse) neutron spin.

still contributes to the depolarization of the neutron. The $[L+, T+]$ (lower left) and $[T+, L+]$ (upper right) probabilities both attain values 1/2 at $p_{pT} = 0$,

$$R_{[T+,L+]}(\alpha_p, \boldsymbol{p}_{pT} = 0) = \tfrac{1}{2}, \tag{4.53a}$$

$$R_{[L+,T+]}(\alpha_p, \boldsymbol{p}_{pT} = 0) = \tfrac{1}{2}, \tag{4.53b}$$

which shows that, in these configurations, the deuteron polarization causes equal neutron polarization along either direction of the perpendicular axis.

(4) All four plots show an approximately semicircular arc (centered at $\alpha_p = 1$, $p_{pT} = 0$, with a radius of $p_{pT} \approx 0.3$ GeV or $\Delta\alpha_p \approx 0.3$), where all ratios take the value $R = 1/2$, and there is no net neutron polarization regardless of the deuteron polarization state. This corresponds to the node in the spin-dependent distributions caused by the vanishing of the factor $(f_0 - f_2/\sqrt{2})$ at $k \approx 0.3$ GeV, discussed in Sec. IV D and shown in Figs. 6 and 7.

(5) A striking spin-orbit effect is observed in the $[L+, T+]$ (lower left) and $[T+, L+]$ (upper right) probabilities. Both probabilities attain values of approximately 1 at $\alpha_p \gtrsim 1.3$ and $p_{pT} \gtrsim 0.3$ GeV, corresponding to complete neutron polarization "sideways" to the deuteron spin. The effect is caused by the entanglement of spin and orbital angular momentum in the deuteron wave function and the selection of configurations by the tagged proton momentum. In the particular kinematics here, the proton momentum has an angle of approximately 45° relative to the $z$ axis and thus lies "between" the direction of the deuteron spin and the neutron spin.

The spin and spin-orbit effects described here can be observed in high-energy electron-deuteron scattering with proton tagging, if the elementary electron-neutron scattering process exhibits a dependence on the neutron spin. This can be realized in quasi-elastic electron scattering (electric vs magnetic neutron current) or in deep-inelastic scattering (spin dependence of neutron structure functions).

The probabilistic distributions of neutrons in a pure deuteron spin state with projection $\Lambda = 0$ along a given axis can be studied in analogy to those in the $\Lambda = \pm 1$ states. In the $\Lambda = 0$ state the vector polarization is absent, $\boldsymbol{S}_D = 0$, see Eqs. (2.28), and only the unpolarized neutron distribution $P_{[U]}$ in Eq. (4.43) is active. The probabilistic distributions therefore do not depend on the neutron spin, longitudinal or transverse. However, the distributions do depend on the angle of the proton momentum relative to the deuteron spin-quantization axis, because tensor polarization is present in the $\Lambda = 0$ state, see Eqs. (2.28).

## V. TAGGED DIS STRUCTURE FUNCTIONS

### A. Unpolarized electron

We now derive the explicit expressions of the structure functions of the polarized tagged DIS cross section. The general decomposition of the cross section in independent structures and notation for the structure functions are described in Part I [1], Sec. IV. The particular kinematic

variables and phase space elements used in tagged DIS on the deuteron are described in Sec. II of the present article.

The structure functions are derived from the master formula for the hadronic tensor in the IA, Eq. (3.38), obtained in the LFQM formulation of the scattering process in Sec. III B. The summation over the neutron LF helicities is performed using the spin density matrix representation Eq. (4.1) developed in Sec. IV A. The expressions of the structure functions are obtained by taking suitable components of the IA hadronic tensor Eq. (3.38) $(++, TT, +T)$ and matching them with the general decomposition in terms of structure functions. The IA results for the tagged structure functions are expressed in terms of the momentum- and spin-dependent neutron distributions introduced in Secs. IV B–IV D, providing a compact and transparent representation.

The calculations are performed in the DIS limit

$$Q \gg \text{mass}, \tag{5.1}$$

where the generic mass scale includes the scale governing power corrections to the nucleon structure functions in DIS,

$$\text{mass} \sim xm, \tag{5.2}$$

and the scales arising from the longitudinal and transverse motion of the nucleons in the deuteron

$$\text{mass} \sim (1-\alpha_p)m,\ |\boldsymbol{p}_{pT}|. \tag{5.3}$$

Power corrections will be denoted simply as $O(1/Q)$, without indicating the mass scale governing the corrections; in most cases, the origin of the mass scale will be clear; if necessary, it will be given explicitly. In kinematic variables that have a finite value in the DIS limit, power corrections $O(1/Q)$ to that value are neglected. The structure functions are computed to leading power accuracy. In the structure functions that are $Q^2$-independent in the DIS limit ("leading-twist" in the terminology of QCD factorization), power corrections $O(1/Q)$ are neglected. The power-suppressed structure functions ("higher-twist") are evaluated to leading nonzero power accuracy where possible.

The symmetric and antisymmetric parts of the hadronic tensor in Eq. (4.1) are

$$W^{\mu\nu} = \tfrac{1}{2}W^{\{\mu\nu\}} + \tfrac{1}{2}W^{[\mu\nu]}, \tag{5.4}$$

$$W^{\{\mu\nu\}}, W^{[\mu\nu]} \equiv W^{\mu\nu} \pm W^{\nu\mu}, \tag{5.5}$$

and give rise to the lepton-unpolarized and lepton-polarized structure functions, see Part I [1], Sec. IV. We first compute the lepton-unpolarized structure functions. The symmetric part of the neutron hadronic tensor is diagonal in the neutron LF helicity and independent of the value of the helicity,[4]

$$W_n^{\{\mu\nu\}}(p_n, \widetilde{q}; \lambda_n', \lambda_n) = \delta(\lambda_n', \lambda_n)\, W_n^{\{\mu\nu\}}(p_n, \widetilde{q}). \tag{5.6}$$

The decomposition of the symmetric neutron tensor is[5]

$$\tfrac{1}{2}W_n^{\{\mu\nu\}} = \tfrac{1}{2}\left(e_L^\mu e_L^\nu - e_q^\mu e_q^\nu - g^{\mu\nu}\right) F_{[UU,T]n} + \tfrac{1}{2}e_L^\mu e_L^\nu\, F_{[UU,L]n}, \tag{5.7}$$

where the basis vectors $e_L$ and $e_q$ are as defined in Part I [1], Eq. (2.6), but constructed with the neutron 4-momentum $p_n$ and the effective 4-momentum transfer $\widetilde{q}$, Eqs. (3.29) and (3.35). [The decomposition in Eq. (5.7) has the same form as the $\phi$-independent part of the unpolarized deuteron tensor in Part I [1], Eq. (4.20).] The neutron structure functions in Eq. (5.7) depend on the invariants formed with $p_n$ and $\widetilde{q}$. The effective invariant momentum transfer in the electron-neutron–scattering process is given by Eq. (3.42),

$$-\widetilde{q}^2 = Q^2[1 + O(1/Q^2)]. \tag{5.8}$$

The effective scaling variable is

$$x_n \equiv \frac{-\widetilde{q}^2}{2\, p_n \cdot \widetilde{q}} = \frac{x}{2-\alpha_p}[1 + O(1/Q^2)]; \tag{5.9}$$

its value is determined by the longitudinal LF momentum of the neutron, as fixed by the tagged proton LF momentum. The neutron structure functions $F_{[UU,T]n}$ and $F_{[UU,L]n}$ in Eq. (5.7) relate to the commonly used structure functions $F_{1n}$ and $F_{2n}$ as

$$F_{1n} = \tfrac{1}{2}F_{[UU,T]n}, \tag{5.10a}$$

$$F_{2n} = x_n(F_{[UU,T]n} + F_{[UU,L]n}), \tag{5.10b}$$

where the coefficients are given up to terms $O(1/Q^2)$.

The neutron tensor is averaged over the neutron LF helicities in Eq. (4.1). Because the symmetric neutron tensor is independent of the neutron LF helicity, the result for the symmetric deuteron tensor involves only the unpolarized neutron distributions. We obtain

$$\frac{1}{2}\langle W_D^{\{\mu\nu\}}\rangle(p_D, q, p_p) = \frac{2[2(2\pi)^3]}{2-\alpha_p} P_{[U]}(\alpha_p, \boldsymbol{p}_{pT}|T_D)\frac{1}{2}W_n^{\{\mu\nu\}}(p_n, \widetilde{q}), \tag{5.11}$$

where $P_{[U]}$ is the unpolarized neutron distribution Eq. (4.17). With respect to deuteron polarization, $P_{[U]}$ contains an unpolarized and a tensor-polarized part, but no vector-polarized part, so for unpolarized electron scattering, only unpolarized deuteron and tensor-polarized deuteron structures appear. Expressions for the individual structure functions are obtained by equating the IA result of Eqs. (5.11) and (5.7) to the general decomposition of the spin-1 semi-inclusive scattering tensor in Part I [1], Eq. (4.20), and taking suitable components of the tensor equation. The calculation is straightforward; an explicit demonstration of the steps is given in Ref. [9], Appendix B. For the unpolarized deuteron structure functions,

[4]We neglect the transverse spin dependence of the unpolarized nucleon tensor due to two-photon exchange effects [71,72].

[5]Neutron and deuteron structure functions are distinguished by adding square brackets and an $n, D$ index to the notation used in Part I [1], i.e., $F_{[UU,T]n}$, $F_{[UU,T]D}$, etc.

we obtain

$$F_{[UU,T]D}(x,Q^2;\alpha_p,\boldsymbol{p}_{pT}) = \frac{2[2(2\pi)^3]}{2-\alpha_p} P_{[U,U]}(\alpha_p,\boldsymbol{p}_{pT})\, F_{[UU,T]n}(x_n,Q^2), \tag{5.12a}$$

$$F_{[UU,L]D}(x,Q^2;\alpha_p,\boldsymbol{p}_{pT}) = \frac{2[2(2\pi)^3]}{2-\alpha_p} P_{[U,U]}(\alpha_p,\boldsymbol{p}_{pT})\, F_{[UU,L]n}(x_n,Q^2), \tag{5.12b}$$

$$\begin{aligned} F^{\cos\phi_p}_{[UU]D}(x,Q^2;\alpha_p,\boldsymbol{p}_{pT}) &= \frac{2[2(2\pi)^3]}{2-\alpha_p} P_{[U,U]}(\alpha_p,\boldsymbol{p}_{pT}) \frac{2x_n|\boldsymbol{p}_{pT}|}{Q} [F_{[UU,T]n} + F_{[UU,L]n}](x_n,Q^2) \\ &= \frac{2[2(2\pi)^3]}{2-\alpha_p} P_{[U,U]}(\alpha_p,\boldsymbol{p}_{pT}) \frac{2|\boldsymbol{p}_{pT}|}{Q} F_{2n}(x_n,Q^2), \end{aligned} \tag{5.12c}$$

$$\begin{aligned} F^{\cos 2\phi_p}_{[UU]D}(x,Q^2;\alpha_p,\boldsymbol{p}_{pT}) &= \frac{2[2(2\pi)^3]}{2-\alpha_p} P_{[U,U]}(\alpha_p,\boldsymbol{p}_{pT}) \frac{2x_n^2|\boldsymbol{p}_{pT}|^2}{Q^2} [F_{[UU,T]n} + F_{[UU,L]n}](x_n,Q^2) \\ &= \frac{2[2(2\pi)^3]}{2-\alpha_p} P_{[U,U]}(\alpha_p,\boldsymbol{p}_{pT}) \frac{2x_n|\boldsymbol{p}_{pT}|^2}{Q^2} F_{2n}(x_n,Q^2), \end{aligned} \tag{5.12d}$$

where $P_{[U,U]}$ is the unpolarized neutron distribution in the unpolarized distribution, Eq. (4.18). Equation (5.12) represents the invariant structure functions of tagged DIS on the deuteron in terms of products of the neutron LF momentum distribution in the deuteron and the ordinary neutron DIS structure functions and embodies the "factorization" of nuclear and hadronic structure. The factor

$$2 \times 1/(2-\alpha_p) \tag{5.13}$$

results from the relation between the neutron and deuteron tensors and ensures the proper sum rules and compositeness relations for the nuclear structure functions (see below).

For the tensor-polarized structure functions, we separate the contributions corresponding to $T_{LL}$, $T_{LT}$ and $T_{TT}$ tensor polarization as described in Sec. IV C, using Eq. (4.22) and the normalized distributions. For the $T_{LL}$ structure functions, we obtain

$$F_{[UT_{LL},T]D}(x,Q^2;\alpha_p,\boldsymbol{p}_{pT}) = \frac{2[2(2\pi)^3]}{2-\alpha_p} \sqrt{\frac{3}{2}} P_{[T_{LL},U]}(\alpha_p,\boldsymbol{p}_{pT})\, F_{[UU,T]n}(x_n,Q^2), \tag{5.14a}$$

$$F_{[UT_{LL},L]D}(x,Q^2;\alpha_p,\boldsymbol{p}_{pT}) = \frac{2[2(2\pi)^3]}{2-\alpha_p} \sqrt{\frac{3}{2}} P_{[T_{LL},U]}(\alpha_p,\boldsymbol{p}_{pT})\, F_{[UU,L]n}(x_n,Q^2), \tag{5.14b}$$

$$F^{\cos\phi_p}_{[UT_{LL}]D}(x,Q^2;\alpha_p,\boldsymbol{p}_{pT}) = \frac{2[2(2\pi)^3]}{2-\alpha_p} \sqrt{\frac{3}{2}} P_{[T_{LL},U]}(\alpha_p,\boldsymbol{p}_{pT})\, \frac{2x_n|\boldsymbol{p}_{pT}|}{Q} [F_{[UU,T]n} + F_{[UU,L]n}](x_n,Q^2), \tag{5.14c}$$

$$F^{\cos 2\phi_p}_{[UT_{LL}]D}(x,Q^2;\alpha_p,\boldsymbol{p}_{pT}) = \frac{2[2(2\pi)^3]}{2-\alpha_p} \sqrt{\frac{3}{2}} P_{[T_{LL},U]}(\alpha_p,\boldsymbol{p}_{pT})\, \frac{2x_n^2|\boldsymbol{p}_{pT}|^2}{Q^2} [F_{[UU,T]n} + F_{[UU,L]n}](x_n,Q^2). \tag{5.14d}$$

For the $T_{LT}$ structure functions, we obtain

$$F^{\cos(\phi_p-\phi_{T_L})}_{[UT_{LT},T]D}(x,Q^2;\alpha_p,\boldsymbol{p}_{pT}) = \frac{2[2(2\pi)^3]}{2-\alpha_p} \sqrt{2} P_{[T_{LT},U]}(\alpha_p,\boldsymbol{p}_{pT})\, F_{[UU,T]n}(x_n,Q^2), \tag{5.15a}$$

$$F^{\cos(\phi_p-\phi_{T_L})}_{[UT_{LT},L]D}(x,Q^2;\alpha_p,\boldsymbol{p}_{pT}) = \frac{2[2(2\pi)^3]}{2-\alpha_p} \sqrt{2} P_{[T_{LT},U]}(\alpha_p,\boldsymbol{p}_{pT})\, F_{[UU,L]n}(x_n,Q^2), \tag{5.15b}$$

$$F^{\cos\phi_{T_L}}_{[UT_{LT}]D}(x,Q^2;\alpha_p,\boldsymbol{p}_{pT}) = F^{\cos(2\phi_p-\phi_{T_L})}_{[UT_{LT}]D}(\ldots) = \frac{2[2(2\pi)^3]}{2-\alpha_p} \frac{1}{\sqrt{2}} P_{[T_{LT},U]}(\alpha_p,\boldsymbol{p}_{pT}) \frac{2x_n|\boldsymbol{p}_{pT}|}{Q} [F_{[UU,T]n} + F_{[UU,L]n}](x_n,Q^2), \tag{5.15c}$$

$$F^{\cos(\phi_p+\phi_{T_L})}_{[UT_{LT}]D}(x,Q^2;\alpha_p,\boldsymbol{p}_{pT}) = F^{\cos(3\phi_p-\phi_{T_L})}_{[UT_{LT}]D}(\ldots) = \frac{2[2(2\pi)^3]}{2-\alpha_p} \frac{1}{\sqrt{2}} P_{[T_{LT},U]}(\alpha_p,\boldsymbol{p}_{pT}) \frac{2x_n^2|\boldsymbol{p}_{pT}|^2}{Q^2} [F_{[UU,T]n} + F_{[UU,L]n}](x_n,Q^2). \tag{5.15d}$$

For the $T_{TT}$ structure functions, we obtain

$$F^{\cos(2\phi_p-2\phi_{T_T})}_{[UT_{TT},T]D}(x,Q^2;\alpha_p,\boldsymbol{p}_{pT}) = \frac{2[2(2\pi)^3]}{2-\alpha_p}\frac{1}{\sqrt{2}}P_{[T_{TT},U]}(\alpha_p,\boldsymbol{p}_{pT})\,F_{[UU,T]n}(x_n,Q^2), \tag{5.16a}$$

$$F^{\cos(2\phi_p-2\phi_{T_T})}_{[UT_{TT},L]D}(x,Q^2;\alpha_p,\boldsymbol{p}_{pT}) = \frac{2[2(2\pi)^3]}{2-\alpha_p}\frac{1}{\sqrt{2}}P_{[T_{TT},U]}(\alpha_p,\boldsymbol{p}_{pT})\,F_{[UU,L]n}(x_n,Q^2), \tag{5.16b}$$

$$F^{\cos(\phi_p-2\phi_{T_T})}_{[UT_{TT}]D}(x,Q^2;\alpha_p,\boldsymbol{p}_{pT}) = F^{\cos(3\phi_p-\phi_{T_T})}_{[UT_{TT}]D}(\ldots) = \frac{2[2(2\pi)^3]}{2-\alpha_p}\frac{1}{2\sqrt{2}}P_{[T_{TT},U]}(\alpha_p,\boldsymbol{p}_{pT})\frac{2x_n|\boldsymbol{p}_{pT}|}{Q}[F_{[UU,T]n}(x_n,Q^2)+F_{[UU,L]n}(x_n,Q^2)], \tag{5.16c}$$

$$F^{\cos 2\phi_{T_T}}_{[UT_{TT}]D}(x,Q^2;\alpha_p,\boldsymbol{p}_{pT}) = F^{\cos(4\phi_p-2\phi_{T_T})}_{[UT_{TT}]D}(\ldots) = \frac{2[2(2\pi)^3]}{2-\alpha_p}\frac{1}{2\sqrt{2}}P_{[T_{TT},U]}(\alpha_p,\boldsymbol{p}_{pT})\frac{2x_n^2|\boldsymbol{p}_{pT}|^2}{Q^2}[F_{[UU,T]n}(x_n,Q^2)+F_{[UU,L]n}(x_n,Q^2)]. \tag{5.16d}$$

Here $P_{[T_{LL},U]}$, $P_{[T_{LT},U]}$, and $P_{[T_{TT},U]}$ are the normalized neutron distributions in the tensor-polarized deuteron defined in Eq. (4.19).

We observe that, in the scattering of unpolarized electrons, the following tagged structure functions are leading-twist ($Q^2$-independent in the DIS limit):

$$\begin{aligned}
&F_{[UU,T]D},\ F_{[UU,L]D},\\
&F_{[UT_{LL},T]D},\ F^{\cos(\phi_p-\phi_{T_L})}_{[UT_{LT},T]D},\ F^{\cos(2\phi_p-2\phi_{T_T})}_{[UT_{TT},T]D},\\
&F_{[UT_{LL},L]D},\ F^{\cos(\phi_p-\phi_{T_L})}_{[UT_{LT},L]D},\ F^{\cos(2\phi_p-2\phi_{T_T})}_{[UT_{TT},L]D},
\end{aligned}$$

for the unpolarized and tensor-polarized deuteron, respectively. All other structure functions are suppressed by one or two powers of $|\boldsymbol{p}_{pT}|/Q$. Note that the leading-twist structure functions also contain power-suppressed terms $|\boldsymbol{p}_{pT}|^2/Q^2$, which have been neglected here.

The general decomposition of the cross section of unpolarized electron scattering in Part I [1], Eq. (4.20), also contains structures proportional to the deuteron vector polarization. These structures are obtained as identically zero in the IA,

$$F^{\sin\phi_p}_{[US_L]D},\ F^{\sin 2\phi_p}_{[US_L]D} = 0, \tag{5.17a}$$

$$F^{\sin(\phi_p-\phi_S)}_{[US_T,L]D},\ F^{\sin(\phi_p-\phi_S)}_{[US_T,T]D} = 0, \tag{5.17b}$$

$$F^{\sin(\phi_p+\phi_S)}_{[US_T]D},\ F^{\sin(3\phi_p-\phi_S)}_{[US_T]D},\ F^{\sin\phi_S}_{[US_T]D},\ F^{\sin(2\phi_p-\phi_S)}_{[US_T]D} = 0. \tag{5.17c}$$

This result is specific to the dynamics of the IA, which does not generate spin-dependent phases of the amplitudes (imaginary parts). FSI or other multistep processes will generate imaginary parts of the amplitudes and yield nonzero values for these structure functions [9].

It should be noted that the IA expressions of the individual structure functions are obtained from the $T$ component of the hadronic current in the deuteron hadronic tensor, which is subject to interaction effects in LF quantization [67]. For the leading-twist structure functions, these interaction effects are generally suppressed in the DIS limit, which is reflected in the fact that the structure functions satisfy the momentum sum rule (see below). For the higher-twist structure functions, interaction effects are generally not suppressed, and corrections to the IA approximations should be expected.

### B. Momentum sum rule

The IA results for the tagged deuteron structure functions satisfy certain sum rules when integrated over $x$ and over the tagged proton momentum. For the structure function

$$\frac{x}{2}[F_{[UU,T]D}+F_{[UU,L]D}](x,Q^2;\alpha_p,\boldsymbol{p}_{pT}), \tag{5.18}$$

corresponding to the conventional $F_{2D}$ deuteron structure function with the scaling variable $x/2 = x_D \in [0,1]$, Eq. (2.4), we obtain [9]

$$\begin{aligned}
&\int_0^2 dx \int d\Gamma_p \frac{x}{2}[F_{[UU,T]D}+F_{[UU,L]D}](x,Q^2;\alpha_p,\boldsymbol{p}_{pT})\\
&\quad=\int_0^2 dx\int_0^{2-x}\frac{d\alpha_p}{\alpha_p}d^2p_{pT}P_{[U,U]}(\alpha_p,\boldsymbol{p}_{pT})\\
&\qquad\times\frac{x}{2-\alpha_p}[F_{[UU,T]n}+F_{[UU,L]n}](x_n,Q^2)\\
&\quad=\int_0^2\frac{d\alpha_p}{\alpha_p}d^2p_{pT}\ (2-\alpha_p)P_{[U,U]}(\alpha_p,\boldsymbol{p}_{pT})\\
&\qquad\times\int_0^1 dx_n\ x_n[F_{[UU,T]n}+F_{[UU,L]n}](x_n,Q^2)\\
&\quad=\int_0^1 dx_n\ x_n[F_{[UU,T]n}+F_{[UU,L]n}](x_n,Q^2).
\end{aligned} \tag{5.19}$$

The integration bounds on $\alpha_p$ follow from the kinematic limit Eq. (2.17). In the second expression, we have substituted the IA results, Eqs. (5.12a) and (5.12b). In the third expression we have changed the order of the integrations over $x$ and $\alpha_p$, and changed the integration variable from $x$ to $x_n$ using Eq. (5.9). In the last expression, we have used the momentum sum rule for the $P_{[U,U]}$ distribution, Eq. (4.24). One observes that the $x$ integral of the spectator-momentum-integrated deuteron structure function is equal to the $x$ integral of the neutron structure function. This realizes the momentum sum rule for the nuclear structure function and provides an important test of the consistency of the approximations. Similar integral relations can be derived for the tensor-polarized tagged structure functions and evaluate to zero due to the angular integral over the tensor-polarized densities; see Eq. (4.25).

### C. Polarized electron

The antisymmetric part of the neutron hadronic tensor depends on the neutron LF helicities. The dependence can be expressed in covariant form as

$$\frac{1}{2}W_n^{[\mu\nu]}(p_n,\widetilde{q};\lambda_n',\lambda_n) = A^{\mu\nu\rho}(p_n,\widetilde{q})\,\bar{u}(p_n,\lambda_n')\left(\frac{-\gamma_\rho\gamma^5}{2m}\right)u(p_n,\lambda_n). \tag{5.20}$$

The bilinear form in nucleon bispinors is the polarization four-vector of the free neutron. The rank-3 tensor is given by

$$A^{\mu\nu\rho}(p_n,\widetilde{q}) = \frac{i}{2}\epsilon^{\mu\nu\sigma\tau}(e_q)_\sigma\Big\{-(e_L)_\tau(e_{L*})^\rho\,F_{[LS_L]n} + \big[(e_{L*})_\tau(e_{L*})^\rho + g_\tau^\rho\big]F_{[LS_T]n}\Big\}. \tag{5.21}$$

Here, the basis vectors $e_q$, $e_L$, and $e_{L*}$ are as defined in Part I [1], Eqs. (2.6) and (2.7), but formed with the 4-momenta $p_n$ and $\widetilde{q}$. The parameter

$$\gamma_n \equiv \frac{2x_nm}{\sqrt{-\widetilde{q}^2}} = \frac{2xm}{(2-\alpha_p)Q}[1+O(1/Q^2)] \tag{5.22}$$

is as defined in Part I [1], Eq. (2.9), but formed with the neutron DIS variables; it is related to the parameter of the deuteron DIS process, Eq. (2.6), by

$$\gamma_n = \gamma/(2-\alpha_p). \tag{5.23}$$

The neutron structure functions in Eq. (5.21) depend on the invariant variables $\widetilde{q}^2$ and $x_n$, which in the DIS limit are given by Eqs. (5.8) and (5.9). The structure functions $F_{[LS_L]n}$ and $F_{[LS_T]n}$ in Eq. (5.21) relate to the conventional neutron spin structure functions $g_{1n,2n}$ as

$$F_{[LS_L]n} = 2g_{1n}, \tag{5.24a}$$

$$F_{[LS_T]n} = -2\gamma_n(g_{1n}+g_{2n}). \tag{5.24b}$$

Note that $F_{[LS_L]n}$ is leading-twist, while $F_{[LS_T]n}$ is higher-twist (power-suppressed).

When averaging the antisymmetric neutron tensor Eq. (5.20) over the LF helicities using Eq. (4.4), only the $\not{s}_n\gamma_5$ term in the covariant neutron spin density matrix Eq. (4.5) contributes. The average therefore takes a simple form: it replaces the free neutron polarization four-vector in Eq. (5.20) by the effective polarization vector provided by the density matrix Eq. (4.5). We obtain

$$\frac{1}{2}\langle W_D^{[\mu\nu]}(p_D,q,p_p)\rangle = \frac{2[2(2\pi)^3]}{(2-\alpha_p)^2}\,A^{\mu\nu\rho}(p_n,\widetilde{q})\,s_{n,\rho}(\alpha_p,\boldsymbol{p}_{pT}|\boldsymbol{S}_D). \tag{5.25}$$

This result is achieved thanks to the covariant representation of the deuteron spin structure. The effective polarization vector in Eq. (5.25) encodes all the information on the deuteron polarization and the tagged proton momentum.

Expressions for the polarized structure functions are obtained by equating the IA result of Eq. (5.25) with the general decomposition of the spin-1 semi-inclusive scattering tensor in Part I [1], Eq. (4.20), and taking suitable components of the tensor equation. The tensor equations involve the $+$ and $T$ components of the deuteron polarization vector, and the structure functions can be expressed in terms of the longitudinally and transversely polarized neutron distributions introduced in Sec. IV D. The $\mu,\nu=1,2$ components of Eq. (5.25) give access to the structures with longitudinal neutron polarization. We obtain

$$F_{[LS_L]D}(x,Q^2;\alpha_p,\boldsymbol{p}_{pT}) = \frac{2[2(2\pi)^3]}{(2-\alpha_p)}P_{[S_L,S_L]}(\alpha_p,\boldsymbol{p}_{pT})\,F_{[LS_L]n}(x_n,Q^2), \tag{5.26a}$$

$$F_{[LS_T]D}^{\cos(\phi_p-\phi_S)}(x,Q^2;\alpha_p,\boldsymbol{p}_{pT}) = \frac{2[2(2\pi)^3]}{(2-\alpha_p)}P_{[S_T,S_L]}(\alpha_p,\boldsymbol{p}_{pT})\,F_{[LS_L]n}(x_n,Q^2), \tag{5.26b}$$

where $P_{[S_L,S_L]}$ and $P_{[S_T,S_L]}$ are given in Eqs. (4.30) and (4.31). One observes that $F_{[LS_L]D}$ is proportional to the favored distribution of longitudinally polarized neutrons in the longitudinally polarized deuteron, $P_{[S_L,S_L]}$, while $F_{[LS_T]D}^{\cos(\phi_p-\phi_S)}$ is proportional to the unfavored distribution in the transversely polarized deuteron, $P_{[S_T,S_L]}$; see Sec. IV D for details. Both structure functions are proportional to the neutron longitudinally polarized spin structure function $F_{[LS_L]n}$ and are leading-twist, see Eq. (5.24).

The $\mu,\nu=+,T$ components of Eq. (5.25) give access to the structures with transverse neutron polarization. We obtain

$$F_{[LS_L]D}^{\cos\phi_p}(x,Q^2;\alpha_p,\boldsymbol{p}_{pT}) = \frac{2[2(2\pi)^3]}{(2-\alpha_p)}P_{[S_L,S_T]}(\alpha_p,\boldsymbol{p}_{pT})\,F_{[LS_T]n}(x_n,Q^2), \tag{5.27a}$$

$$\big[F_{[LS_T]D}^{\cos\phi_S}+F_{[LS_T]D}^{\cos(2\phi_p-\phi_S)}\big](x,Q^2;\alpha_p,\boldsymbol{p}_{pT}) = \frac{2[2(2\pi)^3]}{(2-\alpha_p)}P_{[S_T,S_T]}^{\parallel}(\alpha_p,\boldsymbol{p}_{pT})\,F_{[LS_T]n}(x_n,Q^2), \tag{5.27b}$$

$$\big[F_{[LS_T]D}^{\cos\phi_S}-F_{[LS_T]D}^{\cos(2\phi_p-\phi_S)}\big](x,Q^2;\alpha_p,\boldsymbol{p}_{pT}) = \frac{2[2(2\pi)^3]}{(2-\alpha_p)}P_{[S_T,S_T]}^{\perp}(\alpha_p,\boldsymbol{p}_{pT})\,F_{[LS_T]n}(x_n,Q^2), \tag{5.27c}$$

$$F_{[LS_T]D}^{\cos\phi_S}(x,Q^2;\alpha_p,\boldsymbol{p}_{pT}) = \frac{2[2(2\pi)^3]}{(2-\alpha_p)}\frac{1}{2}[P_{[S_T,S_T]}^{\perp}+P_{[S_T,S_T]}^{\parallel}](\alpha_p,\boldsymbol{p}_{pT}) \times F_{[LS_T]n}(x_n,Q^2), \tag{5.27d}$$

where $P_{[S_T,S_T]}^{\parallel}$, $P_{[S_T,S_T]}^{\perp}$, and $P_{[S_L,S_T]}$ are given in Eqs. (4.36) and (4.38). One observes that $F_{[LS_L]D}^{\cos\phi_p}$ is proportional to the unfavored distributions of transversely polarized neutrons in the longitudinally polarized deuteron, $P_{[S_L,S_T]}$, while $F_{[LS_T]D}^{\cos\phi_S}$ and $F_{[LS_T]D}^{\cos(2\phi_p-\phi_S)}$ are proportional to the favored distributions in the transversely polarized deuteron, $P_{[S_T,S_T]}^{\parallel}$ and $P_{[S_T,S_T]}^{\perp}$; see Sec. IV D for details. All three structure functions are proportional to the neutron transversely polarized spin structure function $F_{[LS_T]n}$ and are consequently higher-twist, see Eq. (5.24).

The structure functions for polarized electron scattering on an unpolarized or tensor-polarized deuteron are zero in the IA,

$$F_{[LU]D}^{\sin\phi_p} = 0, \tag{5.28a}$$

$$F_{[LT_{LL}]D}^{\sin\phi_p},\ F_{[LT_{LT}]D}^{\sin(\phi_p+\phi_{T_\parallel})},\ F_{[LT_{LT}]D}^{\sin\phi_{T_\parallel}},\ F_{[LT_{LT}]D}^{\sin(2\phi_p-\phi_{T_\parallel})},$$
$$F_{[LT_{TT}]D}^{\sin\phi_{T_\perp}},\ F_{[LT_{TT}]D}^{\sin(\phi_p-\phi_{T_\perp})},\ F_{[LT_{TT}]D}^{\sin(3\phi_p-\phi_{T_\perp})} = 0. \tag{5.28b}$$

This immediately follows from the fact that Eq. (5.25) is linear in the deuteron vector polarization parameter $s_n \propto \boldsymbol{S}_D$ and does not give rise to unpolarized or tensor-polarized structures.

### D. Spin sum rules

The IA results for the tagged deuteron structure functions in polarized electron scattering satisfy certain sum rules when integrated over $x$ and over the tagged proton momentum, similar to those in unpolarized electron scattering. For the principal leading-twist spin structure function $F_{[LS_L]D}$, Eq. (5.27a), we obtain

$$\begin{aligned}\int_0^2 \frac{dx}{2}\int d\Gamma_p\, F_{[LS_L]D}(x,Q^2;\alpha_p,\boldsymbol{p}_{pT}) &= \int_0^2 dx \int_0^{2-x} \frac{d\alpha_p}{\alpha_p(2-\alpha_p)} d^2p_{pT} P_{[S_L,S_L]}(\alpha_p,\boldsymbol{p}_{pT}) F_{[LS_L]n}(x_n,Q^2)\\ &= \int_0^2 \frac{d\alpha_p}{\alpha_p} d^2p_{pT} P_{[S_L,S_L]}(\alpha_p,\boldsymbol{p}_{pT}) \int_0^1 dx_n\, F_{[LS_L]n}(x_n,Q^2)\\ &= \left(1-\frac{3}{2}\omega_2\right)\int_0^1 dx_n\, F_{[LS_L]n}(x_n,Q^2).\end{aligned} \tag{5.29}$$

The steps are the same as in the derivation of the momentum sum rule (5.19). In the last step, we have used the sum rule for the polarized neutron distribution, Eq. (4.40). Equation (5.29) is the spin sum rule for the tagged DIS structure function. It shows that the $x$ integral of the tagged spin structure function reduces to that of the neutron spin structure function when integrating over the spectator momentum, and that the only effect of nuclear binding is the neutron depolarization in the initial state.

Similar relations can be derived for the higher-twist tagged spin structure functions. Here, we demonstrate the Burkhardt-Cottingham (BC) sum rule [73,74] for the tagged spin structure function

$$g_{2D} = -\frac{1}{2}F_{[L,S_L]D} - \frac{1}{2\gamma}F_{[L,S_T]D}^{\cos\phi_S} \tag{5.30}$$

by computing the integral

$$\int_0^2 \frac{dx}{2}\int d\Gamma_p\, g_{2D}(x,Q^2;\alpha_p,\boldsymbol{p}_{pT}). \tag{5.31}$$

The integral of the first term in Eq. (5.30) is evaluated in Eq. (5.29); in terms of the neutron spin structure function $g_{1n}$, the result is (we omit the arguments of the functions for brevity)

$$\int_0^2 \frac{dx}{2}\int d\Gamma_p\left[-\frac{1}{2}F_{[LS_L]D}\right] = -\left(1-\frac{3}{2}\omega_2\right)\int_0^1 dx_n g_{1n}. \tag{5.32}$$

The integral of the second term in Eq. (5.30) is computed by going through similar steps:

$$\begin{aligned}\int_0^2 \frac{dx}{2}\int d\Gamma_p\left[-\frac{1}{2\gamma}F_{[L,S_T]D}^{\cos\phi_S}\right] &= \int_0^2 dx\int_0^{2-x}\frac{d\alpha_p}{\alpha_p(2-\alpha_p)} d^2p_{pT}\,\frac{1}{2}\left[P^{\parallel}_{[S_T,S_T]}+P^{\perp}_{[S_T,S_T]}\right]\frac{\gamma_n}{\gamma}(g_{1n}+g_{2n})\\ &= \int_0^2 dx\int_0^{2-x}\frac{d\alpha_p}{\alpha_p(2-\alpha_p)^2} d^2p_{pT}\,\frac{1}{2}\left[P^{\parallel}_{[S_T,S_T]}+P^{\perp}_{[S_T,S_T]}\right](g_{1n}+g_{2n})\\ &= \int_0^2 \frac{d\alpha_p}{\alpha_p(2-\alpha_p)} d^2p_{pT}\,\frac{1}{2}\left[P^{\parallel}_{[S_T,S_T]}+P^{\perp}_{[S_T,S_T]}\right]\int_0^1 dx_n(g_{1n}+g_{2n})\\ &= \left(1-\frac{3}{2}\omega_2\right)\int_0^1 dx_n(g_{1n}+g_{2n}).\end{aligned} \tag{5.33}$$

In the last step, we used the sum rule Eq. (A27) for the $\parallel$ and $\perp$ neutron distributions. Combining Eqs. (5.32) and (5.33), the terms involving $g_{1n}$ cancel, and we obtain

$$\int_0^2 \frac{dx}{2}\int d\Gamma_p g_{2D} = \left(1-\frac{3}{2}\omega_2\right)\int_0^1 dx_n g_{2n}(x_n,Q^2) = 0. \tag{5.34}$$

In the last step, we have used the BC sum rule for the neutron structure function $g_{1n}$. Thus, the BC sum rule for the tagged deuteron structure function is realized by combining the spin sum rule for the neutron LF momentum distributions and the BC sum rule for the neutron structure function.

## VI. TAGGED POLARIZATION OBSERVABLES

### A. Unpolarized deuteron

The IA expresses the structure functions of DIS on the deuteron with proton tagging in terms of calculable neutron momentum distributions and empirical neutron structure functions (or vice versa, with neutron tagging and proton structure functions). As such it offers a simple framework for estimating observables and analyzing the experiments. The general form of the spin observables in polarized semi-inclusive scattering from a spin-1 target is discussed in Part I [1], Sec. V. We now compute the basic observables in polarized tagged DIS using the IA and study the sensitivity to deuteron and neutron structure.

Experiments in polarized tagged DIS can be performed with various goals:

(1) validate the IA by testing the factorization of nuclear and hadronic structure, testing the universality of the elements, and quantifying deviations;
(2) extract the free neutron spin structure functions;
(3) extract the spin-dependent neutron LF momentum distributions in the deuteron, including structures sensitive to the $D/S$ ratio, spin-orbit correlations, and high-momentum components;
(4) study effects beyond the IA, such as initial-state modifications (EMC effect, antishadowing) or FSI ($T$-odd structures).

Each type has its specific requirements and uncertainties and merits a dedicated impact study. Here, we only provide an orientation and assess the basic feasibility of the measurements in EIC kinematics.

The following numerical estimates use the deuteron LF wave function obtained from the AV18 nonrelativistic deuteron wave function [70] using the prescription of Eq. (3.24). The unpolarized neutron structure function $F_{2n}$ is evaluated using the SLAC parametrization [75], and a constant value $R = F_L/F_T = 0.18$ is assumed. The polarized neutron structure function $g_{1n}$ is evaluated using the DSSV09 parametrization [76], and $g_{2n}$ is computed using the Wandzura-Wilczek approximation [74,77]. The simple input is chosen in order to make the results reproducible; the numerical estimates could easily be refined using more elaborate parametrizations.

The estimates are performed in the DIS limit, Eq. (5.1). The contributions of terms in the cross section to observables are ordered by (i) the scaling behavior of the kinematic factors, determined by their dependence on $\gamma$, see Part I [1], Eq. (2.9); and (ii) the scaling behavior of structure functions, determined by their dependence on $|\boldsymbol{p}_{pT}|/Q$ in the IA. The results are presented in leading nonvanishing order of $1/Q$, without power corrections.

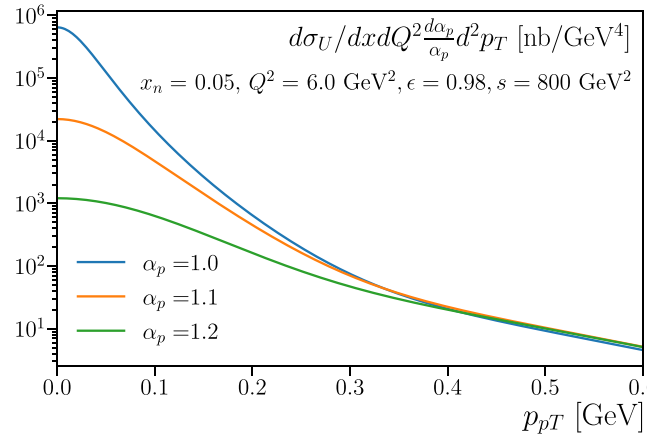



FIG. 9. The differential cross section of unpolarized tagged DIS, Eq. (6.1), as a function of the tagged proton transverse momentum $p_{pT}$, for several values of the longitudinal momentum fraction $\alpha_p$ and fixed $x_n$. The cross section is averaged over the azimuthal angle $\phi_p$.

The unpolarized tagged DIS cross section controls the reaction rates and determines the feasibility of measuring more complex observables such as spin asymmetries. Unpolarized measurements are also used directly for the extraction of unpolarized neutron structure [7,9,10] and studies of nuclear modifications [11,12].

Figure 9 shows the magnitude and spectator momentum dependence of the differential cross section of unpolarized tagged DIS in typical EIC kinematics. The function plotted is

$$d\sigma_U/dxdQ^2(d\alpha_p/\alpha_p)d^2p_{pT}, \tag{6.1}$$

where the differential cross section is given by Eq. (2.19) with $\mathcal{F}_U$ only ($\mathcal{F}_S, \mathcal{F}_T = 0$) and is averaged over the tagged proton azimuthal angle $\phi_p$. This cross section depends only on the leading-twist tagged structure functions $F_{[UU,T]}$ and $F_{[UU,L]}$. It is plotted as a function of $p_{pT}$ for various values of $\alpha_p$ and a fixed value of $x_n$, Eq. (5.9) (the value $x$ is changed when $\alpha_p$ is varied such as to keep $x_n$ fixed). One observes: (i) The dependence on the tagged proton momentum essentially tracks that of the unpolarized neutron distribution $P_{[U,U]}$ shown in Fig. 3. (ii) Even at tagged proton momenta corresponding to exceptional configurations in the deuteron ($|\alpha_p - 1| \gtrsim 0.2$; $p_{pT} \gtrsim 0.2$ GeV), large event numbers can be collected at a projected EIC integrated luminosity of 10 fb$^{-1}$ [28]. The rate for a given finite phase-space element in the tagged proton momentum is essentially the inclusive neutron DIS rate, multiplied by the integral of the $P_{[U,U]}$ distribution over the phase-space element.

Figure 10 shows the azimuthal modulation of the unpolarized tagged DIS cross section. The function plotted is the ratio of the $\phi_p$-dependent and $\phi_p$-averaged differential cross sections,

$$\frac{\mathcal{F}_U(\phi_p)}{\langle \mathcal{F}_U \rangle} = 1 + \sqrt{2\epsilon(1+\epsilon)}\cos\phi_p \frac{F^{\cos\phi_p}_{[U,U]}}{F_{[UU,T]} + \epsilon F_{[UU,L]}} + \epsilon\cos 2\phi_p \frac{F^{\cos 2\phi_p}_{[U,U]}}{F_{[UU,T]} + \epsilon F_{[UU,L]}}, \tag{6.2a}$$

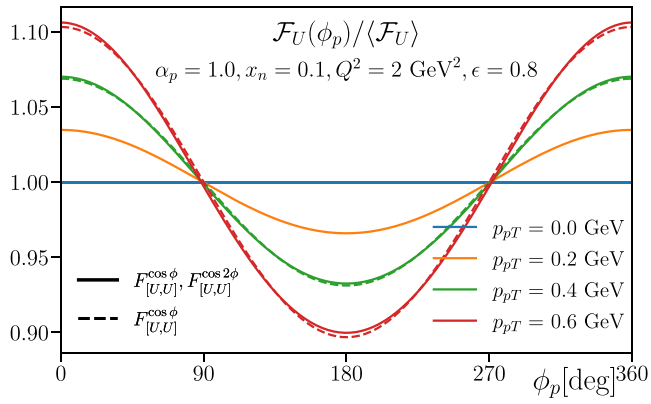



FIG. 10. The ratio of the $\phi_p$-dependent and $\phi_p$-averaged differential cross sections in unpolarized tagged DIS, Eq. (6.2), as a function of the tagged proton azimuthal angle $\phi_p$. Solid lines show the ratio with all $\phi_p$-dependent structures in the numerator. Dashed lines show the ratio with only the $\cos\phi_p$ term in the numerator.

$$\langle\ldots\rangle \equiv \int_0^{2\pi} \frac{d\phi_p}{2\pi}\,(\ldots), \tag{6.2b}$$

which includes the $\epsilon$-dependent factors accompanying the angular structures in the cross section, see Part I [1], Eq. (4.37). In the IA, the two $\phi_p$-dependent structure functions are higher twist, being suppressed by factors $p_{pT}/Q$ (for $\cos\phi_p$) and $(p_{pT}/Q)^2$ (for $\cos 2\phi_p$). This is reflected in the numerical size of the azimuthal modulations, which are generally small and grow with $p_{pT}$. The $\cos\phi_p$ harmonic reaches a magnitude of 10% for $p_{pT} \approx 0.5$ GeV in the chosen kinematics. The $\cos 2\phi_p$ modulations are $\lesssim$1% even for the largest $p_{pT}$ values shown here.

The extraction of the unpolarized neutron structure functions with spectator tagging has been studied extensively for fixed-target experiments [7] and for EIC [9,10]. By extrapolating to nonphysical momenta $|\boldsymbol{p}_{pT}|^2 < 0$ one can reach the free nucleon pole of the deuteron LF wave function, where the IA becomes exact and initial-state modifications and FSI are absent [7,9]; in coordinate space, it corresponds to configurations of infinite transverse size, where the nucleons are free [18]. The main challenge arises from the strong kinematic variation of the cross section as a function of $|\boldsymbol{p}_{pT}|$ at values of a few 10 MeV, which places high demands on the momentum resolution. Pole extrapolation in DIS with proton tagging appears feasible with the EIC far-forward detectors [10]. Neutron tagging with the EIC zero-degree calorimeter is being explored [10]. It would allow one to extract the free proton structure functions from DIS on the deuteron with neutron tagging, which can then be compared with direct measurements in DIS on the proton.

### B. Vector-polarized deuteron

Tagged DIS on the vector-polarized deuteron can be used to extract the neutron spin structure functions for both longitudinal and transverse polarization. It can also be used to determine the effective neutron polarization as a function of the tagged proton momentum and validate the $D/S$ wave ratio in the deuteron LF wave function.

The basic observable is the double spin asymmetry of the differential cross section with respect to the electron helicity $\lambda_e = \pm 1/2$ and the deuteron spin projection $\Lambda = \pm 1$ along a given polarization axis; see Part I [1], Sec. V D. Here we compute the double spin asymmetry of the $\phi_p$-averaged differential cross section, for deuteron polarization along an axis defined relative to the initial electron momentum direction in the deuteron rest frame (or relative to the colliding beam direction in the collider), as defined in Part I [1], Eq. (5.21).

The double spin asymmetry $A^V_\parallel$, for deuteron polarization parallel to the initial electron momentum direction in the deuteron rest frame (or parallel to the deuteron beam direction in the collider), is expressed in terms of the structure functions in Part I [1], Eq. (5.22). In the DIS limit, the kinematic factors are

$$D_{\parallel[S_L]} = \frac{y(1-y/2)}{1-y+y^2/2} + O(1/Q), \tag{6.3a}$$

$$D_{\parallel[S_T]} = O(1/Q), \tag{6.3b}$$

$$D_{\parallel[T_{LL}]} = \frac{1}{3} + O(1/Q), \tag{6.3c}$$

$$D_{\parallel[UT_{LT}]} = O(1/Q), \tag{6.3d}$$

$$D_{\parallel[T_{TT}]} = O(1/Q^2), \tag{6.3e}$$

and, up to power corrections, the asymmetry becomes

$$A^V_\parallel = D_{\parallel[S_L]} \frac{F_{[LS_L]D}}{\Sigma_\parallel F_D}, \tag{6.4a}$$

$$\Sigma_\parallel F_D = F_{[UU,T]D} + \epsilon F_{[UU,L]D} + \tfrac{1}{3}(F_{[UT_{LL},T]D} + \epsilon F_{[UT_{LL},L]D}). \tag{6.4b}$$

The denominator of the structure function ratio includes the $T_{LL}$ tensor-polarized structure functions. In the IA, the structure function ratio factorizes as

$$\frac{F_{[LS_L]D}}{\Sigma_\parallel F_D} = \frac{P_{[S_LS_L]}}{P_{[U,U]} + \frac{1}{\sqrt{6}} P_{[T_{LL},U]}} \frac{F_{[LS_L]n}}{F_{[UU,T]n} + \epsilon F_{[UU,L]n}}. \tag{6.5}$$

The first factor is the ratio of the longitudinally polarized and unpolarized neutron momentum distributions in the deuteron; it describes the effective neutron polarization in the deuteron and depends on the tagged proton momentum. It can also be expressed as the ratio of the probabilistic neutron distributions, Eq. (4.45a),

$$\frac{P_{[L+,L+]} - P_{[L+,L-]}}{P_{[L+,L+]} + P_{[L+,L-]}}, \tag{6.6}$$

which can be directly connected with the form of the spin asymmetry in Part I [1], Eq. (5.21). The second factor in Eq. (6.5) is the ratio of the longitudinally polarized and unpolarized neutron structure functions; it depends on the subprocess DIS variables and is what would be measured in DIS on the free neutron in the subprocess kinematics.

Figure 11 shows the deuteron structure function ratio in the parallel spin asymmetry, Eq. (6.5), as a function of the tagged proton momentum. The ratio is plotted for a fixed value of $x_n$ (the value of $x$ is changed as $\alpha_p$ is varied such as to keep

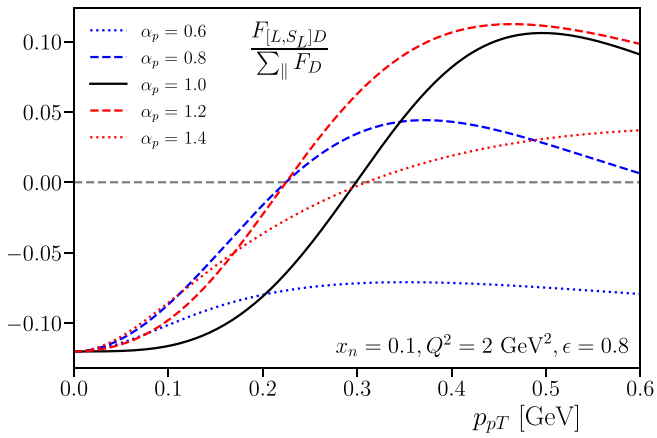



FIG. 11. The deuteron structure function ratio Eq. (6.5), as a function of $p_{pT}$, for several fixed values of $\alpha_p$. The ratio determines the double spin asymmetry for deuteron polarization parallel to the electron direction in tagged DIS, $A_\parallel^V$, Eq. (6.4). The observable asymmetry includes also the depolarization factor $D_{\parallel[S_L]}$, Eq. (6.3a).

$x_n$ fixed), which is how the measurement would be performed to extract the neutron spin structure function at fixed $x_n$. One observes the following: (i) At $p_{pT} = 0$ the ratio has a negative value of approximately $-0.1$ and is independent of $\alpha_p$. At these proton momenta the $D$ wave is absent in the deuteron LF wave function and the neutron is 100% polarized along the deuteron spin direction (see Fig. 8, upper-left panel). The value of the deuteron structure function ratio is equal to that of the neutron structure function ratio in Eq. (6.5). (ii) As $p_{pT}$ increases to approximately 0.1 to 0.2 GeV, the deuteron structure function ratio decreases in magnitude. The depolarization effect is caused by the $D$ wave. (iii) Above $p_{pT} \approx 0.3$ GeV the deuteron structure function ratio changes its sign. For $\alpha_p \approx 1$ and $p_{pT} \approx 0.5$ GeV, the ratio attains values of approximately $+0.1$, corresponding to complete reversal of the neutron polarization by the $D$ wave. This illustrates how the tagged proton momentum controls the effective neutron polarization in tagged DIS.

The double spin asymmetry $A_\parallel^V$ can be used to extract the neutron spin structure function $F_{[LS_L]n} \propto g_{1n}$. The pole extrapolation of the asymmetry is discussed in Ref. [17]. Note that Fig. 11 shows only the deuteron structure function ratio in Eq. (6.4). The experimental asymmetry includes also the depolarization factor $D_{\parallel[S_L]}$, Eq. (6.3a), whose value can be $\ll 1$ depending on $y$.

The double spin asymmetry $A_\perp^V$, for deuteron polarization perpendicular to the initial electron direction in the deuteron rest frame (or perpendicular to the deuteron beam direction in the collider), is expressed in terms of the structure functions in Part I [1], Eq. (5.23). In the DIS limit, the kinematic factors are

$$D_{\perp[S_L]} = \frac{\gamma y(1-y/2)\sqrt{1-y}}{1-y+y^2/2}\cos\psi_N + O(1/Q^2), \tag{6.7a}$$

$$D_{\perp[S_T]} = \frac{y\sqrt{1-y}}{1-y+y^2/2}\cos\psi_N + O(1/Q), \tag{6.7b}$$

$$D_{\perp[T_{LL}]} = -\frac{1}{6} + O(1/Q), \tag{6.7c}$$

$$D_{\perp[UT_{LT}]} = O(1/Q), \tag{6.7d}$$

$$D_{\perp[T_{TT}]} = O(1), \tag{6.7e}$$

where $\psi_N$ is the angle of the polarization axis relative to the lepton plane defined in Part I [1], Sec. V A and Fig. 2. Taking into account the combined scaling behavior of the kinematic factors and the structure functions, the asymmetry in the DIS limit becomes

$$A_\perp^V = D_{\perp[S_L]}\frac{F_{[LS_L]D}}{\Sigma_\perp F_D} + D_{\perp[S_T]}\frac{F^{\cos\phi_S}_{[LS_T]D}}{\Sigma_\perp F_D}, \tag{6.8a}$$

$$\Sigma_\perp F_D \equiv F_{[UU,T]D} + \epsilon F_{[UU,L]D} - \frac{1}{6}(F_{[UT_{LL},T]D} + \epsilon F_{[UT_{LL},L]D}). \tag{6.8b}$$

The two terms in Eq. (6.8a) are both $O(1/Q)$ and thus of the same order in the DIS limit. In the first term, $D_{\perp[S_L]} = O(1/Q)$ and $F_{[LS_L]D} = O(1)$; in the second term $D_{\perp[S_T]} = O(1)$ and $F_{[LS_T]D} = O(1/Q)$; see Eq. (5.24). The denominator Eq. (6.8b) again contains a tensor-polarized contribution. Of the various tensor-polarized structures in the original expression in Part I [1] only the $T_{LL}$ structure survives in the DIS limit, because $D_{\perp[T_{LL}]} = O(1)$ and $F_{[UT_{LL},T]D}, F_{[UT_{LL},L]D} = O(1)$; the $T_{LT}$ structure is suppressed because $D_{\perp[UT_{LT}]} = O(1/Q)$; and $T_{TT}$ is suppressed because the structure function Eq. (5.16d) is

$$F^{\cos 2\phi_{T_T}}_{[UT_{TT}]D} = O(1/Q^2). \tag{6.9}$$

In the IA, the structure function ratios in Eq. (6.8) factorize as

$$\frac{F_{[LS_L]D}}{\Sigma_\perp F_D} = \frac{P_{[S_LS_L]}}{P_{[U,U]} - \frac{1}{2\sqrt{6}}P_{[T_{LL},U]}}\frac{F_{[LS_L]n}}{F_{[UU,T]n} + \epsilon F_{[UU,L]n}}, \tag{6.10a}$$

$$\frac{F^{\cos\phi_S}_{[LS_T]D}}{\Sigma_\perp F_D} = \frac{\frac{1}{2}\left(P^\parallel_{[S_TS_T]} + P^\perp_{[S_TS_T]}\right)}{P_{[U,U]} - \frac{1}{2\sqrt{6}}P_{[T_{LL},U]}}\frac{F_{[LS_T]n}}{F_{[UU,T]n} + \epsilon F_{[UU,L]n}}. \tag{6.10b}$$

The first ratio involves the leading-twist neutron structure function $F_{[LS_L]n}$; the second involves the higher-twist structure function $F_{[LS_T]n}$. Note that the contributions of the two structures to the asymmetry, Eq. (6.8), can be separated only using the $y$ dependence of the kinematic factors (varying $y$ by changing the electron-deuteron collision energy), or by performing an independent measurement of $F_{[LS_L]n}$ using the parallel spin asymmetry, Eq. (6.4).

Figure 12 shows the deuteron structure function ratio Eq. (6.10b), describing the contribution of the neutron structure function $F_{[LS_T]n}$ to the perpendicular spin asymmetry, as a function of the tagged proton momentum. One observes the following: (i) The values of the transversely polarized structure function ratio are an order of magnitude smaller than those of the longitudinally polarized ratio in Fig. 11, because of the power suppression of the transversely polarized structure functions. (ii) At moderate values of the tagged proton momentum, $|1-\alpha_p| \lesssim 0.2$ and $p_{pT} \lesssim 200$ MeV, the transversely polarized structure function ratio depends strongly on $|1-\alpha_p|$ but not on $p_{pT}$, in marked contrast to the longitudi-

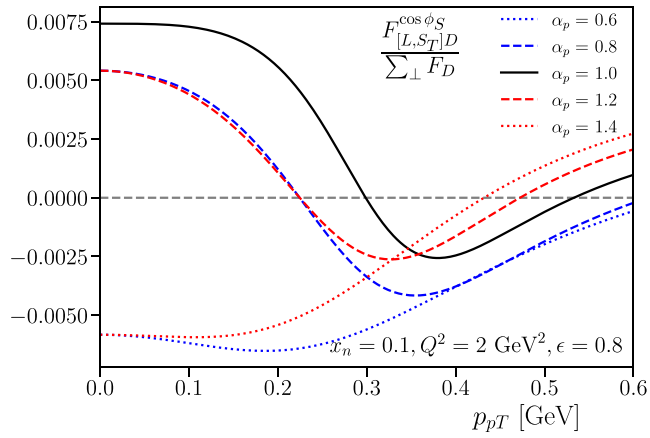



FIG. 12. The deuteron structure function ratio Eq. (6.10b), as a function of $p_{pT}$, for several fixed values of $\alpha_p$. The ratio enters in the double spin asymmetry for perpendicular deuteron polarization in tagged DIS, $A^V_\perp$, Eq. (6.8), and controls the contribution of the transversely polarized neutron structure function $F_{[LS_T]n}$ (or $g_{2n}$). The observable asymmetry includes also the term with the longitudinally polarized neutron structure function $F_{[LS_L]n}$ and the depolarization factors.

nally polarized ratio in Fig. 11. This happens because $\alpha_p \neq 1$ selects configurations with nonzero longitudinal nucleon momentum and therefore transverse orbital angular momentum, which causes $D$-wave depolarization of the transversely polarized neutron. Note that the values at $p_{pT} = 0$ depend only on $|1 - \alpha_p|$, the magnitude of the longitudinal momentum.

The extraction of the neutron structure functions from the perpendicular asymmetry is more complex than in the parallel case, because the terms with $F_{[LS_L]n}$ and $F_{[LS_T]n}$ appear at the same order. A future study should explore whether proton tagging could be used to separate $F_{[LS_L]n}$ and $F_{[LS_T]n}$, or $g_{1n}$ and $g_{2n}$, in measurements at fixed $y$, using the different dependence of the terms on the tagged proton momentum, including possibly the dependence on the azimuthal angle $\phi_p$.

### C. Tensor-polarized deuteron

Tensor-polarized deuteron observables are particularly clean probes of the $D$ wave in the deuteron LF wave function. In the tensor-polarized spin asymmetries the neutron structure functions cancel out in the IA, so that the asymmetries depend only on deuteron structure. Tagging makes it possible to select configurations where the $D$ wave is dominant, producing asymmetries of order unity.

The basic observable is the tensor-polarized asymmetry of the differential cross section averaged over the electron helicity, computed with the deuteron spin states with projection $\Lambda = \pm 1$ and 0 along a given polarization axis; see Part I [1], Sec. V D. Here we compute the tensor-polarized asymmetry of the $\phi_p$-averaged cross section for deuteron polarization along an axis defined relative to the initial electron momentum direction in the deuteron rest frame (or relative to the colliding beam direction in the collider), as defined in Part I [1], Eq. (5.24). The steps are the same as in the study of the vector-polarized asymmetries above.

The tensor-polarized asymmetry for deuteron polarization parallel to the initial electron direction, $A^T_\parallel$, is expressed in terms of the deuteron structure functions in Part I [1], Eq. (5.25). In the DIS limit the kinematic factors are given by Eq. (6.3), and, up to power corrections, the asymmetry becomes

$$A^T_\parallel = \frac{2}{3}\frac{F_{[UT_{LL},T]D} + \epsilon F_{[UT_{LL},L]D}}{F_{[UU,T]D} + \epsilon F_{[UU,L]D}}. \tag{6.11}$$

In the IA, substituting the factorized expressions of the deuteron structure functions, Eqs. (5.14) and (5.12), the neutron structure functions cancel, and we obtain

$$A^T_\parallel = \sqrt{\frac{2}{3}}\frac{P_{[T_{LL},U]}}{P_{[U,U]}} = \frac{\left(2f_0 + \frac{1}{\sqrt{2}}f_2\right)\frac{1}{\sqrt{2}}f_2}{f_0^2 + f_2^2}(1 - 3\cos^2\theta_k). \tag{6.12}$$

The asymmetry is given by a ratio of quadratic forms in the $S$- and $D$-wave radial wave functions in the c.m. frame, multiplied by an angular factor. One can easily verify that the expression takes values in $[-2, 1]$. The ratio of quadratic forms attains a maximum value of $+1$ when

$$f_2/f_0 = \sqrt{2} \tag{6.13}$$

(this is the location where the polarized neutron distributions have a node), and a minimum value of $-1/2$ when

$$f_2/f_0 = -1/\sqrt{2}. \tag{6.14}$$

The angular factor is proportional to the second-order Legendre polynomial $P_2(\cos\theta_k)$ and has a maximum value of $+1$ (at $\theta_k = \pi/2$) and a minimum value of $-2$ (at $\theta_k = 0, \pi$).

In inclusive measurements, where the numerator and denominator in the asymmetry are separately averaged over the nucleon configurations in the deuteron, most of the events come from momenta $k$ of several tens of MeV, where $|f_2| \ll |f_0|$, and the asymmetry has values $\ll 1$. In tagged measurements, where the configuration is fixed by the spectator momentum, one can select configurations where the asymmetry has values of order unity or even reaches its extremal values $-2$ and 1.

With the AV18 radial wave functions, the condition Eq. (6.13) is satisfied for $k = 0.30$ GeV. At this value of the c.m. momentum, the minimal and maximal value of $A^T_\parallel$ are attained with $\theta_k = 0$ and $\theta_k = \pi/2$, respectively. In terms of the LF momentum variables, this corresponds to $|\alpha_p - 1| \approx 0.3$, $p_{pT} = 0$ and $|\alpha_p - 1| = 0$, $p_{pT} = 0.3$ GeV, respectively. These momentum values are in the domain where the present treatment of deuteron structure is well applicable and the results are robust (see below). Our findings therefore imply that the extremal values $A^T_\parallel = 1$ and $-2$ can be achieved in experiments with these kinematic settings.

The condition Eq. (6.14) is satisfied only at $k \approx 1$ GeV with the AV18 radial wave functions. At such large momenta, the treatment of the deuteron as an $NN$ bound state becomes questionable and the results are model-dependent. While formally $A^T_\parallel$ attains extremal values at this c.m. momentum, we cannot suggest this as a realistic prediction. Table II summarizes the kinematic settings in which $A^T_\parallel$ reaches its extremal

TABLE II. Kinematic settings for which the tensor-polarized asymmetry $A_{\parallel}^{T}$, Eq. (6.12), attains its minimal or maximal values. The spectator momentum is given in terms of the c.m. and LF variables. The numerical values are based on the AV18 radial wave functions. (The high-momentum setting in the last line is not presumed to be a realistic prediction and is listed only for completeness.)

| | | c.m. variables | | LF variables | |
|---|---|---|---|---|---|
| $A_{\parallel}^{T}$ | $f_2/f_0$ | $k$ | $\theta_k$ | $\lvert\alpha_p-1\rvert$ | $p_{pT}$ |
| $-2$ | $\sqrt{2}$ | 0.3 GeV | 0 | 0.3 | 0 |
| 1 | $\sqrt{2}$ | 0.3 GeV | $\pi/2$ | 0 | 0.3 GeV |
| 1 | $-1/\sqrt{2}$ | 1 GeV | 0 | 0.7 | 0 |

values in the c.m. variables $k$ and $\theta_k$ and the corresponding LF variables $\alpha_p$ and $p_{pT}$.

Figure 13 shows the dependence of $A_{\parallel}^{T}$ on the tagged proton momentum variables $\alpha_p$ and $p_{pT}$. The extremal values in the first two lines of Table II can be identified in the graphs. The functional dependence reflects the interplay of the two factors in Eq. (6.12). In the lower panel one sees that, as a function of $\alpha_p$, $A_{\parallel}^{T}$ always peaks at $\alpha_p = 1$ (maximum of the angular factor at $\theta_k = \pi/2$), and always has a minimum at

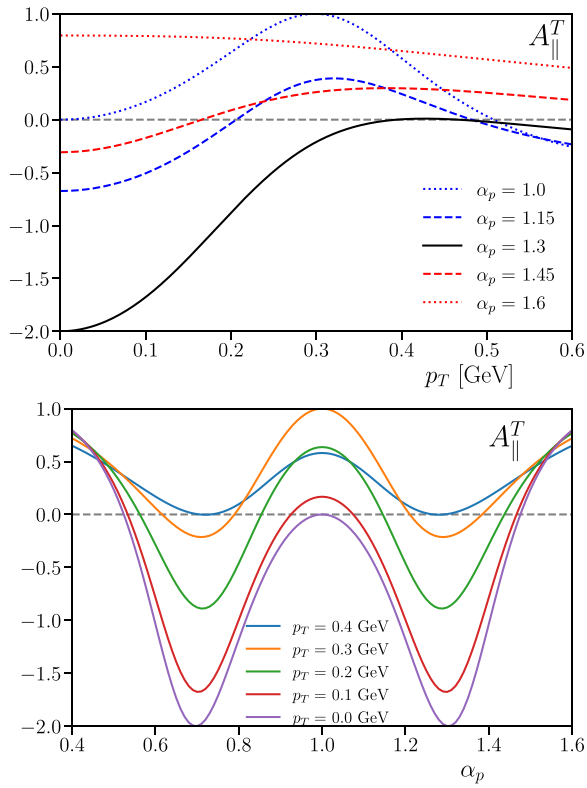



FIG. 13. The tensor-polarized asymmetry $A_{\parallel}^{T}$ in $\phi_p$-averaged tagged DIS in the IA, Eq. (6.12), as a function of the tagged proton momentum variables $\alpha_p$ and $p_{pT}$. The deuteron is polarized parallel to the electron direction. The upper panel shows the asymmetry as a function of $p_{pT}$, for fixed $\alpha_p$. The lower panel shows the results as a function of $\alpha_p$, for fixed $p_{pT}$. The extremal values correspond to the settings listed in Table II.

$|\alpha_p - 1| \approx 0.3$ (maximum of the ratio of quadratic forms in the radial wave function).

The tensor-polarized asymmetry for deuteron polarization along an axis perpendicular to the electron momentum is expressed in terms of the structure functions in Part I [1], Eq. (5.26). In the DIS limit the kinematic factors are given by Eq. (6.7). Taking into account the combined scaling behavior of the kinematic factors and the structure functions, neglecting power corrections, the asymmetry becomes

$$A_{\perp}^{T} = -\frac{1}{3}\frac{F_{[UT_{LL},T]D} + \epsilon F_{[UT_{LL},L]D}}{F_{[UU,T]D} + \epsilon F_{[UU,L]D}}; \tag{6.15}$$

the other structures in the original expression in Part I [1] are power-suppressed either in the kinematic factors or in the structure functions, see Eq. (6.9). The asymmetry is independent of the angle of the perpendicular polarization axis, $\psi_N$. Therefore, in the DIS limit

$$A_{\perp}^{T} = -\frac{1}{2}A_{\parallel}^{T} = -\sqrt{\frac{1}{6}}\frac{P_{[T_{LL},U]}}{P_{[U,U]}}. \tag{6.16}$$

The perpendicular asymmetry is $-1/2$ times the parallel asymmetry in the IA, Eq. (6.12), and thus contains no new information. An experimental test of the relation Eq. (6.16) would test the accuracy of the IA predictions and quantify possible deviations.

So far, we have considered the tensor-polarized asymmetries of the $\phi_p$-averaged differential cross section. We can also compute the tensor-polarized asymmetry of the $\phi_p$-dependent differential cross section, defined as in Part I [1], Eq. (5.24), but with $d\sigma$ now the full $\phi_p$-dependent differential cross section. These asymmetries involve the $\phi_p$-dependent structures of the cross section in both numerator and denominator and exhibit a rich structure. In particular, certain $\phi_p$-dependent structures corresponding to a given tensor polarization ($T_{LL}, T_{LT}, T_{TT}$) can be $O(1)$ in cases where the $\phi_p$-averaged structures are suppressed, implying a change in the counting of structures.

Here we illustrate the behavior of the $\phi_p$-dependent tensor-polarized asymmetry for deuteron polarization perpendicular to the initial electron momentum in the rest frame, at the same angle as the final electron direction ($\psi_N = 0$). For this polarization direction, the $\phi_p$-averaged asymmetry is given by Part I [1], Eq. (5.26). In the $\phi_p$-dependent case, the numerator includes the leading-twist $T_{TT}$ structure functions of Eq. (5.16),

$$F_{[UT_{TT},T]D}^{\cos(2\phi_p - 2\phi_{T_T})}, \quad F_{[UT_{TT},L]D}^{\cos(2\phi_p - 2\phi_{T_T})}, \tag{6.17}$$

which qualitatively changes the form compared with Eq. (6.15). The denominator remains unchanged at the leading-twist level, as the $\phi_p$-dependent structure functions of the $U$ cross section in Eq. (5.12) are $O(|\boldsymbol{p}_{pT}|/Q)$. Figure 14 shows the $\phi_p$-dependent $A_{\perp}^{T}$, as a function of $\phi_p$, for $\alpha_p = 1$ and several values of $p_{pT}$. One observes the following: (i) The asymmetry shows a clear $\cos 2\phi_p$ modulation, whose amplitude grows with increasing $p_{pT}$. (ii) The higher-order modulations in the numerator, which are associated with power-suppressed structure functions, are tiny in the kinematics shown. The same applies to the $\cos\phi_p$ and

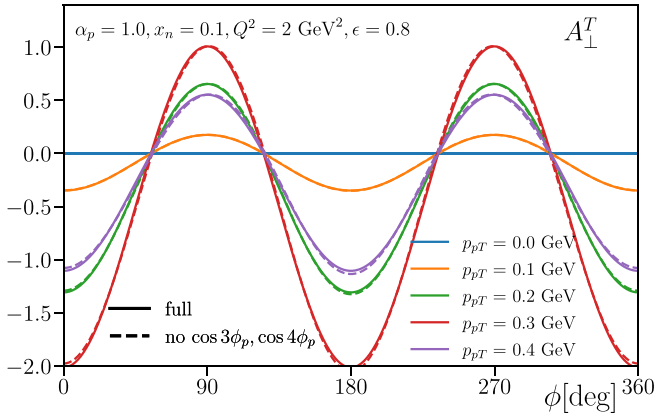



FIG. 14. The tensor-polarized asymmetry $A_\perp^T$ in $\phi_p$-dependent tagged DIS, as a function of $\phi_p$, for $\alpha_p = 1$ and several values of $p_{pT}$. Here the deuteron is polarized perpendicular to the initial electron direction in the rest frame, at the same angle as the final electron direction (see text). The denominator is the full $\phi_p$-dependent unpolarized cross section.

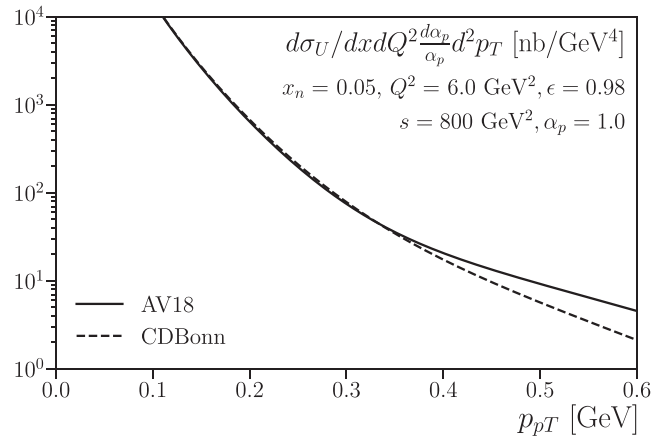



FIG. 15. Same as Fig. 9, but now comparing results obtained with the AV18 and CDBonn deuteron wave functions.

$\cos 2\phi_p$ modulations in the denominator, which could otherwise distort the clear $2\phi_p$ modulation in the curves. (iii) The asymmetry respects the bounds $[-2, 1]$ and is able to attain its extremal values for $p_{pT} \approx 0.3$ GeV, which again corresponds to c.m. momenta where Eq. (6.13) is satisfied.

The tensor-polarized asymmetries can be used to extract the $D/S$ wave ratio of the deuteron radial wave functions, which is an important characteristic of short-range deuteron structure. Tensor-polarized asymmetries of order unity can be achieved in spectator tagging, qualitatively changing the magnitude compared with inclusive measurements. The asymmetries for parallel and perpendicular polarization contain the same information in a different form and can be compared for validation.

The tensor-polarized asymmetries are, in principle, sensitive to FSI, because the deuteron spin states with different spin projections have different spatial distributions of the nucleons and therefore different probabilities for rescattering in the final state. The effect of FSI on the tensor-polarized asymmetries should be investigated in a dedicated study.

### D. Nuclear structure model dependence

The numerical estimates of tagged DIS observables in the IA rely on the deuteron LF wave function as a dynamical input. In our approach, the deuteron LF wave function is constructed from the nonrelativistic wave function in the approximation described in Sec. III C, see Eq. (3.24). The deuteron nonrelativistic wave function is obtained from empirical $NN$ potentials constrained by $NN$ scattering and nuclear bound-state data; see Ref. [78] for a review. At small nucleon momenta $|\boldsymbol{k}| \lesssim 100$ MeV, the $NN$ potentials and the deuteron wave function are well determined in this scheme; at larger momenta $|\boldsymbol{k}| \gtrsim 300$ MeV there are substantial differences between the various parametrizations. We now estimate the numerical uncertainty of the IA predictions resulting from the $NN$ interaction model.

The observables in this section have been computed with the deuteron wave function from the AV18 potential [70], which is considered a "hard" $NN$ interaction (strong high-momentum components). To estimate the uncertainty, we compare the results with those computed with the wave function from the CDBonn potential [79], which is a "softer" interaction.

Figure 15 compares the unpolarized tagged DIS cross sections for two different deuteron wave functions at $\alpha_p = 1$ (see Fig. 9). One observes that at $p_{pT} \lesssim 300$ MeV the results agree at the few percent level, but that at 500 MeV the CDBonn result is only approximately 60% of the AV18 one.

Figure 16 compares the deuteron structure function ratios in the vector-polarized asymmetry (see Fig. 11). One observes the same pattern: for small $p_{pT}$ the results are virtually the same, but discrepancies appear at larger values $p_{pT} \gtrsim 300$ MeV.

Figure 17 compares the predictions for the tensor-polarized asymmetry $A_\parallel^T$ (see Fig. 13, lower panel). Here an interesting situation arises. While the maximum value occurs at $\alpha_p = 1$ and shows no dependence on the deuteron wave function,

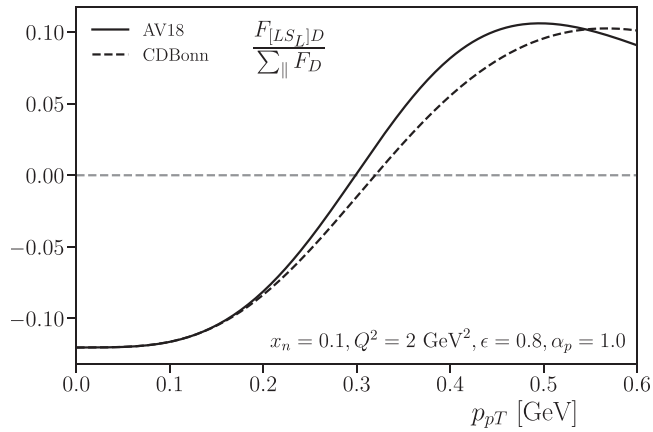



FIG. 16. Same as Fig. 11, but now comparing results obtained with the AV18 and CDBonn deuteron wave functions.

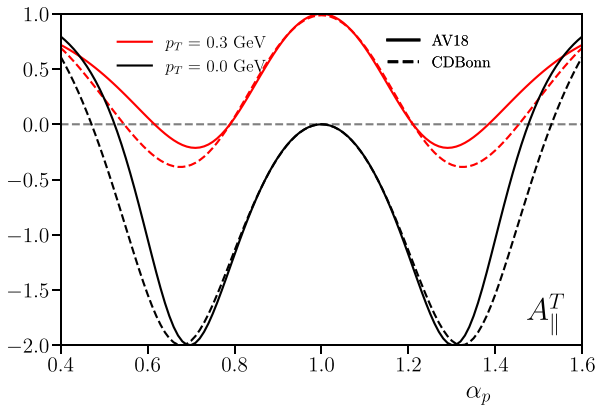



FIG. 17. Same as the lower panel in Fig. 13, but now comparing results obtained with the AV18 and CDBonn deuteron wave functions.

the minimum value occurs at values $\alpha_p \neq 1$ and shows a substantial model dependence, especially for $p_{pT} \gtrsim 300$ MeV. The tensor-polarized asymmetry can therefore be used to discriminate between deuteron wave function models, especially since it is independent of neutron structure in the IA (see the comments regarding FSI in Sec. VI C).

It is worth noting that the nuclear structure uncertainty estimated here is not the only uncertainty affecting the tagged DIS cross section, and may not even be the dominant one for tagged spectator momenta of a few 100 MeV. Other uncertainties arise from the implementation of the LF description in the IA (the restriction to $NN$ states, the matching with the nonrelativistic wave function) and from FSI neglected in the IA. In the differential cross section, FSI effects are expected to have a strong dependence on the angle of the spectator momentum ($\theta_k$ in the c.m. frame) and reach a magnitude comparable to the IA for momenta $\gtrsim$300 MeV [9].

## VII. CONCLUSIONS AND EXTENSIONS

In this work we have computed the cross section and spin observables of DIS on the polarized deuteron with spectator nucleon tagging, combining methods of LF quantization, the IA, and dynamical input from nonrelativistic nuclear structure. The main results can be summarized as follows:

(1) The LFQM formulation enables an efficient description of deuteron LF structure including the spin degrees of freedom. The collinear boost invariance transports the deuteron polarization parameters from the deuteron rest frame (where they are given experimentally) to the $pn$ c.m. frame (where the spin wave function is constructed) and to any collinear frame (where the scattering process happens). The resulting formulas have quasi three-dimensional appearance yet embody the full LF spin structure.

(2) The tagged DIS structure functions can be represented as products of the active neutron structure functions and the neutron LF momentum distributions in the deuteron, which depend on the tagged proton momentum and the neutron and deuteron spin variables (or vice versa for active proton and tagged neutron). This form expresses the factorization of hadronic and nuclear structure and provides a compact and transparent representation of the structure functions (effective neutron polarization, subprocess kinematics).

(3) The spin-dependent neutron (or proton) LF momentum distributions can be used to quantify and visualize relativistic deuteron structure and are interesting objects of study in themselves. They have the same structural properties as the TMD parton distributions in QCD [41] (spin-orbit couplings, $T$-even and odd structures) but are governed by nuclear dynamics and can be computed from empirical interactions. Within the IA, the nucleon distributions are process-independent and can be extracted and validated using various nucleon-level scattering processes, i.e., quasi-elastic scattering.

(4) Spectator tagging is a special case of target fragmentation in DIS. The treatment of nuclear breakup by soft nuclear interactions is consistent with the factorization theorem and the twist expansion of the structure functions. The tagged structure functions computed here can be connected with the fracture functions in the conventions of Refs. [2–4]. The dynamical modeling of target fragmentation involves matrix elements of twist-2 QCD operators and is simpler than the current fragmentation involving TMD operators.

(5) Spectator tagging enables the selection of specific nuclear configurations during the DIS process. The spectator momentum controls the $D/S$ wave ratio in the $pn$ configuration. This produces striking effects in spin observables. The vector-polarized spin asymmetry changes sign between low and high spectator momenta, as the effective neutron polarization changes from along the deuteron spin ($S$ wave) to opposite to it ($D$ wave).

(6) The tensor-polarized spin asymmetry in tagged DIS is generally of order unity and attains its minimal and maximal values of $-2$ and 1 in configurations where the $D/S$ ratio is $f_2/f_0 = \sqrt{2}$, which occurs at spectator momenta of approximately 300 MeV and certain angles. This is very different from untagged (inclusive) DIS, where the tensor-polarized asymmetry is $\ll 1$ because the scattering is dominated by $S$-wave configurations.

The main limitations of the present study are as follows:

(1) The present treatment of the scattering process is limited to the IA and should be extended to include FSI. FSI has a large effect on the unpolarized tagged DIS differential cross section at spectator momenta $\gtrsim$300 MeV (the rescattering process changes the tagged nucleon momentum and thus the functional dependence of the cross section) and shows a strong dependence on the spectator momentum angle [9]. The effect on the polarized tagged DIS differential cross section and the spin asymmetries should be studied. Interesting questions are as follows: (a) Can a possible spin

dependence of the rescattering process enable interference of scattering amplitudes with $S$ and $D$ wave in the initial state? (b) What is the effect of FSI on tensor-polarized asymmetries, where the polarization state controls the spatial configuration of the nucleons? (c) What is the size of $T$-odd structure functions, which are zero in the IA and provide a sensitive test of FSI?

(2) The expansion of the deuteron state in the LFQM calculation is restricted to the $pn$ component. While this approximation is adequate for c.m. momenta $\lesssim$300 MeV [6], for higher momenta non-nucleonic components ($NN\pi$, $\Delta\Delta$) should be included in the expansion [63]. These components then participate in the DIS process, bringing in new hadronic structure functions and interference effects at the amplitude level. A proper treatment of these components in tagged DIS remains a major challenge. A study of quasi-elastic scattering, where the final state is simpler and limits the interference of amplitudes, would be a good first step.

The results of the present study can be applied and extended in several other ways:

The structure function models can be used to simulate polarized tagged DIS with the EIC, using the far-forward detectors to capture spectator protons or neutrons. Measurements of the unpolarized $\phi_p$-integrated tagged cross sections have been simulated in Ref. [10]. The predictions for the $\phi_p$ dependence obtained in this work can be used to control the systematic uncertainties in measurements with incomplete azimuthal coverage. They can also be used to simulate the extraction of $\phi_p$ harmonics, valuable observables which provide critical tests of the IA and possible FSI effects. The predictions for the spin dependence can be used to simulate measurements of polarized tagged DIS with possible polarized deuteron beams at EIC [29–31]. Important questions are as follows: (a) What magnitude and uncertainty of the deuteron polarization in the various spin states are required to measure vector- and tensor-polarized asymmetries? (b) What are the luminosity requirements for measuring spin asymmetries at spectator momenta $\gtrsim$100 MeV, which correspond to rare configurations in the deuteron? (c) What are the tradeoffs in measuring the tensor-polarized asymmetry at spectator momenta $\approx$ few 100 MeV, where it takes values of order unity (low rates vs large spin asymmetry)?

The treatment can be extended to exclusive processes in electron scattering on the deuteron with spectator tagging, $e + D \to e' + M + n + p$, where $M$ = meson or photon. For such exclusive processes the dynamical calculations are performed at the amplitude level (in inclusive scattering they are performed at the cross section level). The nucleon-level process is now described by the exclusive amplitude $e + N \to e' + M + N'$. In the regime of QCD factorization, this amplitude can be expressed in terms of quark or gluon scattering amplitudes and the nucleon generalized parton distributions (GPDs). A new aspect in the nuclear breakup calculations (compared with inclusive scattering) is that the active nucleon appears intact in the final state, which creates the possibility of the interference of amplitudes with different active nucleons. Exclusive processes on the deuteron with spectator tagging would provide valuable new information on the neutron GPDs.

The technique of spectator nucleon tagging and nuclear breakup detection can be extended to scattering on $A > 2$ nuclei, i.e., $^3$He. While this greatly expands the range of possibilities, the theoretical challenges are very considerable. The implementation of the LF structure of the three-body system is much more complex than for the two-body system. The realization of rotational invariance using c.m. frame variables (see Sec. III C) is more complicated, because each two-body subsystem has its own c.m. frame, which is boosted relative to the nuclear rest frame in a way that depends on the third particle [69,80–82]. Because the spectator system now consists of multiple nucleons subject to nuclear interactions, the amplitudes of the nuclear breakup into defined channels are determined by wave function overlap integrals that show large model uncertainties. Also, FSI are much more complex than in $A = 2$ nuclei, because of the many possible configurations of the remnant system and the resulting interaction trajectories. Substantial further efforts are needed to extend the present methods to $A > 2$ nuclei.

## ACKNOWLEDGMENTS

This study greatly benefited from earlier work and exchanges with D. Higinbotham, Ch. Hyde, A. Jentsch, S. Kumano, P. Nadel-Turonski, M. Sargsian, M. Strikman, and Zhoudunming Tu. This material is based upon work supported by the U.S. Department of Energy, Office of Science, Office of Nuclear Physics under Contract No. DE-AC05–06OR23177, and by the U.S. National Science Foundation under Awards No. PHY-2111442 and No. PHY-2239274.

## DATA AVAILABILITY

There are no publicly available research data or software supporting this paper. Requests for further information or data should be sent to the authors.

## APPENDIX: SUM RULES FOR POLARIZED NEUTRON DISTRIBUTIONS

### 1. Longitudinally polarized neutron

In this Appendix we compute the integrals of the longitudinally and transversely polarized neutron distributions over the tagged proton momentum. The integrals describe the contribution of the neutron spin to the total spin of the deuteron, in analogy to the spin sum rules for the quarks and gluons in the nucleon in QCD. The exercise demonstrates the realization of rotational invariance in the LF description and the role of relativistic effects in deuteron structure.

The integral of the longitudinally polarized neutron distribution Eq. (4.27) over the tagged proton momentum can be expressed as [18]

$$\int_0^2 \frac{d\alpha_p}{\alpha_p}\, d^2 p_{pT} P_{[S_L]}(\alpha_p, \boldsymbol{p}_{pT}|\boldsymbol{S}_D) = I_{[S_L]} S_D^z. \tag{A1}$$

That it is proportional to $S_D^z$, and independent of $\boldsymbol{S}_{DT}$, is required by rotational invariance and confirmed by the explicit expressions below. The integral is evaluated as an integral over the c.m. momentum using Eq. (3.21),

$$\begin{aligned}
&\int_0^2 \frac{d\alpha_p}{\alpha_p}\, d^2p_{pT} P_{[S_L]}(\alpha_p, \boldsymbol{p}_{pT}|\boldsymbol{S}_D) \\
&= \int \frac{d^3k}{E}\left(f_0 - \frac{f_2}{\sqrt{2}}\right) \\
&\quad \times \left[A\left(f_0 - \frac{f_2}{\sqrt{2}}\right) + B(f_0 + \sqrt{2}f_2)\right], \\
&= 4\pi \int \frac{dk\, k^2}{E}\left(f_0 - \frac{f_2}{\sqrt{2}}\right) \\
&\quad \times \left[\bar{A}\left(f_0 - \frac{f_2}{\sqrt{2}}\right) + \bar{B}(f_0 + \sqrt{2}f_2)\right],
\end{aligned} \tag{A2}$$

where

$$\bar{A} \equiv \int \frac{d\Omega_k}{4\pi} A(\boldsymbol{k}), \quad \bar{B} \equiv \int \frac{d\Omega_k}{4\pi} B(\boldsymbol{k}) \tag{A3}$$

are the angular averages of the coefficients given in Eqs. (4.27b) and (4.27). The angular averages can be computed exactly. Here we evaluate them by expanding the coefficients in $k/m$, which produces simple analytic expressions, explains the connection with nonrelativistic nuclear structure, and provides an excellent numerical approximation to the exact results. Expanding in $k/m$, the coefficients become

$$\begin{aligned}
A(\boldsymbol{k}) &= \cos^2\theta_k\, S_D^z - \sin^2\theta_k \cos\theta_k \frac{|\boldsymbol{k}|}{m} S_D^z \\
&\quad + \left(\cos\theta_k - \sin^2\theta_k \frac{|\boldsymbol{k}|}{m}\right) \frac{\boldsymbol{S}_{DT}\cdot\boldsymbol{k}_T}{|\boldsymbol{k}|} \\
&\quad + O\left(\frac{k^2}{m^2}\right),
\end{aligned} \tag{A4a}$$

$$\begin{aligned}
B(\boldsymbol{k}) &= \sin^2\theta_k\, S_D^z + \sin^2\theta_k \cos\theta_k \frac{|\boldsymbol{k}|}{m} S_D^z \\
&\quad - \cos\theta_k \left(1 + \cos\theta_k \frac{|\boldsymbol{k}|}{m}\right) \frac{\boldsymbol{S}_{DT}\cdot\boldsymbol{k}_T}{|\boldsymbol{k}|} \\
&\quad + O\left(\frac{k^2}{m^2}\right).
\end{aligned} \tag{A4b}$$

Only the first terms $\propto S_D^z$ survive in the angular averaging; the terms $\propto \boldsymbol{S}_{DT}$ average to zero because of rotational invariance. We obtain

$$\bar{A} = \tfrac{1}{3} S_D^z, \quad \bar{B} = \tfrac{2}{3} S_D^z. \tag{A5}$$

We can thus identify the scalar integral in Eq. (A1) as

$$\begin{aligned}
I_{[S_L]} &= 4\pi \int \frac{dk\, k^2}{E}\left(f_0 - \frac{f_2}{\sqrt{2}}\right)\left(f_0 + \frac{f_2}{\sqrt{2}}\right) \\
&= 4\pi \int \frac{dk\, k^2}{E}\left(f_0^2 - \frac{f_2^2}{2}\right) \\
&= 4\pi \int \frac{dk\, k^2}{E}\left(f_0^2 + f_2^2 - \frac{3}{2} f_2^2\right) \\
&= 1 - \frac{3}{2}\omega_2.
\end{aligned} \tag{A6}$$

In the last step we have used the normalization condition of the radial wave functions in the c.m. frame, Eq. (3.23), and substituted the expression of the $D$-state probability of the deuteron wave function in the c.m. frame,

$$\omega_2 \equiv 4\pi \int \frac{dk\, k^2}{E(k)} [f_2(k)]^2. \tag{A7}$$

The longitudinally polarized neutron distribution satisfies a spin sum rule, with a depolarization correction proportional to the $D$-state probability.

The integrals of the normalized longitudinally polarized distributions Eqs. (4.30) and (4.31) are computed in the same way. They are given by expressions similar to Eq. (A2), in which the coefficients $A, B$ are replaced by $A_{[=]}, B_{[=]}$ and $A_{[\neq]}, B_{[\neq]}$, respectively. Expanding the coefficients in $k/m$,

$$A_{[=]}(\boldsymbol{k}) = \cos^2\theta_k - \sin^2\theta_k \cos\theta_k \frac{k}{m} + O\left(\frac{k^2}{m^2}\right), \tag{A8a}$$

$$B_{[=]}(\boldsymbol{k}) = \sin^2\theta_k + \sin^2\theta_k \cos\theta_k \frac{k}{m} + O\left(\frac{k^2}{m^2}\right), \tag{A8b}$$

$$A_{[\neq]}(\boldsymbol{k}) = \sin\theta_k \cos\theta_k - \sin^3\theta_k \frac{k}{m} + O\left(\frac{k^2}{m^2}\right), \tag{A8c}$$

$$B_{[\neq]}(\boldsymbol{k}) = \sin\theta_k \cos\theta_k + \cos^2\theta_k \sin\theta_k \frac{k}{m} + O\left(\frac{k^2}{m^2}\right), \tag{A8d}$$

we obtain the angular averages (A3) as

$$\bar{A}_{[=]} = \frac{1}{3}, \quad \bar{B}_{[=]} = \frac{2}{3}, \tag{A9a}$$

$$\bar{A}_{[\neq]} = -\frac{3\pi}{16}\frac{k}{m}, \quad \bar{B}_{[\neq]} = \frac{\pi}{16}\frac{k}{m}. \tag{A9b}$$

Going through the same steps as in Eq. (A6), we obtain for the favored distribution

$$\int_0^2 \frac{d\alpha_p}{\alpha_p}\, d^2p_{pT} P_{[S_L,S_L]}(\alpha_p, \boldsymbol{p}_{pT}) = 1 - \frac{3}{2}\omega_2; \tag{A10}$$

for the unfavored distribution

$$\int_0^2 \frac{d\alpha_p}{\alpha_p}\, d^2p_{pT} P_{[S_T,S_L]}(\alpha_p, \boldsymbol{p}_{pT}) = \varepsilon_{[S_L]}, \tag{A11}$$

where

$$\varepsilon_{[S_L]} = \frac{\pi^2}{4} \int \frac{dk k^2}{E} \frac{k}{m}\left(f_0 - \frac{f_2}{\sqrt{2}}\right)\left(-4f_0 + \frac{f_2}{\sqrt{2}}\right). \tag{A12}$$

For the favored distribution, the depolarization correction to the integral is not suppressed in $k/m$ (present in the nonrelativistic limit) and quadratic in the $D$ wave. For the unfavored distribution, the correction is of first order in $k/m$ (relativistic correction) and quadratic in the $S$ wave. These findings are naturally explained by the angular momentum addition implied by rotational invariance in the c.m. frame.

Table III gives the numerical values of the depolarization corrections, computed with the AV18 deuteron radial wave functions [70]. The $D$-state probability $\omega_2$ is a basic prediction of the $NN$ potential parametrization. The integral $I_{[S_L]}$ is given

TABLE III. Values of the integrals appearing in the sum rules of the polarized neutron distributions, evaluated with the AV18 deuteron wave function. The second column shows the results obtained with exact numerical integration. The third column shows the results obtained with integrand expanded in $k/m$, neglecting $O(k^2/m^2)$ (see text). The fourth column shows the references in text.

| integral | exact | expanded | Ref. |
|---|---|---|---|
| $\omega_2$ | 0.0576 | | (A7) |
| $I_{[S_L]}$ | 0.911 | 0.913 | (A1) |
| $I_{[S_T]}$ | 0.912 | 0.913 | (A13) |
| $\delta^{\parallel}$ | 0.125 | 0.122 | (A20) |
| $\delta^{\perp}$ | 0.0512 | | (A22) |
| $\varepsilon_{[S_L]}$ | −0.0568 | −0.0579 | (A11) |
| $\varepsilon_{[S_T]}$ | 0.0550 | 0.0552 | (A28) |

as computed exactly using Eq. (A1), and approximately by expanding in $k/m$ using Eq. (A6); the difference between the two values is seen to be of order $10^{-3}$. The relativistic correction $\epsilon_{[S_L]}$ is of the order of a few percent.

### 2. Transversely polarized neutron

The integral of the distribution of transversely polarized neutrons Eq. (4.34) is computed in the same way as for the longitudinally polarized neutrons. The integral is expressed as

$$\int_0^2 \frac{d\alpha_p}{\alpha_p}\, d^2p_{pT}\, \boldsymbol{P}_{[S_T]}(\alpha_p, \boldsymbol{p}_{pT}|\boldsymbol{S}_D) = I_{[S_T]}\boldsymbol{S}_{DT}. \tag{A13}$$

The integral is again evaluated in the c.m. momentum variables,

$$\begin{aligned}
&\int_0^2 \frac{d\alpha_p}{\alpha_p}\, d^2p_{pT}\, \boldsymbol{P}_{[S_T]}(\alpha_p, \boldsymbol{p}_{pT}|\boldsymbol{S}_D) \\
&\quad = \int \frac{d^3k}{E}\left(f_0 - \frac{f_2}{\sqrt{2}}\right) \\
&\qquad \times \left[\boldsymbol{A}_T(f_0 + \sqrt{2}f_2) + \boldsymbol{B}_T\left(f_0 - \frac{f_2}{\sqrt{2}}\right)\right] \\
&\quad = 4\pi \int \frac{dk\, k^2}{E}\left(f_0 - \frac{f_2}{\sqrt{2}}\right) \\
&\qquad \times \left[\bar{\boldsymbol{A}}_T(f_0 + \sqrt{2}f_2) + \bar{\boldsymbol{B}}_T\left(f_0 - \frac{f_2}{\sqrt{2}}\right)\right],
\end{aligned} \tag{A14}$$

where now

$$\bar{\boldsymbol{A}}_T \equiv \int \frac{d\Omega_k}{4\pi}\boldsymbol{A}_T(\boldsymbol{k}), \quad \bar{\boldsymbol{B}}_T \equiv \int \frac{d\Omega_k}{4\pi}\boldsymbol{B}_T(\boldsymbol{k}), \tag{A15}$$

are the angular averages of the transverse vector-valued coefficients Eqs. (4.34b) and (4.34c). Expanding in $k/m$, the coefficients become

$$\begin{aligned}
\boldsymbol{A}_T &= \boldsymbol{S}_{DT} - \left(1 + \cos\theta_k \frac{|\boldsymbol{k}|}{m}\right)\frac{(\boldsymbol{S}_{DT}\cdot\boldsymbol{k}_T)\boldsymbol{k}_T}{|\boldsymbol{k}|^2} \\
&\quad - \left(\cos\theta_k - \sin^2\theta_k \frac{|\boldsymbol{k}|}{m}\right)\frac{\boldsymbol{k}_T}{|\boldsymbol{k}|}S_D^z + O\left(\frac{k^2}{m^2}\right),
\end{aligned} \tag{A16a}$$

$$\begin{aligned}
\boldsymbol{B}_T &= \left(1 + \cos\theta_k \frac{|\boldsymbol{k}|}{m}\right)\frac{(\boldsymbol{S}_{DT}\cdot\boldsymbol{k}_T)\boldsymbol{k}_T}{|\boldsymbol{k}|^2} \\
&\quad + \cos\theta_k\left(1 + \cos\theta_k \frac{|\boldsymbol{k}|}{m}\right)\frac{\boldsymbol{k}_T}{|\boldsymbol{k}|}S_D^z + O\left(\frac{k^2}{m^2}\right).
\end{aligned} \tag{A16b}$$

Now the terms $\propto S_D^z$ average to zero and the terms $\propto \boldsymbol{S}_{DT}$ survive. We obtain

$$\bar{\boldsymbol{A}}_T = \tfrac{2}{3}\boldsymbol{S}_{DT}, \quad \bar{\boldsymbol{B}}_T = \tfrac{1}{3}\boldsymbol{S}_{DT}. \tag{A17}$$

We thus identify the scalar integral in Eq. (A13) as

$$\begin{aligned}
I_{[S_T]} &= 4\pi \int \frac{dk\, k^2}{E}\left(f_0 - \frac{f_2}{\sqrt{2}}\right)\left(f_0 + \frac{f_2}{\sqrt{2}}\right) \\
&= I_{[S_L]} = 1 - \frac{3}{2}\omega_2.
\end{aligned} \tag{A18}$$

The scalar integral in the sum rule for the transversely polarized neutron distribution is the same as that in the longitudinally polarized distribution [Eq. (A1)]. This result would be expected for a nonrelativistic system. In our LF description it is obtained including terms of the order $\boldsymbol{k}/m$, neglecting only terms of order $k^2/m^2$, and is thus a nontrivial consequence of the realization of rotational invariance by the c.m. frame representation of the deuteron LF wave function.

The integrals of the normalized transversely polarized distributions, Eqs. (4.36) and (4.38), can be computed in a similar way. Here we have to take into account that the vectors used for the projections of the transverse spins, Eq. (4.29), depend on the transverse momentum $\boldsymbol{k}_T$ and thus are affected by the angular averaging in the integrals. For the $\parallel$ favored distribution Eq. (4.36a),

$$\begin{aligned}
&\int_0^2 \frac{d\alpha_p}{\alpha_p}\, d^2p_{pT} P^{\parallel}_{[S_T,S_T]}(\alpha_p, \boldsymbol{p}_{pT}|\boldsymbol{S}_D) \\
&\quad = \int \frac{d^3k}{E}\left(f_0 - \frac{f_2}{\sqrt{2}}\right) \\
&\qquad \times \left[A_{[=]}(f_0 + \sqrt{2}f_2) + B_{[=]}\left(f_0 - \frac{f_2}{\sqrt{2}}\right)\right] \\
&\quad = 4\pi \int \frac{dk\, k^2}{E}\left(f_0 - \frac{f_2}{\sqrt{2}}\right) \\
&\qquad \times \left[\bar{A}_{[=]}(f_0 + \sqrt{2}f_2) + \bar{B}_{[=]}\left(f_0 - \frac{f_2}{\sqrt{2}}\right)\right],
\end{aligned} \tag{A19}$$

and using the angular averages [Eq. (A9)], we obtain

$$\begin{aligned}
&\int_0^2 \frac{d\alpha_p}{\alpha_p}\, d^2p_{pT} P^{\parallel}_{[S_T,S_T]}(\alpha_p, \boldsymbol{p}_{pT}|\boldsymbol{S}_D) \\
&\quad = 4\pi \int \frac{dk\, k^2}{E}\left(f_0 - \frac{f_2}{\sqrt{2}}\right) f_0 \\
&\quad = 4\pi \int \frac{dk\, k^2}{E}\left[f_0^2 + f_2^2 - (f_0 + \sqrt{2}f_2)\frac{f_2}{\sqrt{2}}\right] \\
&\quad = 1 - \delta^{\parallel},
\end{aligned} \tag{A20}$$

where

$$\delta^{\parallel} \equiv 4\pi \int \frac{dk\, k^2}{E}(f_0 + \sqrt{2}f_2)\frac{f_2}{\sqrt{2}}. \tag{A21}$$

For the $\perp$ favored distribution [Eq. (4.36b)], we obtain

$$\int_0^2 \frac{d\alpha_p}{\alpha_p} d^2p_{pT} P^{\perp}_{[S_T,S_T]}(\alpha_p, \boldsymbol{p}_{pT}|\boldsymbol{S}_D) = \int \frac{d^3k}{E}\left(f_0 - \frac{f_2}{\sqrt{2}}\right)(f_0 + \sqrt{2}f_2) = 1 - \delta^{\perp}, \tag{A22}$$

where

$$\delta^{\perp} \equiv 4\pi \int \frac{dk\, k^2}{E}(-f_0 + 2\sqrt{2}f_2)\frac{f_2}{\sqrt{2}}. \tag{A23}$$

In both the $\parallel$ and the $\perp$ distribution the depolarization effects are caused by the $D$ wave; however, the corrections are not simply quadratic in the $D$-wave radial wave function as in the sum rule for the unprojected distribution, Eqs. (A7) and (A18), but involve the product of the $D$- and $S$-wave functions. These differences are a consequence of the angular momentum addition implied by the projection of the distribution on the angular-dependent transverse vectors Eq. (4.29). The numerical values of $\delta^{\parallel}$ and $\delta^{\perp}$ are given in Table III. Comparing the integrals in Eqs. (A7), (A21), and (A23), we observe that

$$\tfrac{1}{2}(\delta^{\parallel} + \delta^{\perp}) = \tfrac{3}{2}\omega_2, \tag{A24}$$

so that

$$\int_0^2 \frac{d\alpha_p}{\alpha_p} d^2p_{pT} \frac{1}{2}\left[P^{\parallel}_{[S_T,S_T]} + P^{\perp}_{[S_T,S_T]}\right] = 1 - \frac{3}{2}\omega_2. \tag{A25}$$

In the sum of the $\parallel$ and $\perp$ projected distributions, the mixed $D$- and $S$-wave terms in the depolarization correction cancel, and the correction is proportional to the square of the $D$ wave, as it should be.

In the sum rule for the tagged spin structure function $g_{2D}$ in Sec. V D we encounter the integral Eq. (A25) with an additional factor

$$\frac{1}{2-\alpha_p} = 1 + \cos\theta_k \frac{k}{m} + O\left(\frac{k^2}{m^2}\right) \tag{A26}$$

in the integrand. This integral can be computed in the same manner as above and is equal to Eq. (A25) up to corrections $O(k^2/m^2)$,

$$\int_0^2 \frac{d\alpha_p}{\alpha_p(2-\alpha_p)} d^2p_{pT} \frac{1}{2}\left[P^{\parallel}_{[S_T,S_T]} + P^{\perp}_{[S_T,S_T]}\right] = 1 - \frac{3}{2}\omega_2. \tag{A27}$$

This result is again a consequence of rotational invariance in the c.m. frame.

For the unfavored distribution of transversely polarized neutrons, Eq. (4.38), we obtain

$$\int_0^2 \frac{d\alpha_p}{\alpha_p} d^2p_{pT} P_{[S_L,S_T]}(\alpha_p, \boldsymbol{p}_{pT}|\boldsymbol{S}_D) = \varepsilon_{[S_T]}, \tag{A28}$$

where

$$\varepsilon_{[S_T]} = \frac{\pi^2}{4}\int \frac{dkk^2}{E}\frac{k}{m}\left(f_0 - \frac{f_2}{\sqrt{2}}\right)\left(4f_0 + 5\frac{f_2}{\sqrt{2}}\right). \tag{A29}$$

The angular averages of the coefficients $A_{[\neq]}$, $B_{[\neq]}$ were used, see Eq. (A9). The result Eq. (A29) is of the same form as that for the unfavored distribution of longitudinally polarized neutrons, Eq. (A12), but with different numerical coefficients of the radial wave functions in the second factor in the integrand. Overall,

$$\varepsilon_{[S_T]} \approx -\varepsilon_{[S_L]}, \tag{A30}$$

as can be seen by comparing the sign of the squared $S$-wave term in the integrals. The numerical value of $\varepsilon_{[S_T]}$ is given in Table III. The sum rules for the unfavored distributions show that there is some net longitudinal neutron polarization induced by transverse deuteron polarization, and vice versa. The effect is of the order $k/m$ (relativistic correction) and approximately of the same size in either direction.


[1] W. Cosyn and C. Weiss, preceding paper, Semi-inclusive deep-inelastic scattering on a polarized spin-1 target. I. Cross section and spin observables, Phys. Rev. C **114**, 025201 (2026).

[2] L. Trentadue and G. Veneziano, Fracture functions: An improved description of inclusive hard processes in QCD, Phys. Lett. B **323**, 201 (1994).

[3] J. C. Collins, Proof of factorization for diffractive hard scattering, Phys. Rev. D **57**, 3051 (1998); **61**, 019902(E) (2000).

[4] M. Anselmino, V. Barone, and A. Kotzinian, SIDIS in the target fragmentation region: Polarized and transverse momentum dependent fracture functions, Phys. Lett. B **699**, 108 (2011).

[5] L. L. Frankfurt and M. I. Strikman, High momentum transfer processes with polarized deuterons, Nucl. Phys. A **405**, 557 (1983).

[6] L. L. Frankfurt and M. I. Strikman, High-energy phenomena, short range nuclear structure and QCD, Phys. Rep. **76**, 215 (1981).

[7] M. Sargsian and M. Strikman, Model independent method for determination of the DIS structure of free neutron, Phys. Lett. B **639**, 223 (2006).

[8] W. Cosyn and M. M. Sargsian, High-$x$ structure function of the virtually free neutron, Phys. Rev. C **93**, 055205 (2016).

[9] M. Strikman and C. Weiss, Electron-deuteron deep-inelastic scattering with spectator nucleon tagging and final-state interactions at intermediate $x$, Phys. Rev. C **97**, 035209 (2018).

[10] A. Jentsch, Z. Tu, and C. Weiss, Deep-inelastic electron-deuteron scattering with spectator nucleon tagging at the future Electron Ion Collider: Extracting free nucleon structure, Phys. Rev. C **104**, 065205 (2021).

[11] W. Melnitchouk, M. Sargsian, and M. I. Strikman, Probing the origin of the EMC effect via tagged structure functions of the deuteron, Z. Phys. A: Hadrons Nucl. **359**, 99 (1997).

[12] M. M. Sargsian *et al.*, Hadrons in the nuclear medium, J. Phys. G **29**, R1 (2003).

[13] O. Hen, D. W. Higinbotham, G. A. Miller, E. Piasetzky, and L. B. Weinstein, The EMC effect and high momentum nucleons in nuclei, Int. J. Mod. Phys. E **22**, 1330017 (2013).

[14] E. P. Segarra, J. R. Pybus, F. Hauenstein, D. W. Higinbotham, G. A. Miller, E. Piasetzky, A. Schmidt, M. Strikman, L. B. Weinstein, and O. Hen, Short-range correlations and the nuclear EMC effect in deuterium and helium-3, Phys. Rev. Res. **3**, 023240 (2021).

[15] S. Ratliff and A. Schmidt, Studying the impact of virtuality-dependent nucleon structure modification on spectator-tagged deep inelastic scattering, Eur. Phys. J. A **60**, 5 (2024).

[16] O. Hen, G. A. Miller, E. Piasetzky, and L. B. Weinstein, Nucleon-nucleon correlations, short-lived excitations, and the quarks within, Rev. Mod. Phys. **89**, 045002 (2017).

[17] W. Cosyn and C. Weiss, Neutron spin structure from polarized deuteron DIS with proton tagging, Phys. Lett. B **799**, 135035 (2019).

[18] W. Cosyn and C. Weiss, Polarized electron-deuteron deep-inelastic scattering with spectator nucleon tagging, Phys. Rev. C **102**, 065204 (2020).

[19] A. Airapetian *et al.* (HERMES Collaboration), First measurement of the tensor structure function $b_1$ of the deuteron, Phys. Rev. Lett. **95**, 242001 (2005).

[20] J. Poudel, A. Bacchetta, J.-P. Chen, and N. Santiesteban, Experimental study of tensor structure function of deuteron, Eur. Phys. J. A **61**, 81 (2025).

[21] N. Baillie *et al.* (CLAS Collaboration), Measurement of the neutron $F_2$ structure function via spectator tagging with CLAS, Phys. Rev. Lett. **108**, 142001 (2012); **108**, 199902(E) (2012).

[22] S. Tkachenko *et al.* (CLAS Collaboration), Measurement of the structure function of the nearly free neutron using spectator tagging in inelastic $^2\mathrm{H}(e, e' p_s)X$ scattering with CLAS, Phys. Rev. C **89**, 045206 (2014); **90**, 059901 (2014).

[23] W. Armstrong *et al.*, Partonic structure of light nuclei, arXiv:1708.00888.

[24] I. Albayrak *et al.*, Design, construction, and performance of the GEM based radial time projection chamber for the BONuS12 experiment with CLAS12, Nucl. Instrum. Methods Phys. Res., Sect. A **1062**, 169190 (2024).

[25] A. V. Klimenko *et al.* (CLAS Collaboration), Electron scattering from high-momentum neutrons in deuterium, Phys. Rev. C **73**, 035212 (2006).

[26] S. Gilad, O. Hen, L. B. Weinstein, S. A. Wood, *et al.*, In medium nucleon structure functions, SRC, and the EMC effect, JLAB-PR12-11-107 (2011), http://www.jlab.org/exp_prog/proposals/11/PR12-11-107.pdf

[27] E. P. Segarra *et al.*, The CLAS12 backward angle neutron detector (BAND), Nucl. Instrum. Methods Phys. Res., Sect. A **978**, 164356 (2020).

[28] R. Abdul Khalek *et al.*, Science requirements and detector concepts for the Electron-Ion Collider: EIC Yellow Report, Nucl. Phys. A **1026**, 122447 (2022).

[29] H. Huang, F. Méot, V. Ptitsyn, V. Ranjbar, and T. Roser, Polarization preservation of polarized deuteron beams in the electron ion collider at Brookhaven National Laboratory, Phys. Rev. Accel. Beams **23**, 021001 (2020).

[30] H. Huang, F. Méot, V. Ptitsyn, V. Ranjbar, and T. Roser, Feasibility of polarized deuteron beam in the EIC, in *12th International Particle Accelerator Conference* (JACoW Publishing, Campinas, Brazil, 2021).

[31] H. Huang, K. Hock, F. Meot, V. Ptitsyn, V. Ranjbar, V. Schoefer, and V. Morozov, Hadron polarization in the Electron Ion Collider, PoS **PSTP2024**, 022 (2025).

[32] P. A. M. Dirac, Forms of relativistic dynamics, Rev. Mod. Phys. **21**, 392 (1949).

[33] S. Weinberg, Dynamics at infinite momentum, Phys. Rev. **150**, 1313 (1966).

[34] J. B. Kogut and D. E. Soper, Quantum electrodynamics in the infinite momentum frame, Phys. Rev. D **1**, 2901 (1970).

[35] H. Leutwyler and J. Stern, Relativistic dynamics on a null plane, Ann. Phys. (NY) **112**, 94 (1978).

[36] S. J. Brodsky, H.-C. Pauli, and S. S. Pinsky, Quantum chromodynamics and other field theories on the light cone, Phys. Rep. **301**, 299 (1998).

[37] L. A. Kondratyuk and M. I. Strikman, Relativistic correction to the deuteron magnetic moment and angular condition, Nucl. Phys. A **426**, 575 (1984).

[38] M. V. Terentev, On the structure of wave functions of mesons as bound states of relativistic quarks, Sov. J. Nucl. Phys. **24**, 106 (1976).

[39] L. L. Frankfurt, M. M. Sargsian, and M. I. Strikman, Feynman graphs and generalized eikonal approach to high energy knock-out processes, Phys. Rev. C **56**, 1124 (1997).

[40] M. M. Sargsian, Selected topics in high energy semi-exclusive electro-nuclear reactions, Int. J. Mod. Phys. E **10**, 405 (2001).

[41] R. Boussarie *et al.*, TMD handbook, arXiv:2304.03302.

[42] C. Ciofi degli Atti, L. P. Kaptari, and D. Treleani, On the effects of the final state interaction in the electrodisintegration of the deuteron at intermediate-energies and high-energies, Phys. Rev. C **63**, 044601 (2001).

[43] C. Ciofi degli Atti, L. P. Kaptari, and B. Z. Kopeliovich, Final state interaction effects in semi-inclusive DIS off the deuteron, Eur. Phys. J. A **19**, 145 (2004).

[44] W. Cosyn and M. Sargsian, Final-state interactions in semi-inclusive deep inelastic scattering off the deuteron, Phys. Rev. C **84**, 014601 (2011).

[45] W. Cosyn and M. Sargsian, Nuclear final-state interactions in deep inelastic scattering off the lightest nuclei, Int. J. Mod. Phys. E **26**, 1730004 (2017).

[46] D. W. Sivers, Single spin production asymmetries from the hard scattering of point-like constituents, Phys. Rev. D **41**, 83 (1990).

[47] V. Dmitrasinovic and F. Gross, Polarization observables in deuteron photodisintegration and electrodisintegration, Phys. Rev. C **40**, 2479 (1989); **43**, 1495(E) (1991).

[48] H. Arenhövel, W. Leidemann, and E. L. Tomusiak, General formulae for polarization observables in deuteron electrodisintegration and linear relations, Few-Body Syst. **15**, 109 (1993).

[49] H. Arenhövel, W. Leidemann, and E. L. Tomusiak, General multipole expansion of polarization observables in deuteron electrodisintegration, Eur. Phys. J. A **14**, 491 (2002).

[50] H. Arenhövel, W. Leidemann, and E. L. Tomusiak, General survey of polarization observables in deuteron electrodisintegration, Eur. Phys. J. A **23**, 147 (2005).

[51] J. Flores, S. S. Chabysheva, and J. R. Hiller, Reduced nuclear helicity amplitudes for deuteron electrodisintegration and other processes, Phys. Rev. C **107**, 045205 (2023).

[52] W. Leidemann, E. L. Tomusiak, and H. Arenhövel, Inclusive deuteron electrodisintegration with polarized electrons and a polarized target, Phys. Rev. C **43**, 1022 (1991).

[53] H. Arenhövel, W. Leidemann, and E. L. Tomusiak, Exclusive deuteron electrodisintegration with polarized electrons and a polarized target, Phys. Rev. C **46**, 455 (1992).

[54] S. Jeschonnek and J. W. Van Orden, Target polarization for $^2\vec{\mathrm{H}}(e, e'p)n$ at GeV energies, Phys. Rev. C **80**, 054001 (2009).

[55] S. Jeschonnek and J. W. Van Orden, Factorization breaking of $A_d^T$ for polarized deuteron targets in a relativistic framework, Phys. Rev. C **95**, 044001 (2017).

[56] M. P. Rekalo, G. I. Gakh, and A. P. Rekalo, Inclusive electrodisintegration of polarized deuterons, J. Phys. G: Nucl. Phys. **13**, 1209 (1987).

[57] G. I. Gakh, A. P. Rekalo, and E. Tomasi-Gustafsson, Relativistically invariant analysis of polarization effects in exclusive deuteron electrodisintegration process, Ann. Phys. (NY) **319**, 150 (2005).

[58] A. Grassi, J. Golak, W. N. Polyzou, R. Skibiński, H. Witała, and H. Kamada, Electron and neutrino scattering off the deuteron in a relativistic framework, Phys. Rev. C **107**, 024617 (2023).

[59] F. D. Aaron *et al.* (H1 Collaboration), Measurement of the inclusive $ep$ scattering cross section at low $Q^2$ and $x$ at HERA, Eur. Phys. J. C **63**, 625 (2009).

[60] J. R. Cooke and G. A. Miller, Deuteron binding energies and form-factors from light front field theory, Phys. Rev. C **66**, 034002 (2002).

[61] D. E. Soper, Infinite-momentum helicity states, Phys. Rev. D **5**, 1956 (1972).

[62] H. J. Melosh, Quarks: Currents and constituents, Phys. Rev. D **9**, 1095 (1974).

[63] L. Frankfurt and M. Strikman, Short-range correlations in nuclei as seen in hard nuclear reactions and light-cone dynamics, *Modern Topics in Electron Scattering*, edited by B. Frois and I. Sick (World Scientific, Singapore, 1992), pp. 645–694.

[64] J. Carbonell and V. A. Karmanov, Relativistic deuteron wave function in the light front dynamics, Nucl. Phys. A **581**, 625 (1995).

[65] M. M. Sargsian and F. Vera, New structure in the deuteron, Phys. Rev. Lett. **130**, 112502 (2023).

[66] O. Benhar, N. Farina, H. Nakamura, M. Sakuda, and R. Seki, Electron- and neutrino-nucleus scattering in the impulse approximation regime, Phys. Rev. D **72**, 053005 (2005).

[67] L. L. Frankfurt and M. I. Strikman, Hard nuclear processes and microscopic nuclear structure, Phys. Rep. **160**, 235 (1988).

[68] M. M. Sargsian, Large $Q^2$ electrodisintegration of the deuteron in virtual nucleon approximation, Phys. Rev. C **82**, 014612 (2010).

[69] R. Alessandro, A. Del Dotto, E. Pace, G. Perna, G. Salmè, and S. Scopetta, Light-front transverse momentum distributions for $J = 1/2$ hadronic systems in valence approximation, Phys. Rev. C **104**, 065204 (2021).

[70] R. B. Wiringa, V. G. J. Stoks, and R. Schiavilla, Accurate nucleon-nucleon potential with charge-independence breaking, Phys. Rev. C **51**, 38 (1995).

[71] N. Christ and T. D. Lee, Possible tests of $C_{\mathrm{st}}$ and $T_{\mathrm{st}}$ invariances in $l^{\pm} + N \to l^{\pm} + \Gamma$ and $A \to B + e^+ + e^-$, Phys. Rev. **143**, 1310 (1966).

[72] A. Afanasev, M. Strikman, and C. Weiss, Transverse target spin asymmetry in inclusive DIS with two-photon exchange, Phys. Rev. D **77**, 014028 (2008).

[73] H. Burkhardt and W. N. Cottingham, Sum rules for forward virtual Compton scattering, Ann. Phys. (NY) **56**, 453 (1970).

[74] J. Kodaira and K. Tanaka, Polarized structure functions in QCD, Prog. Theor. Phys. **101**, 191 (1999).

[75] A. Bodek *et al.*, Experimental studies of the neutron and proton electromagnetic structure functions, Phys. Rev. D **20**, 1471 (1979).

[76] D. de Florian, R. Sassot, M. Stratmann, and W. Vogelsang, Extraction of spin-dependent parton densities and their uncertainties, Phys. Rev. D **80**, 034030 (2009).

[77] S. Wandzura and F. Wilczek, Sum rules for spin dependent electroproduction: Test of relativistic constituent quarks, Phys. Lett. B **72**, 195 (1977).

[78] R. Machleidt and I. Slaus, The nucleon-nucleon interaction: Topical review, J. Phys. G **27**, R69 (2001).

[79] R. Machleidt, The high-precision, charge-dependent Bonn nucleon-nucleon potential (CD-Bonn), Phys. Rev. C **63**, 024001 (2001).

[80] S. N. Sokolov and A. N. Shatnyi, Physical equivalence of three forms of relativistic dynamics and addition of interactions in the front and instant forms, Theor. Math. Phys. **37**, 1029 (1978).

[81] B. L. G. Bakker, L. A. Kondratyuk, and M. V. Terentev, On the formulation of two-body and three-body relativistic equations employing light front dynamics, Nucl. Phys. B **158**, 497 (1979).

[82] F. M. Lev, Relativistic quantum mechanics and its applications to few-nucleon systems, Riv. Nuovo Cimento **16**, 1 (1993).